

S T A T E M E N T

This study and the investigations conducted by the author are primarily concerned with the cosmic ray fluctuations of very short periods, of the order of a few minutes. This was not possible in the past because large area detectors that could give a very high counting rate, were not available. For cosmic ray modulation pattern to be perceptible, it must show above the statistical fluctuations, which at times for a small area detector, can be higher than the signal. In one of the earlier attempts by Torizuka and Wada (1960), where they had used detectors giving counting rates of the order of 10^5 counts per minute, some studies of short period variations were made. A very general indication was that the amplitude of the short period fluctuations decreased, with the decrease of the meson intensity. They improved the analysis further in (1962), but the statistical accuracy was not so high as to warrant any definite conclusions.

With the availability of a mu meson detector with scintillators of 60 Sq. meter area operated by BASJE at Chacaltaya (Bolivia), altitude 17,200 ft., geographic latitude $S 16^{\circ} - 19'$, longitude $W 68^{\circ} - 10'$, it became possible to study short period fluctuations with a counting rate of about 10^6 counts per minute. The Bolivian Air Shower Joint Experiment had been set up jointly by

M.I.T., University of Tokyo and the University of Michigan with the main object of studying showers produced by very high energy cosmic ray particles (Suga et al 1962). An array of 15 scintillator detectors, each of 4 Sq. meter area, formed the main element of the mu meson detecting system. The whole area of the detecting system was housed in a cave shielded with galena to about 3 M.W.E. The author built a digitized recording unit at M.I.T. during the latter half of 1963. This was later installed at Chacaltaya and the recording of the data was started from April, 1964. The author maintained the unit throughout the I.Q.S.Y. period and up to the end of June, 1966. The basic interval of data recording was fixed at 12 second, with time recorded every 1 minute. Also, a digitized servo-barometer was used for recording pressure every minute. Three groups of 5 detectors each, recorded separately. Maximum care was taken to ensure stabilized conditions of the whole recording system. Using a pulse height analyser, differential spectra of the dark current pulses of the photo-tubes, and of mu meson scintillator pulses were recorded. Thus a check could be maintained on the noise level, and it helped in fixing the levels of the discriminator circuits. The data was recorded on punched paper tape, and was later converted to I.B.M. cards by a tape to card converter. These cards formed the basis of the further analysis, performed by using a 1620 I.B.M. computer.

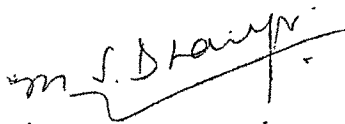
Power spectrum and digital filtering methods of analysis are used (Blackman and Tukey 1959). The power is given in the frequency domain. The signal to noise ratio is improved because of the random nature of noise, and the frequency selective pattern makes the signal frequency to appear more predominantly even in a condition where the signal to noise ratio is not high. The range of frequencies selected for the present study is from 1 to 30 cycles per hour.

Each sample, comprising of a 3-hourly interval, shows a variability of spectral estimates. In the range of 1 to 6 cycles per hour, the spectral estimates tend to average out as more and more samples are superposed upon one another. But as the range is extended up to 30 cycles per hour, consistent peaks are observed at 18 CPH and 25 CPH. The 18 CPH (200 sec. period) which is persistent, has also been detected with high activity in magnetic measurements taken in the magnetosheath by Mariner IV (Siscoe et al 1967). The dynamic power spectrum taken for one sample shows the existence of peaks at 6, 11, 17 and 26 cycles per hour. Frequencies close to these have also been found in the measurements of the interplanetary magnetic field recorded simultaneously by Pioneer VI (Ness et al 1966). Magnetic field measurements conducted in the magnetosphere by Explorer VI, show oscillations with period of 200 sec.

(Judge and Coleman 1962), and Explorer XII, periods of 180 and 120 sec. (Patel and Cahill 1964).

Detailed analysis is carried out to find the behaviour of the prominent frequencies during quiet and disturbed epochs. The possibility, that the magnetic field fluctuations produced by the interplanetary wind in the magnetosheath are responsible for modulating the cosmic rays through changes of the geomagnetic cut off rigidity, is considered.


(VIKRAM A. SARABHAI)


(M. S. DHANJU)

A C K N O W L E D G E M E N T S

I wish to express my deep gratitude to Professor Vikram A. Sarabhai for his inspiring guidance and continued interest throughout the course of this work.

Thanks are due to Prof. H. S. Bridge of M.I.T. and Dr. M. Wada then at M.I.T. for the valuable help rendered in the initial stages of the experiment. The experiment would have been impossible without the active help of the BASJE investigators particularly Prof. I. Escobar, Dr. Suga and Dr. K. Kamata. The author is indebted to Prof. I. Escobar, the Director and the staff, for providing facilities at Laboratorio de Fisica Cosmica, U.M.S.A., LAPAZ (Bolivia), where the author stayed for the bulk of the period of the experimental investigation.

The author is thankful to Dr. U. R. Rao for the helpful suggestions rendered during the preparation of this thesis. It is a pleasure to acknowledge fruitful discussions with Dr. R. P. Kane, in the initial stages of the analysis work.

The analysis was carried out at the computing centre, Physical Research Laboratory. I am extremely thankful to Mr. S. R. Thakore for offering very valuable suggestions and advice during the course of the computer analysis. Thanks are also due to Mr. P. S. Shah,

: vi :

Mr.C.G.Rathod and Mr.M.V.Bhavsar for help in programming,
and for computational help, to Mr.D.H.Shah and Mr.
P.V.Bhavsar.

Financial help by the U.S.Air Force office of
Scientific Research under grant AF-AFOSR 4-63 and 4-65,
and by the Department of Atomic Energy, Govt.of India,
is gratefully acknowledged.

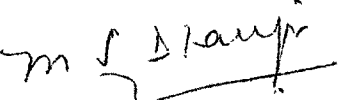

M. S. Dhanju.

TABLE OF CONTENTS

SUMMARY	i - iv
CHAPTER I. INTRODUCTION				
1.1	<u>Primary and secondary cosmic rays</u>	1
1.11	Primary cosmic rays	1
1.111	Nature of primary cosmic rays			1
1.112	Energy spectrum	2
1.12	Secondary Components	4
1.13	Effects of pressure and temperature on secondary components	8
1.131	General aspects	8
1.132	Corrections for meson component			9
1.2	<u>Cosmic rays in geomagnetic field</u>	10
1.21	Geomagnetic field and particle trajectories..	10
1.22	Threshold rigidity	12
1.23	Asymptotic directions	14
1.3	<u>Cosmic ray variations</u>	16
1.31	General aspects	16
1.32	Spectral variation by method of coupling constants	17
1.33	Variation of cut off rigidity	19
1.34	Energy spectrum variations	22
1.4	<u>Conditions in interplanetary space</u>	23
1.41	Solar wind	23
1.42	Interplanetary magnetic field	26

1.43	Sector structure	30
1.5	<u>Interaction of solar wind with geomagnetic field</u>	32
1.51	Magnetosheath and magnetospheric cavity			32
1.52	Bow shock	36
1.53	Theoretical models of the magnetosphere			37
1.6	<u>Geomagnetic micropulsations</u>	39
1.61	Characteristics of geomagnetic micropulsations	39
1.62	Amplitude and frequency dependence on latitude.	40
1.63	Hydrodynamical nature of PC 5	..		41
1.64	Telluric currents	42

CHAPTER II. EXPERIMENTAL SET UP

2.1	<u>General remarks</u>	43
2.2	<u>Operation</u>	45
2.3	<u>Detectors and associated electronics</u>	..		47
2.31	Scintillators	47
2.32	Phototube	48
2.33	H.V. connection to the phototube	..		49
2.34	H.V. Power supply	50
2.4	<u>Amplifiers</u>	51
2.41	Pre-amplifier	51
2.42	Main amplifier	52
2.43	Discriminator, pulse shaper, mixer and driver	53

2.5	<u>Counting circuits</u>	57
2.51	Pre-scaler	57
2.52	Count decades	59
2.6	<u>Electronic clock calender</u>	60
2.61	DC/DC converter	64
2.7	<u>Integral circuits and temporary storage</u>			66
2.8	<u>Print out circuits</u>	70
2.81	Serial converter	70
2.82	Printing of calender and pressure..			74
2.83	Coupler	76
2.84	Punchers	77
2.85	Typewriter	77
2.9	<u>Digital Servo-barometer</u>	78
2.91	DEC to BCD converter	81
2.10	<u>Tests and checks</u>	83
2.101	Stability of the discriminator	..		83
2.102	Pulse Height Analyser checks	..		85
2.103	Temperature checks	88

CHAPTER III. METHOD OF ANALYSIS

PART A:	TREATMENT OF DATA	89
3A.1	<u>Introduction</u>	89
3A.2	<u>Format and duration of data</u>	89
3A.3	<u>Self consistency of the data</u>	..		91
3A.4	<u>Data used for Power Spectrum Analysis..</u>			93

PART B. POWER SPECTRUM ANALYSIS

3B.1	<u>Introductory remarks</u>	94
	3B.11 Auto-covariance function	95
	3B.12 Fourier transforms	97
	3B.13 Numerical formulas	98
3B.2	<u>Aliasing</u>	99
3B.3	<u>Filters</u>	100
	3B.31 General digital filters	100
	3B.32 Hamming or Hanning filter	102
3B.4	<u>Pre-whitening</u>	103
3B.5	<u>Chi-square test</u>	105
3B.6	<u>Superposition of power density estimates</u>			106
3B.7	<u>Choice of the constants for the spectral Analysis</u>			106
3B.8	<u>Method of epochs</u>	109

CHAPTER IV. RESULTS OF THE ANALYSIS

4.1	<u>Variability of spectral estimates</u>	110
4.2	<u>Pressure variations in the frequency range of 1-30 CPH and their effect on cosmic rays</u>	111
4.3	<u>Search for persistent frequencies</u>	111
4.4	<u>Comparison of cosmic ray frequencies with the frequencies found in the magnetic field measurements by Pioneer VI, range 1-30 CPH</u>			114
4.5	<u>Behaviour of cosmic ray frequencies in different interplanetary conditions</u>			116
	4.51 Condition of increase and decrease of cosmic ray intensity	116

4.52 Fast and slow changes in interplanetary conditions				118
4.53 Forbush decrease		120
4.6 <u>Behaviour of cosmic ray frequencies in different ΣKp epochs</u>		123
CHAPTER V. CONCLUSIONS		125
Appendix I	133
Appendix II	134
Appendix III	135
References	i - ix
List of tables	x
Reprint of paper published in Phy.Rev.Letters		

S U M M A R Y

The data relate to a counting rate of 10^6 counts per minute from 60 sq.meters of plastic scintillators under a Galena shielding of 3 M.W.E. at Chacaltaya. Geomagnetic cut off rigidity in the vertical is 13.2 Bv. The counting rate refers essentially to secondary mu-mesons. The counts integrated over successive one minute intervals are used for the analysis. Atmospheric pressure readings from a digital servo-barometer are simultaneously recorded at one minute interval. Data have been analysed for the period from November 1965 to June 1966.

The data are subjected to power spectrum analysis following the well known method given by Blackman and Tukey, having spectral window from 1 to 30 cycles per hour and an analysis period for successive 3 hours.

Fluctuations of the cosmic ray intensity are found to occur in the range of frequencies 6 to 30 cycles per hour. These fluctuations have average amplitude of about .04%. Taking the data as a whole, fluctuations occur most prominently at the frequencies of 16 and 27 cycles per hour corresponding to a period of 225 and 130 second. These have been established at the confidence limits of 99%.

For individual 3 hour periods the prominent peaks occur at one or more frequencies within the range and are not always at 16 or 27 cycles per hour. Moreover, there are some three hourly periods when all frequencies seem to be active, and the average power level in the entire spectrum is raised. There are then no peaks indicative of activity at particular frequencies.

Pioneer 6 measurements in the magnetosheath field at a distance of about 10 earth radii from the centre of the earth on the sunlight side gives a power spectrum with prominent peaks in the range of 6 to 30 cycles per hour (Ness et al 1966). At the same time at Chacaltaya, data show peaks which correspond in an approximate way, but not identically. Pioneer 6 results of the fluctuations of the interplanetary magnetic field over a 3 hour period show prominent peaks in the spectral range 6 to 30 cycles per hour (Ness et al 1966). These roughly correspond with the peaks simultaneously observed in the meson intensity but are not at identical frequencies.

High level of geomagnetic disturbance as characterised by Kp is associated with a low average power of the fluctuations in cosmic ray intensity in the 6 to 30 cycles per hour range. However, during this time prominent peaks appears at the frequencies of 9, 17 and 28 cycles per hour.

Low level of geomagnetic activity corresponding to small K_p is characterised by a high average power in the spectral range 6 to 30 cycles per hour and a prominent frequency only at 27 cycles per hour. When a major Forbush decrease occurs in cosmic rays, even though K_p is high at the time of onset, the average power in the cosmic ray fluctuations in the range of 6 to 30 cycles is always high.

The dependence on the geomagnetic activity of PC 4 micropulsations is similar to the dependence on geomagnetic activity of cosmic ray oscillations i.e. for high K_p the occurrence of PC 4 is less (Troilskaya and Gul'elmi 1967) and the average power of cosmic ray oscillations decreases. Study of velocity fields at the solar photosphere reveal that oscillatory motions with periods of 200 to 400 seconds are present (Howard 1967). The sun seems to be constantly active in this range of periodicities (De Jager 1965).

Thus, it is possible that the main driving force for the cosmic ray oscillations in the range of 6 to 30 GPH arises on the sun. When the magnetic field lines connecting the sun and the earth are relatively undisturbed with few magnetic-field irregularities, the solar excitation gets communicated from these fields without attenuation. But, when the magnetic field lines have irregularities, they provide a preferential passage for transmission of certain frequencies and not others. So,

the fluctuations of the energy density impinging on the magnetosphere could be the means through which the periodicities are generated in the geomagnetic field, thereby producing cosmic ray fluctuations by the change of geomagnetic cut-off rigidity.

CHAPTER I

INTRODUCTION

The turn of the present century saw the start of simple observations for the study of cosmic rays. The refinements in the experimental techniques, later on, greatly added to the reliability and authenticity of the measurements. It was soon realised that the studies of cosmic ray variations, interpreted on the basis of electrodynamics and plasma physics, have vast potentialities. The time variations are proving to be an extremely useful method for investigating the electromagnetic conditions of the interplanetary space. The studies of cosmic rays have also become an integral part of the adjacent disciplines of Nuclear Physics and Astrophysics.

1.1 Primary and secondary cosmic rays:

1.11 Primary Cosmic rays:

1.111 Nature of primary cosmic rays:

There is a continuous influx of energetic particles at the top of the earth's atmosphere. The energy and composition of these particles vary widely. There is evidence to indicate that galactic cosmic rays in interstellar space are largely isotropic and constant but as these rays traverse through interplanetary space they are modulated by solar activity.

To know the energy and composition of the primary cosmic rays, measurements have to be carried out at the top of the atmosphere, by using balloons and rockets. With ground based detectors secondary components are measured, and with the knowledge of certain parameters connecting the primary and secondary particles the characteristics of the primary cosmic rays can be derived. Their intensity is described in terms of the number of particles per meter⁻² sec.⁻¹ sterad⁻¹.

We neglect here solar cosmic rays since they are generally of energy below 1 GeV and do not normally relate to the intensity measured at sea level at the geomagnetic equator.

1.112 Energy Spectrum:

The incoming primary flux of particles is found to be a decreasing function of particle energy. The energy spectrum can be expressed by a power law,

$$N(E) = K E^{-\gamma}$$

where $N(E)$ is the number of incoming particles greater than E , K is a constant and γ is an exponent which is found to be energy dependent. For the determination of the energy spectrum shown in figure 1.1, different methods are used in different regions of energy.

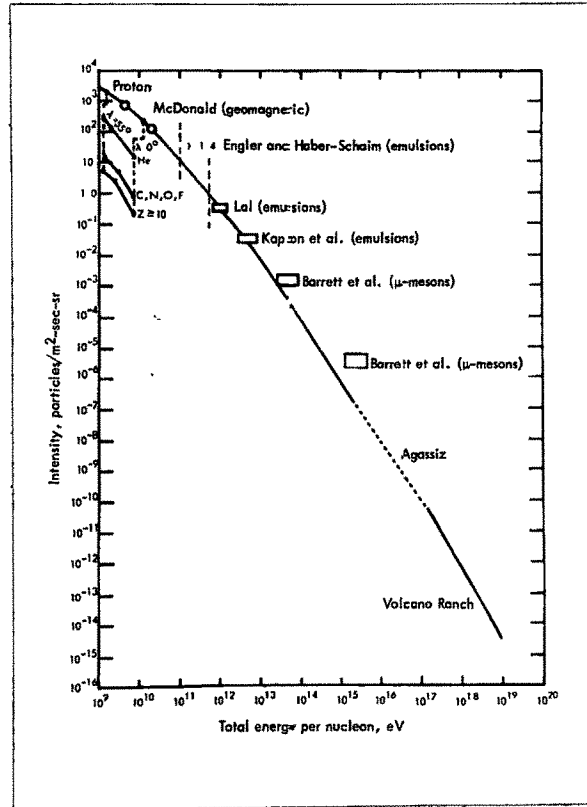


Fig. 1.1 Integral energy spectrum of galactic cosmic rays.

The latitude effect can determine the energy spectrum up to about 17 GeV. Nuclear emulsion techniques are used for higher energies in the range of 10^{12} to 10^{13} eV (Bethe 1933, Frier et al 1948, Kaplan et al 1952, Singer 1958). For very high energies extending towards the tail end of the energy spectrum, extensive air showers can give information regarding the spectrum (Rossi and Greisen 1941, Clark et al 1957 a).

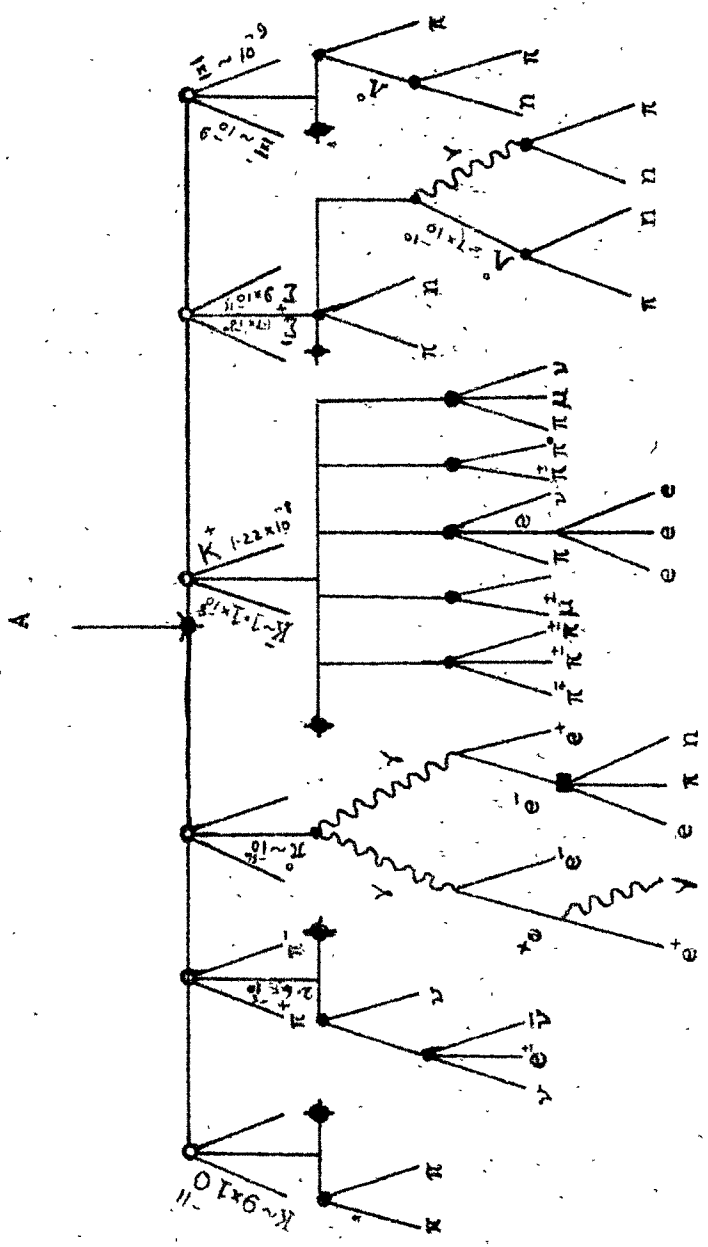
The values of the exponent γ in the integral energy spectrum in the different regions of energy, are given in the following table.

Table 1.1

γ	Energy range GeV	References
1.7 - 1.8	10 to 50	Charakhch'yan, A.N., and T.N. Charakhch'yan 1959.
1.53 ± 0.20	15 to 2×10^6	Barrett et al 1952
2.2 ± 0.1	10^7 to 2×10^8	Clark et al 1962
2.17 ± 0.1	5×10^6 to 10^9	Rossi 1960

1.12 Secondary components:

High energy primary particles in passing through the atmosphere collide with the air nuclei and the resulting nuclear interactions produce mesons (charged and neutral), nucleons, sometimes heavier fragments and strange particles. There are individual collisions between the incident particles and the air nuclei or the secondaries produced in such collisions and the air nuclei. For the cascades produced, considerations are given to the computation of the cumulative effect of the fundamental particle interactions over finite thickness of the matter, assuming the



* Star o Multiple □ Collision with • Decay
 Production a nucleus

A schematic diagram indicating the possible interactions of elementary particles

FROM "PARTICLES AND NUCLEI"
 BY R. H. COHEN, 1954

cross-sections for the individual processes. A general classification of the important particles encountered is given in the following table (from Muirhead 1965). The masses are given in the m_e units.

Table No. 1.2

Bosons	Fermions			
	Leptons		Baryons	
Photon	0	Neutrino ν	0	Nucleon $N \sim 1840$
Pion	$\pi \sim 270$	Electron e	1	$\Lambda \sim 2200$
Kaon	$K \sim 965$	Muon $\mu \sim 207$	Hyperons	$\Sigma \sim 2350$
				$\Xi \sim 2600$

The production of the secondaries is schematically shown in figure 1.2 (from Ramakrishnan 1962). A primary particle enters at A and collides with a nucleus of the air. The horizontal lines in the diagram represent the particles produced in a single collision and the decay products of a particle are shown by lines diverging from a point.

The charged mesons either decay into mu mesons or interact with air nuclei in a nucleon - nucleus collision. The neutral meson either interacts with the nucleus or with a high probability decays almost immediately into two

highly energetic gamma rays which generate soft cascades. The particles K mesons if they have high energies, interact with the nuclei producing the same type of particles as in a pion - nucleon collision at low energies. The hyperons at very high energies reproduce the nucleon collision phenomena while at low energies decay or interact with nuclei forming hyper-fragments which in turn decay into ordinary nuclei with or without emission of pions.

The mu mesons which are highly energetic and weakly interacting, mostly decay, but, since the decay time is comparable to the time for traversing the atmosphere, they comprise the major part of penetrating component at sea level.

A detector fixed at the surface of the earth records secondary component depending upon the sensitivity to the particular particles. To estimate the changes of the secondary component into primary component, it is necessary to know the counting rate yield of the detector for a primary incident particle. The specific yield function $Y(P, h)$ for a cosmic ray detector of a particular type located at a certain atmospheric pressure can be defined as:

$$J(P) Y(P, h) = \frac{\partial N(P, h)}{\partial P}$$

where $J(P)$ is the differential primary spectrum as a function of rigidity and $N(P, h)$ is the counting rate of

the detector that receives particles of threshold rigidity P . Only the vertical threshold values are used because most of the response of the detector is directed in the vertical direction. $\partial N/\partial P$ can be calculated from the latitude curve, and if the primary spectrum is known then the yield function $Y(P, h)$ can be found out. Webber and Quenby (1959) have derived a method by which the yield function can be split for different primary particles. At great depths in the atmosphere the yield function assumes small value due to the absorption of most of the secondary component. Differential response curves for meson component at different depths are shown in figure 1.3.

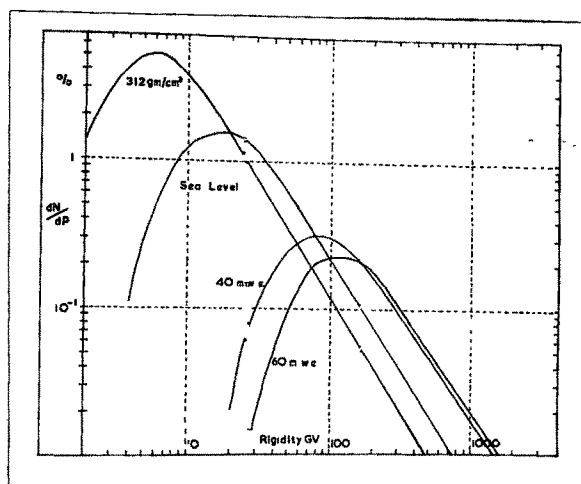


Fig.1.3 Differential response curves for meson detectors at different depths(after Mathews 1963).

For Chacaltaya situated at 545 gm/cm^2 of atmospheric depth and 13.2 Bv cut off rigidity, the value of $\partial n/\partial p$ (for mesons) is about $1.5/\text{par}$ BV. found by interpolating the differential response curve for sea level and for 312 gm/cm^2 (given by Mathews 1963), shown in figure 1.3.

1.13 Effects of pressure and temperature on secondary components:

1.131 General aspects:

The secondary components, produced by the nuclear interaction of the primary cosmic rays with the atmosphere and for the decay processes are affected by the conditions of the atmosphere. The counting rate of a detector varies inversely with the changes in atmospheric pressure. This can be expressed by an empirical relation of the cosmic ray intensity as a function of the atmospheric pressure. The principal components recorded at low level of the atmosphere are nucleons and mesons and as the formation mode in each case is different, the factors applied for their correction vary. The formula used for correction has the exponential form.

$$N = N_c \exp (\beta \Delta h)$$

where N_c is the corrected value, β is called the pressure coefficient and h is the pressure variation. In case β is small, it can be expanded in a simple form,

$$N = N_c (1 + \beta \Delta h)$$

For meson component, pressure coefficient is of the order of -0.1% per mb but for the nucleonic component, it is -0.7% per mb.

1.132 Corrections for Meson component:

For the meson component the meteorological effects are far more complicated than for the nucleonic component. This is because the mesons are unstable and the height of their production over the point of observation is also important. Thus the vertical distribution of the temperature in the atmosphere and of density become relevant. Duperier (1948, 1949) has demonstrated a positive temperature effect and has shown that it is connected with the mean level of production at the height of about 100 Millibar. Olbert (1953) in a more rigorous treatment takes into consideration the continuous production of mu mesons throughout the atmosphere, and also, that the mu mesons suffer from ionization losses. The conception of a production layer at a certain height is not completely justified because of the continuous production of mu mesons. To take into account the ionization losses, additional terms have to be added to the regression equation. Dorman (1957) has made detailed study of the atmospheric effects and the method of correction. It has been shown by him that the empirical method is not justified because of the few parameters used in their calculation (Dorman 1960).

Quenby and Thambyahpillai (1960) estimate the temperature effect by comparing meson and neutron diurnal variations observed at Huancayo during the 1953-1954 solar minima, and arrive at an average temperature effect of 0.11%. Deep River meson and neutron data relating to large counting rate monitors are used by Bercovitch (1966) to derive amplitude of the variation of meson intensity due to atmospheric temperature. He estimates an average amplitude of 0.046% and a time of maxima 5.6 hour local time. The temperature related variations in the neutron component (Kaminer et al 1965) are too small to make any noticeable contribution.

1.2 Cosmic rays in geomagnetic field:

1.21 Geomagnetic field and particle trajectories:

Stormer (1965), in connection with the understanding of auroral phenomena, calculated the trajectories of charged particles in the terrestrial magnetic field. The force F acting on a charged particle with charge e , moving with a velocity v in a magnetic field H is expressed by the well known relation.

$$F = |e| H \times V$$

Using numerical integration methods and dipole simulation for the geomagnetic field, Stormer found that certain directions are forbidden to the particles of certain energy i.e. at a certain point on earth particles of certain energy

cannot approach it from all directions and there are certain directions that are preferred than the others. The cone that forms the allowed directions is called the Stormer cone. Applying Liouville's theorem, it follows that the intensity of cosmic ray particles in any allowed direction will remain the same as it is at their starting point. So, if the distribution of cosmic rays is isotropic at infinity, it remains the same in all allowed directions for any given energy.

Even though a general dipole field suffices for most of the applications, for some cosmic ray phenomena it has been found that a higher degree of simulation of the geomagnetic field is required. The geomagnetic field could be expressed in terms of the spherical harmonic function. If V is the geomagnetic potential then:

$$V = \sum_{n=1}^{\infty} r_e \left(\frac{r_e}{r}\right)^{n+1} T_n$$

where r is the distance from the earth and r_e is the radius of the earth, and

$$T_n = \sum_{m=0}^n (g_n^m \cos m w + h_n^m \sin m w) P_n^m(\theta)$$

where g_n^m and h_n^m are gauss coefficients, θ is the geographic co-latitude, w geographic longitude and $P_n^m(\theta)$ are spherical harmonics.

Finch and Leaton (1957) and Jensen and Cain (1962) have calculated the constants up to sixth spherical harmonics.

1.22 Threshold rigidity:

The Stormer theory states that at a particular point on the Earth's surface it is impossible for certain direction to be accessible for particles from infinity below a certain rigidity. The minimum rigidity is

$$P = \frac{M}{r_e^2} \frac{\cos^4 \lambda}{(1 + (1 - \sin \theta \cos^3 \lambda))^2}$$

where M is the magnetic moment of the Earth's dipole field, r_e is radius of the earth, θ is the angle between the velocity vector of the particle and the meridian plane, and λ is the geomagnetic latitude.

If the particles are incident vertically, the minimum rigidity will be,

$$\begin{aligned} P &= \frac{M}{4 r_e^2} \cos^4 \lambda \\ &= 14.9 \cos^4 \lambda \text{ G.V.} \end{aligned}$$

Some of the trajectories of the particles intersect the earth elsewhere before arriving in the allowed direction. These penumbral trajectories contain loops representing turning away and turning towards the dipole. But at higher rigidities, the main cone threshold is reached and above

this value all trajectories come from infinity without loop and are not obstructed by the Earth (Lemaitre and Vallarate 1933, 1936, Swann 1933).

Calculations of rigidities carried out with a simple dipole field representation of the geomagnetic field showed discrepancies with the observed values (Johnson 1938). Surveys were carried out by two identical neutron monitors aboard a ship and the results confirmed the inadequacy of the rigidity calculations on the dipole model basis (Rose et al 1956). Further surveys were carried out during IGY aboard the ship 'Soya' and nucleon and meson components were measured during the voyage to and from Antarctic (Kodama and Miyazaki 1957). An airborne neutron monitor surveyed the equatorial region and it was possible to establish cosmic ray equator from 12 experimentally determined points (Katz et al 1958). A detailed survey has been carried out by 'Project Magnet' by putting a neutron monitor aboard an air craft (Pomerantz and Agarwal 1962).

Quenby and Webber (1959) introduced the non-dipole terms up to 6th degree for the rigidity calculation. They obtained a better fit with the experimental values of the cosmic ray equator. Kellogg (1960) has also computed the cosmic ray equator. Quenby and Wenk (1962) have formulated an empirical relation that takes into account the ideal dipole latitude and the true latitude where the same value

of the field exists. They have derived corrections that can be applied to give the true cut off rigidity at a given point.

A more rigorous method of computing the cut off rigidities is by deriving the orbits of the particles of different rigidities. McCracken (1962) has developed a widely used programme that takes into account the geomagnetic field upto sixth degree simulation. The directions are followed up to a distance of 25 earth radii, because beyond this distance the geomagnetic field has insignificant effect on the motion of a particle. Using this programme, calculations have been made of cut off rigidities for different stations (Shea et al 1965).

1.23 Asymptotic directions:

The Stormer's calculations give the trajectories of the particles arriving at the surface of the earth in the geomagnetic field. For the study of the spatial dependence of anisotropies in the flux of incident primary particles, it is necessary to know in detail the asymptotic directions far out in space i.e. the direction of propagation of the particle before it enters the geomagnetic field.

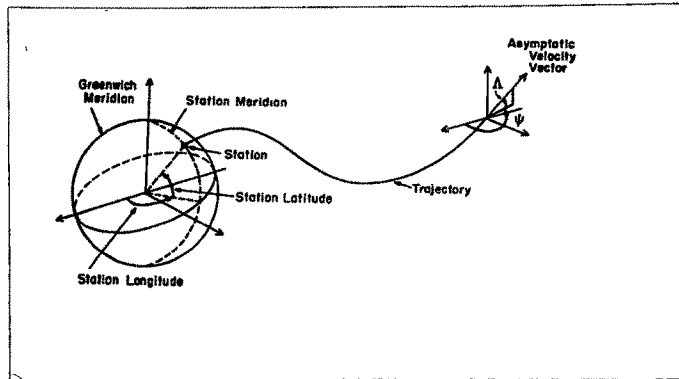


Fig.1.4 Asymptotic directions of approach of a particle trajectory.

As shown in the figure 1.4 the asymptotic direction can be described by two angles λ and ψ , where λ represents the asymptotic latitude and ψ is the asymptotic longitude of the particle with respect to the meridian passing through the observation point. Therefore, ψ is a measure of the bending in longitude (time) suffered by the cosmic ray particle while passing through the geomagnetic field.

In the initial stages asymptotic directions were determined by model experiments using a magnetised terrella for the earth, to which a beam of electrons was projected (Malmfors 1945, Brunberg 1953, and Bland 1962). Numerical integrations of trajectories have been performed by various authors for a dipole field (Firor 1954, Jory 1956, Lust 1957), and non-dipole terms up to sixth degree have been

included in the geomagnetic field representation by others (McCracken 1962, McCracken et al 1962, Shea et al 1965).

Asymptotic cone of acceptance is defined as a solid angle containing the asymptotic directions that make significant contribution to the counting rate of the detector. An important consequence of this idea is that it gives the particular directions in space sampled by the detector (McCracken 1962). Since each detector looks in a uniquely defined direction in space, different detectors fixed to the spinning earth scan the celestial sphere; they will record anisotropy in space at different times (Rao et al 1963, Webber 1963).

1.3 Cosmic ray intensity variations:

1.31 General aspects:

The general classification of the cosmic ray variations is very much dependent upon the nature of their origin. It is found that directly or indirectly the sun plays an important part in cosmic ray variations. The sun's role in this respect is two fold. Firstly, it modulates galactic cosmic rays by changing the conditions in the interplanetary space, and secondly, it injects at the time of solar flares cosmic ray particles in the low energy end of the differential energy spectrum. 11 year variation of galactic cosmic rays at the low energy end (Forbush 1957,

1958), the displacement of the knee of the latitude effect and 27 day recurrences due to solar rotation (Venkatesan 1958), are connected with the different aspects of solar activity.

The early studies of the daily variations were carried out by analysing if these were the residual atmospheric effects. Telescopes pointing towards north and south directions recorded cosmic ray particles that had traversed the same amount of atmosphere under similar conditions. Data were averaged out over long periods, to cancel any effects that might be present due to the inhomogeneous atmosphere. The time variations of the difference of the two directions showed diurnal variations that were much higher than the statistical inaccuracy of the recordings (Malmfors 1949, Elliot and Dolbear 1950, 1951). Extensive investigations have been carried out concerning diurnal variations especially after the availability of I.G.Y. data from world-wide network of cosmic ray recording stations. Excellent reviews on these topics have been given by various authors (Elliot 1952, Sarabhai and Nerurkar 1956, Singer 1958, Forbush 1966, Quenby 1967).

1.32 Spectral variation by Method of coupling coefficients:

The variations present in the measurements of cosmic ray particles at the ground based stations need to be

connected to the corresponding variations of the primary particles. Following Dorman (1963), consider the cosmic ray variations at a point with threshold rigidity P and at atmospheric pressure height h_0 . The observed intensity of cosmic rays can be expressed as,

$$N_p(h_0) = \int_P^{\infty} D(E) \cdot m(E, h_0) dE$$

where $D(E)$ is differential energy spectrum of the particles, and $m(E, h_0)$ is the integral multiplicity, which is the number of secondary particles at pressure depth h_0 formed from a single primary particle of energy E . In the most general case there can be changes in the threshold rigidity P , in the differential energy spectrum $D(E)$ and in the multiplicity $m(E, h_0)$.

So taking partial differentials:

$$\delta N_p(h_0) = -\delta P \cdot D(E) m(E, h_0) + \int_P^{\infty} D(E) \cdot \delta m(E, h_0) dE + \int_P^{\infty} \delta D(E) \cdot m(E, h_0) dE$$

and the relative change is,

$$\frac{\delta N_p(h_0)}{N_p(h_0)} = \delta P \cdot W(E, h_0) + \int_P^{\infty} \frac{\delta m(E, h_0)}{m(E, h_0)} W_p(E, h_0) dE + \int_P^{\infty} \frac{\delta D(E)}{D(E)} W(E, h_0) dE$$

where $W_p(E, h_0) = \frac{D(E) \cdot m(E, h_0)}{N_p(h_0)}$ is called the coupling

coefficient between the primary and secondary variations.

The relative variations are composed of three terms. The first one indicates the changes that occur due to the variation of the cut off rigidity. The second term contains changes in the multiplicity or at times called the yield function. These are associated with the changes occurring in the terrestrial atmosphere. The third term contains changes associated with the primary spectrum variation.

The coupling coefficient can be calculated in terms of the integral multiplicity factor. In the energies sensitive to the geomagnetic field, this can be calculated by taking into consideration the latitude effect for the different secondary components.

1.33 Variation of cut off rigidity:

Using a network of world wide stations Yoshida and Wada (1959) showed the association of cosmic ray variations with the geomagnetic field variations. Kondo et al (1960) have computed the expected variation in neutron intensity for different values of charges in the geomagnetic field. The graphs indicating the computed values are shown in figure 1.5.

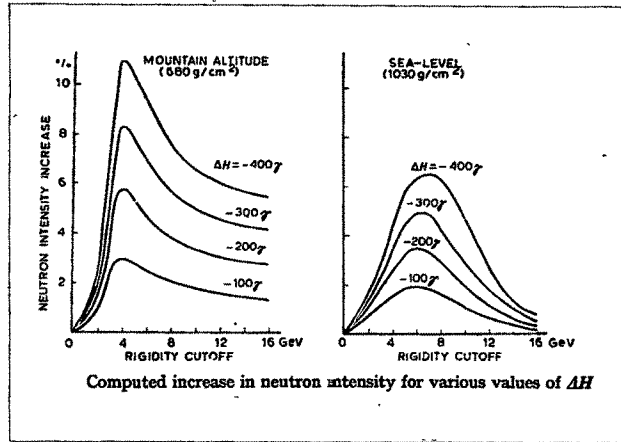


Fig.1.5

Rothwell (1959) showed that the most significant changes in the threshold occur at high latitudes and these should correspondingly affect the cosmic ray intensity. Taking into consideration the changes in the magnetic field and the changes in dimensions of the magnetospheric cavity, Obayashi (1959) has calculated the variation of the cut off rigidity shown in figure 1.6.

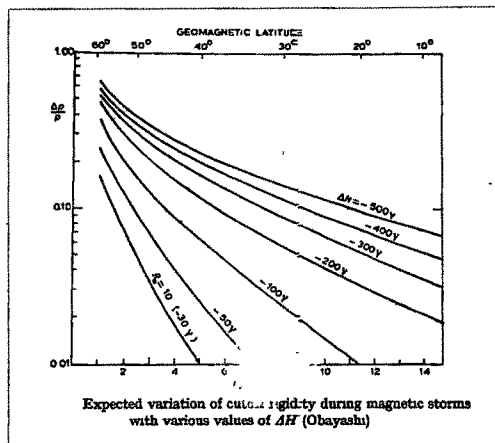


Fig.1.6.

Dorman et al (1961) have computed the expected changes of cosmic ray intensity for changes in the magnetic field. These graphs shown in figure 1.7 are very useful in interpreting the changes found in the cosmic ray intensity and their corresponding relation with the geomagnetic variations.

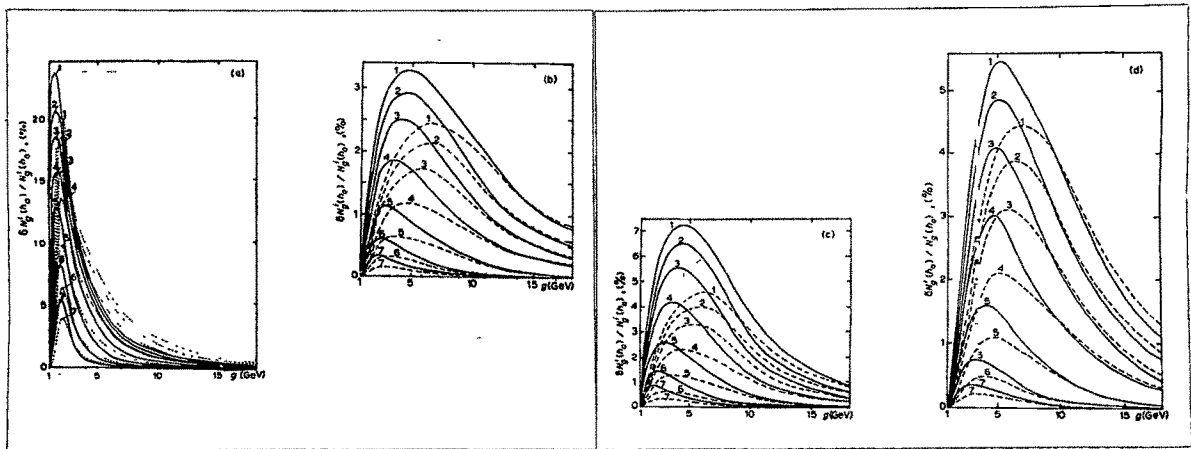


Fig.1.7 Curves 1.....7 for $H = 500, 400, 300, 200, 100, 50$ and 30γ ; a, b, for the ionizing component at stratosphere, and at 4.3 km altitude; c, d, for neutron measurements at mountain altitude (700 mb), and at sea level (from Dorman 1963).

For any cut off rigidity the counting rate N of a detector can be compared to the integral primary intensity. The differential counting rate between E and $E + dE$ will be $\frac{dN}{dE} \sim n(E) E^{-\gamma}$ where E is the cut off energy and $n(E)$ is the yield function and γ is the exponent, of the integral energy spectrum,

$$N \sim \int_E^{\infty} n(E) E^{-\gamma} dE$$

This equation gives the relation between the differential primary spectrum and the effective spectrum.

1.34 Energy Spectrum Variations:

The cosmic ray events found to be energy dependent can best be expressed by spectral variations. This is very useful method for studying anisotropies. In case, data from ground based detectors are used, coupling constants or specific yield functions play an important part in connecting variations of primary and secondary cosmic rays (Treiman 1952, Simpson et al 1953, Dorman 1963). Using data from world-wide network of recording stations, extensive studies in energy spectrum variations have been carried out by various authors (Rao and Sarabhai 1961, Rao et al 1963, Kane 1963, 1964).

In the latitude sensitive region of cosmic rays, direct measurements of the primary cosmic rays have been carried out by various authors. The measurements are mostly performed at the top of the atmosphere by balloon borne detectors, and lately satellites have been used for measurements in space. The latitude curves for either the ion chamber or the counter may be used for obtaining the primary spectrum. The spectra during sunspot minima and

maxima have been determined. Studies of various solar events have also been carried out (Winckler 1960, Balsubramanya and McDonald 1964, Fichtel et al 1964).

1.4 Conditions in Interplanetary space:

1.41 Solar wind:

Based on the observations that comet tails point away from the sun, Biermann (1957) concluded that the emission of corpuscular radiation from the sun is not a sporadic phenomenon occurring only during active periods but takes place even on quiet days when not much activity is observed on the surface of the sun. Starting from Chapman's (1957, 1959) idea that the thermal conductivity of the corona is very high and that the corona populated by the hot ionized Hydrogen, extends far into space, Parker (1958) suggested that the energy transfer takes place from the coronal base by hydrodynamic heating of the plasma, rather than by thermal conduction. The necessary consequences of the temperature distribution of the corona is an outward streaming of the plasma which Parker termed 'solar wind'. Even during quiet periods the solar wind is ejected with hypersonic velocities in the range of 300 to 400 km/second, which increases to about 1000 to 1500 km/second over active regions of the sun.

The behaviour of the plasma can be described by Boltzmann equations for the hydrodynamic motion of a fluid.

Even though the plasma is in a highly ionized condition, an overall condition of neutrality is maintained. Hence the solar wind can be defined as highly ionized neutral gas in which most of the kinetic energy is associated with the radial outward bulk motion (and not with the thermal or random motions). The kinetic energy is carried by the ions (Protons), because although, electrons have the same streaming velocity as the ions, they have much smaller masses.

Since the kinetic energy density of the solar wind is everywhere greater than the magnetic energy density except in the lower corona, the solar wind will be propagated radially outward. The magnetic field lines which are firmly anchored to the sun, however, will be stretched in the form of spirals called Archimedes spiral, due to the rotation of the sun. The streaming angle is defined as the angle between the field direction and the local radius vector, and can be computed from the plasma velocity and the solar angular velocity. For normal solar wind velocities of 300 km/second, the streaming angle at a distance of 1 A.U. is about 45° , as shown in figure 1.8.

It is obvious that the solar wind pressure gets attenuated at distances far away from the sun, where the pressure becomes comparable to the interstellar pressure. The wind velocity is reduced to subsonic values and the

random motion of the individual particle increases. The plasma cools down by mixing with the interstellar gas and ultimately forms a part of it. The distance to which the solar wind extends is estimated to be about 50 A.U. or may be more. It is expected that this distance increases with the increase in solar activity due to the enhanced solar wind velocity.

The characteristics of the solar wind are determined by its bulk velocity, particle density and temperature. Series of satellite experiments have been performed to measure the solar wind parameters. Bridge (1964) has summarised the results of the different plasma probes starting from Pioneer 1 to Explorer 18. The typical values observed by Mariner II are; solar wind velocity 360 to 700 km/second, particle density $0.3 - 10/\text{cm}^3$ and temperature 6×10^4 to 5×10^5 k. (Snyder and Neugebauer 1964). The observations have also revealed close correlation of solar wind velocity with k_p and its association with M-region storms (Snyder, Neugebauer and Rao 1963). The Mariner II plasma measurements demonstrate the existence of 27 day recurrent plasma events. The recurrent increases in plasma density are generally preceded by peaks in plasma velocity (Neugebauer and Snyder 1966). The close association of the recurrent high velocity plasma events in the recurrent M-type geomagnetic storms have also been.

established. The solar wind streams connected to the active regions that persist for many months, can create recurrent magnetic disturbance of M-type characterised by 27 days recurrent tendency (Mustel 1964).

In general, there are three modes of wave propagation in an ionized gas having frozen in magnetic field. The transverse Alfvén wave propagates along the field lines with a velocity $V_A = B / (4 \pi \rho)^{1/2}$ where B is the unperturbed magnetic field, ρ is the density of the ionized gas. The magneto-acoustic waves propagate in a direction transverse to the lines of force with a velocity $V_S = (\gamma P / \rho)^{1/2}$, where γ is the ratio of the specific heat at constant pressure to the specific heat at constant volume, P is the gas pressure. The phase velocity is given by $(V_A^2 + V_S^2)^{1/2}$. The solar wind having velocity of 300-600 km/second is considered to be supersonic with a mach no. of about 5.

1.42 Interplanetary magnetic field:

The sun has a general field of the order of a few gauss which is extended by the radially outward moving plasma (Parker 1963). The active regions of the sun can have magnetic fields as large as a few thousand gauss, consequently, the interplanetary field between the sun and the earth will be different during active periods. During quiet periods, as already explained, the angular rotation of the sun causes the field lines to be stretched in the form of spirals.

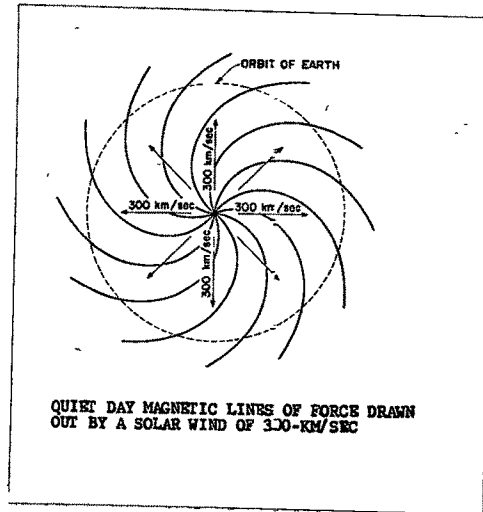


Fig.1.8

Figure 1.8 gives the sketch of field lines and the radially moving outward plasma. This has been verified by direct measurements of the field and plasma with instruments aboard space crafts of IMP and Pioneer series.

During periods of high solar activity when the velocity of the solar wind is very high, the field configuration in the interplanetary space changes considerably. Different models have been proposed for understanding the field configuration during these periods.

Gold (1959) proposed that the sunspots and other solar disturbances form the origin of the field lines that constitute a kind of a magnetic bottle. The intense magnetic field in the bottle will prevent the low energy galactic cosmic rays from entering inside it, thus causing

an intensity depression within the bottle. Recent evidence, however, does not favour this model.

Parker (1961), on the other hand, considers the imposition of blast wave in order to explain the condition of field during disturbed days. Since the magnetic lines of force move with the medium, a spherical symmetric blast wave moving radially will not affect the radial component but will compress the azimuthal component, producing a kink in the magnetic field. So, the quiet day interplanetary field is sheared by the blast wave generated due to solar activity producing a kink. The direction of the field lines in the kink is shown in figure 1.9.

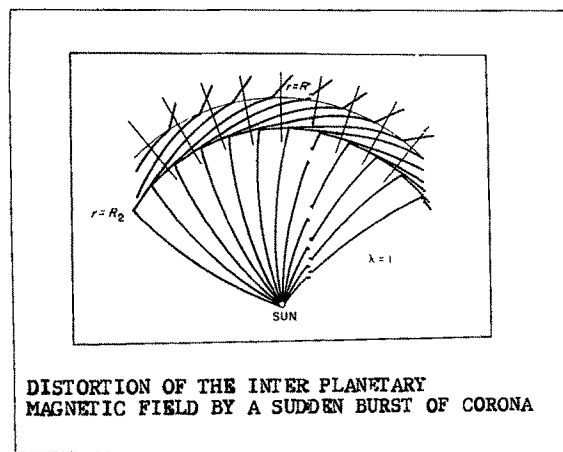


Fig.1.9.

Based on the background of Parker's theory, Sarabhai (1963) has pointed out interesting consequences that arise when slow plasma from solar region A follows fast plasma

from solar region B. The resulting conditions in interplanetary space are shown in figure 1.10.

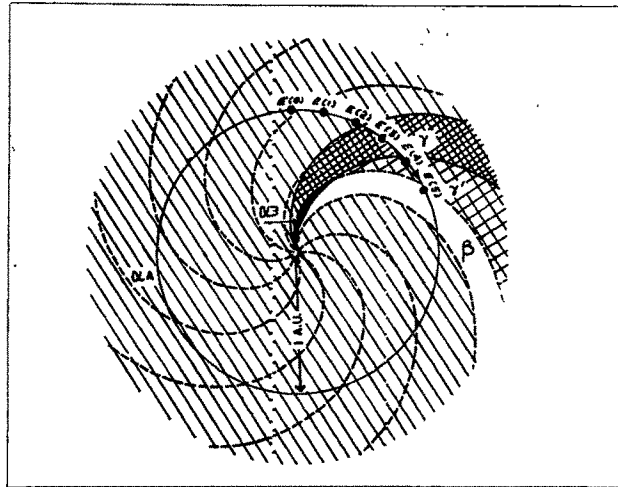


Fig.1.10 Region (α_A α_B β) Cavity and γ (turbulent) formed in interplanetary space along the solar equatorial plane by the interaction of slow and fast moving plasma (after Sarabhai 1963).

The interface generates a cavity almost free from plasma and bounded by intense magnetic field. This results in forming a scattering centre for low energy cosmic rays. If it continues to persist longer, then it can be responsible for 27 - day recurrent Forbush decreases and other geomagnetic effects.

Solar modulation of galactic cosmic rays can be described to be the result of the inward diffusion of cosmic rays through magnetic field irregularities carried outward

from the sun by solar wind (Mayer and Simpson 1957, Parker 1958a). The diffusion coefficient describing the motion of cosmic rays in the interplanetary space was discussed mostly on the concept of magnetic scattering centers and the basis of treatment, in general, was phenomenological. Jokipii (1966, 1967), for describing the motion of cosmic rays in the interplanetary field, determines diffusion coefficient from the power spectra of magnetic irregularities observed on space crafts. Using some of the reported spectra (Coleman 1966, and Siscoe et al 1967), he finds the diffusion coefficient to be proportional to $R \beta$, where R is the particle magnetic rigidity and β is particle velocity. The relation seems to be valid for particles of kinetic energy of 10 MeV/nucleon to about a few GeV/nucleon. Thus, the motion of cosmic rays in the interplanetary space may be quantitatively related to the observed magnetic field.

1.43 Sector structure:

The interplanetary magnetic field measurements by a clean IMP I satellite have clearly indicated that the intensity of the interplanetary magnetic field is in general about 5 gammas and is along the garden hose direction (Ness and Wilcox 1964), as predicted by Parker (1958), although, it varies considerably in direction and magnitude at times. Further, Wilcox and Ness (1965) find that the interplanetary field is divided in the form of sectors, the field in

alternate sectors being oppositely directed to each other, either predominantly away or towards the sun. The sectorial passage was observed for number of solar rotations. The field directions near the earth in each sector were well correlated with the directions of the average solar photospheric magnetic field within 15° of the solar equator, with solar wind velocity of 385 km/second carrying the frozen field with in it.

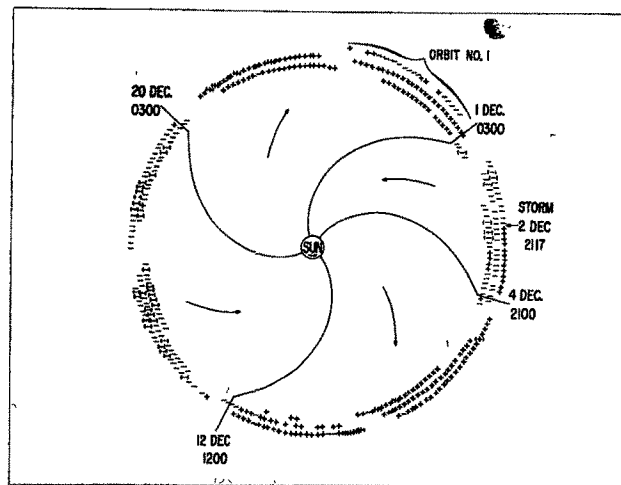


Fig.1.11 Interplanetary magnetic field sector structure (after Wilcox and Ness 1965)

The gross pattern of the field found by Wilcox and Ness is shown in figure 1.11. It is seen that the inter-

planetary space is divided during this period into four sectors, three of which occupied $2/7$ of the longitudinal width and one $1/7$ of the width. This sector structure corotates with the sun and so, sweeps past the earth every 27 days.

The sector boundaries are characterised by a sudden change of direction of the magnetic field. There seems to be a tendency for the proton density and solar wind velocity to change at the boundaries of the sector structure (Lyon et al 1964). The sector structures seem to persist over successive solar rotations. Field measurements aboard IMP II and Mariner IV have provided further evidence of the existence of corotating sector structures (Fairfield and Ness 1967).

1.5 Interaction of solar wind with geomagnetic field:

1.51 Magnetosheath and magnetospheric cavity:

The formation of the geomagnetic cavity due to the impinging of solar corpuscular particles was first discussed by Chapman and Ferraro (1931). The outward streaming plasma will sweep any external field ahead of it in order to prevent any change of field within itself. This is accomplished by surface currents at the magnetopause which cancel the field due to external currents at all interior points. It is this property of the plasma which causes the geomagnetic field to be compressed and confined

within a cavity by the solar wind. In other words, the plasma stream interacting with the geomagnetic field can penetrate upto a distance where the kinetic pressure of the solar wind is balanced by the geomagnetic pressure given by,

$$\frac{H^2}{8\pi} = n m v^2$$

where n is the particle density and m is the proton mass. The total magnetic field H at the surface of the stream, which is twice the original geomagnetic field at that point (Obayashi 1959) is given by,

$$H = \frac{2H_0}{R^3} \quad \text{where } H_0 = 0.3 \text{ T}$$

By substituting the appropriate values in the above equations it can be shown that the magnetopause is at a distance of approximately 10 earth radii in the sunlit side. In the antisolar direction where the forward motion of the plasma is not able to exert any influence, the tail of the magnetosphere is stretched in the form of a tear drop. The streaming plasma is not able to close the tail because it does not exert transverse pressure. The boundary will assume the shape where the external pressure exerted by the plasma and the interplanetary magnetic field balances the internal pressure due to the interior magnetic field, the plasma contained in the tail and hydrodynamical waves propagating inside the tail. A magnetically neutral region called the neutral sheet has also been identified. Its formation

can be explained on the basis of the outgoing and incoming lines of force. There are indications that the length of the tail extends beyond the orbit of the moon.

Magnetometer and plasma probe data from satellites have been used to map the form of the geomagnetic cavity and the extent of the turbulent region (Bonetti et al 1963, Happner et al 1963). Extensive mapping of the magnetosphere boundary was carried out by Cahill and Amazeen (1963), with a magnetometer aboard Explorer 12 satellite. They found abrupt changes in the magnetic field directions at a distance of about 10 earth radii on the sunlit side, implying that the magnetic field was in a turbulent state at that point. This marked the boundary of the magnetosphere. It was observed that during storm conditions the boundary moved closer to the earth. This could be explained on the basis of the increased kinetic pressure of solar wind (Cahill and Bailey 1965).

Detailed magnetometer measurements using IMP satellites have been performed from the sub-solar point to the night-time extending far into the tail (Ness et al 1964, Ness 1965). The shape of the cavity derived from these measurements is shown in figure 1.12.

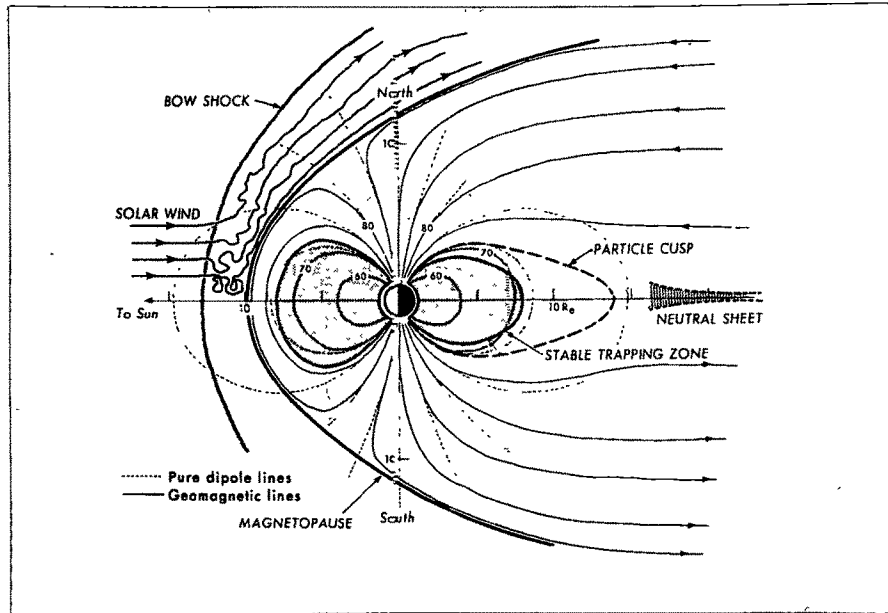


Fig.1.12 Projection of the magnetic field topology on noon-midnight meridian plane (after Ness 1965).

As indicated in the diagram, the magnetopause is at a distance of about 10 earth radii towards the sunlit side. The extent of magnetosheath is from a geocentric distance of about 10 to 15 earth radii bounded by a bow shock. The extent of the magnetosheath is dependent upon the hydrodynamical pressure exerted by solar wind. Beyond that the interplanetary field becomes very ordered and the average direction is confined to the general Archimedes spiral. In the tail side there is a neutral sheet. From

the study of the simultaneous records of magnetic fields and energetic particles, Anderson and Ness (1966), for most of the orbits of IMP I on the dark side of the earth, found depressions in the magnetic field in the particle cusp region.

1.52 Bow Shock:

The particles of solar wind have no transverse component of bulk velocity, and the coulomb interactions between the particles are extremely rare as the mean free path is of the order of 1 A.U. The magnetic field forms an obstruction to the solar wind flow.

The obstacle offered by the geomagnetic field to the supersonic solar wind will make it to go around the magnetic field and thermalize in the tail side. By analogy to the hydrodynamic flow around an obstacle a bow shock will be formed towards the sunlit side.

The hydrodynamic waves crossing the boundary of the magnetosphere transfer energy and momentum. The geomagnetic phenomena are evidence of such a dissipative interaction, which implies the existence of transverse stresses at the magnetosphere boundary. These stresses can have profound influence on the shape of the magnetosphere (Axford 1964). Inflations and distortions of the magnetosphere have been observed by Explorer 12 and 26 (Cahill and Bailey 1965, Cahill and Patel 1967).

1.53 Theoretical models of the magnetosphere:

Starting from an initial assumption of a uniform magnetic field bounded by a plane current sheet, iterative and self consistent methods of successive approximation up to fourth degree are used to compute the shape of the geomagnetic field boundary in solar wind (Midgley and Davis 1963, and Mead and Beard 1964).

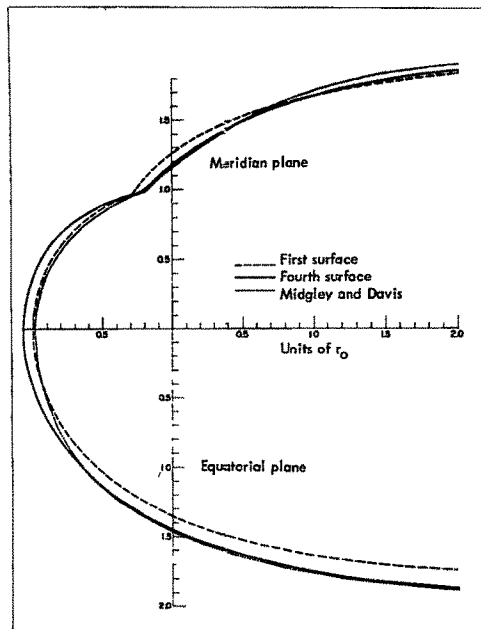


Fig. 1.13 Computed shape of the magnetosphere boundary (after Mead and Beard 1964).

Figure 1.13 shows the boundary surface in two planes cut through the dipole. The curve above the horizontal axis is the solution in the meridian plane and the curve

below is in the equatorial plane of the dipole. The solar wind is incident from the left side and the distance is measured in units of r_0 , the distance to the boundary along the Earth-Sun line in the first approximation surface.

At the points within the magnetosphere resultant field due to geomagnetic field and the component due to surface currents has been computed by Mead (1964).

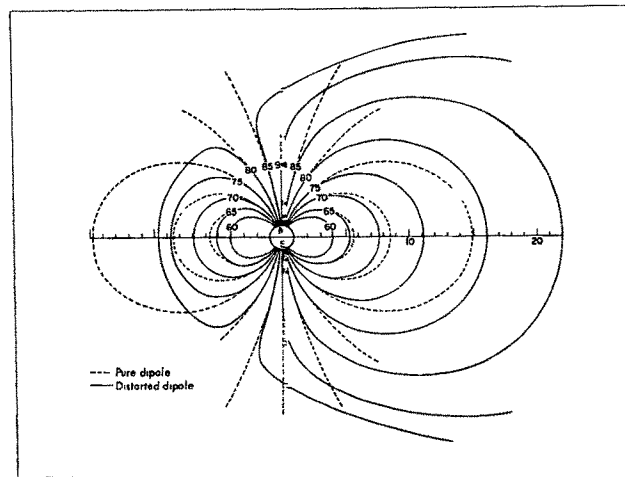


Fig. 1.14 Computed field line configuration on noon-midnight meridian plane (after Mead 1964).

The comparison of the resultant field and the dipole field is shown in figure 1.14. The field is compressed on both the day and the night side of the Earth. At a distance of 10 Earth radii along the Earth-Sun line there exists a critical latitude of 83° above which the field lines originating on the day side of the Earth are thrown

back to the night side, thereby creating a neutral surface. An interesting application of Mead's spherical harmonic representation of the cavity field to the cosmic ray threshold rigidity shows that an increase in the rigidity value occurs due to the presence of the cavity (Makino and Kondo 1965).

1.6 Geomagnetic Micropulsations:

1.62 Characteristics of geomagnetic micropulsations:

The geomagnetic micropulsations of regular type in the range of 0.5 to 600 seconds periods are subdivided in five groups designated as Pc 1 to Pc 5 (Jacobs et al 1964). The pulsations of short periods, Pc 1 and Pc 2 are, in general, connected with auroral phenomena. But, towards the larger periods these assume hydrodynamical character and show certain asymmetries and polarization. Amplitude of Pc 5 is latitude dependent and shows polarization of the perturbed vector (Kato 1965 a).

Large fluctuations in the range of 2 to 10 minutes periods have been observed at polar stations, having morning and afternoon maxima (O1' 1963). Using micropulsation data from three stations around the geomagnetic equator, Mason (1963 a) has not found any consistent frequencies in the range of 1-6 cycles per hour. The intercomparison of the spectral densities for the simultaneous data of these stations does not indicate any consistency of peaks, although individually several frequencies are prominent.

With the magnetic data from New Jersey, Davidson (1964) has made some studies aimed at investigating the source and propagation mechanism of the micropulsations by means of the variability of their power spectral densities. In the range of 4.5 to 1000 seconds periods, it is demonstrated by him that much of the variability of the fine structure of the spectrum disappears as sufficiently large quantity of data are averaged, but certain characters assume stability. Hence, in the range of 1 to 6 cycle per hour no prominent peaks are present over long periods of time, although, there are indications of their periodic behaviour at about 40 minutes period during magnetic storm conditions (Pai and Sarabhai 1964).

Studies aimed at the theoretical calculation of the amplitude and the polarization characteristics of the micropulsations have been carried out by Prince et al(1964), Field (1966) and others.

1.62 Amplitude and frequency dependence on latitude:

It has been observed that amplitude of Pc 5 is latitude dependent. The activity is found to be larger at higher latitudes than at lower ones. A single event, in general, shows an increase of amplitude with latitude, although, not all the events behave in the same way (Duffus et al 1954, Mason 1963 b).

The latitude dependence of the frequency of the micropulsations can be explained on the basis of the increase of the length of lines of force along which the hydrodynamic waves are propagated. The relationship is formulated by an analogy of an elastic string to the lines of force connecting two conjugate points having geomagnetic latitude θ_+ and θ_- (Obayashi 1958). The period T can be expressed as,

$$T = \int_{\theta_-}^{\theta_+} \frac{\delta l}{V_a}$$

where δl is the element of the line of force, V_a is the Alfvén velocity and is equal to $H/\sqrt{4\pi\rho}$, H being the magnetic field strength and $\rho = m_p n_p$, m_p is the particle mass and n_p , the plasma concentration. Assuming Parker's distribution of charged particles in the magnetic field (Parker 1957), and the relationship $H^2/8\pi \sim n_p m_p V^2/2$ at the magnetospheric boundary, we get, $T \propto \cos^{-2} \theta$, which shows the period to be dependent on θ , the latitude.

1.63 Hydrodynamical nature of Pc 5:

The velocity and density gradients of solar wind produce time and space fluctuations in the field of the magnetosheath. These fluctuations produce stresses at the boundary of the magnetospheric cavity and transmit hydrodynamic waves towards the Earth. It has been observed that fluctuations in the interplanetary magnetic field are

capable of producing geomagnetic micropulsations (Kato 1965b). The waves are reflected at a certain geocentric distance that corresponds to their period and their energy is transmitted along the lines of force. The asymmetric radial stresses are capable of producing polarization effects in the fluctuations. These effects have been observed for Pc 5 pulsations.

1.64 Telluric currents:

The measurements of the earth currents can also give good indication of the geomagnetic activity. Some of the interference problems common with magnetic measurements are reduced, and so the recordings have more reliability (Hessler and Wescott 1959). Hence the earth currents data can as well be used for micropulsation studies.

CHAPTER II

EXPERIMENTAL SET UP

2.1 General Remarks:

Operation of a large area of detectors presents diverse problems; the very high counting rate demands fast circuits, but to be free from intermodulation. The problem of insuring stability assumes greater proportions and the grounding arrangements become critical. Since the detectors are spread over a large area, they become much more susceptible to noise. As the scintillators formed the part of the Air Shower Experiment (BASJE), their performance requirements were not so rigid and had a sensitivity over the area uniform to within $\pm 5\%$ (Suga et al 1962). With the help of the BASJE group and using a Multi-channel Pulse Height Analyser, the author carried out detailed checks of differential spectrum of the output pulses from each of the phototubes. It was found necessary to carry out certain modifications which resulted in bringing down the level of noise.

Time variation experiments require very stringent standards of accuracy and stability. So, not only the individual module should be geared to that standard, but also the complete unit should be in the optimum operational condition. Any lapse on these counts can result in producing not very meaningful data.

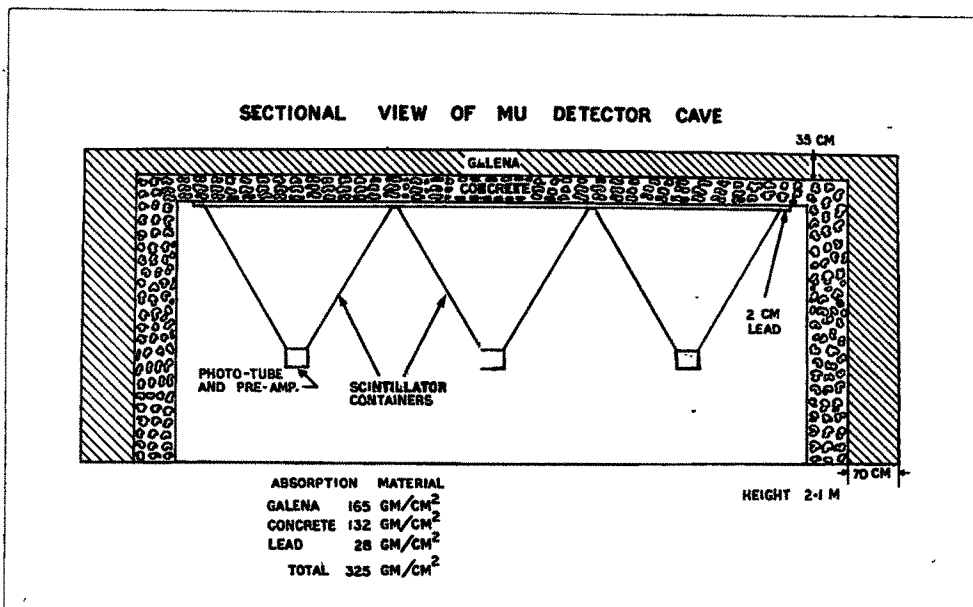


FIG. 2.1

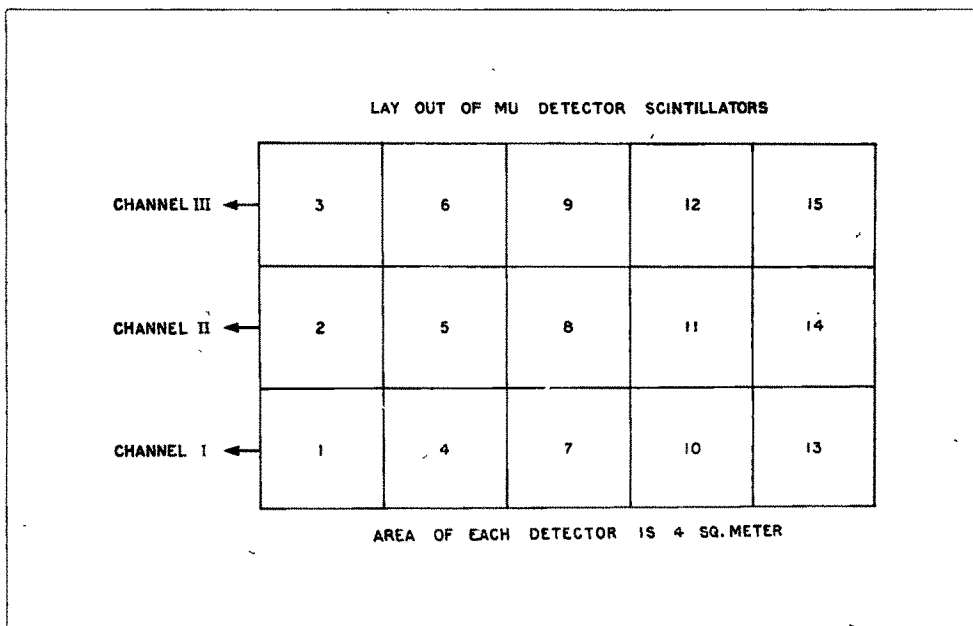


FIG. 2.2

2.2 Operation:

Fifteen scintillators occupying an area of 60 Sq. meter are housed in a cave, with about 3 M.W.E. absorber over it.

The sectional view of the cave is shown in figure 2.1 indicating the absorption material around the detecting system. Each scintillator has 4 square meter area and is fixed at the top inside of a container that acts as a light coupler to a photo-tube fitted at its apex with a preamplifier just below it.

Three rows each of five scintillators form the geometry of the detector. The lay out is shown in figure 2.2, indicating also the recording channel in which each scintillator's counts are accumulated.

Following the block diagram shown in figure 2.3, we find that after discrimination, the pulses are mixed into three independent channels each containing pulses from 5 detectors. The output pulses are then fed to the decades where these keep accumulating until the start of a punching cycle. An electronic clock sends an initiating pulse to an integrator and this results in initiating from the Integrator a read pulse to the decades and the information is transferred to the temporary storage. Another pulse resets the decades that start counting again for the next punching cycle.

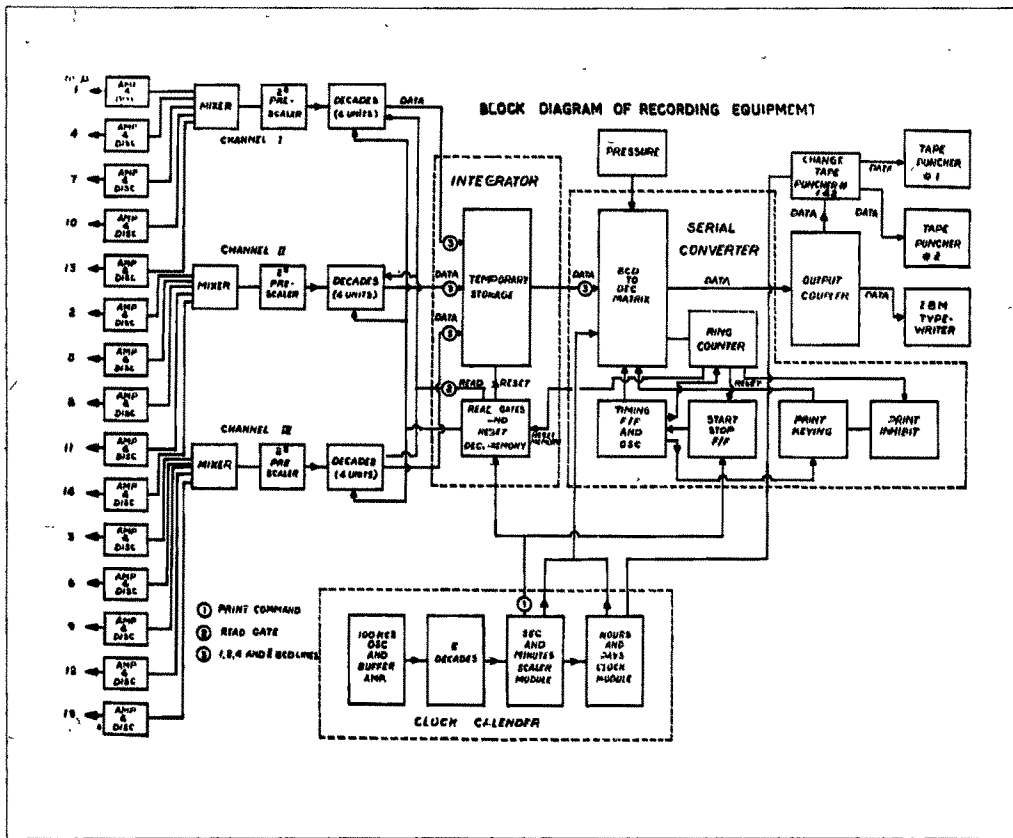


FIG. 2-3

A simultaneous clock pulse actuates a start stop F/F (flip-flop) in a serial converter. This unlocks a ring counter that starts advancing step by step. At each step, information in BCD code is converted in DEC code by a Matrix, after which through a coupler it is punched out on 5 track paper tape and also printed by an IBM typewriter. This process continues until all the BCD information has been scanned. When calendar and pressure are also to be included, a relay switches in more stages of the ring counter and this results in the BCD information of the calendar and the pressure, getting scanned and punched out. Print inhibit circuits lock the Matrix when a functional code is being punched. At the end of the punching cycle the last pulse from the ring counter resets the start stop F/F and also the temporary storage stage. There is an arrangement for automatically changing the tape puncher by using a 24-hour pulse from the clock.

The clock can be adjusted to generate initiating pulses that will start a punching cycle of 1 sec, 12 sec, 1 mt. and 4 mts. In the serial converter the punch speed can be adjusted so that the punching operation is over before the new cycle starts.

2.3 Detectors and associated electronics:

2.31 Scintillators:

The Scintillators used in the present investigation

have been prepared at M.I.T (Clark et al 1957 b), using methods developed by Buck and Swank (1953) and Fischer (1955). The photo-tube is placed at a certain distance from the scintillator; so, it is necessary to have optical coupling of the photo-tube to the scintillator by using proper light pipes (Akimov 1965). The problem is to be considered in terms of the multiple reflection of the fluorescent light inside the detector and its gradual absorption by the walls and the scintillator. White paint is used for the inside surface so as to increase its reflectivity. To improve uniformity of response over the sensitive area, the photo-tube is to be placed in such a position so that the optical path length to various parts of the scintillator is as nearly equal as possible. Detailed tests have been described by Clark et al (1957 b). Sixteen scintillation slabs that form the 4 Sq. meter area of the detector are so constructed as to have a depression in the middle, so that the optical distance to the photo-tube fitted at the apex of the conical box is nearly equal. The sensitivity of the scintillator is uniform over the area to within $\pm 5\%$ (Suga et al 1962).

2.32 Photo-tube:

The photo-tube, Du Mont K 1328 used in the experiment has 14" photo-cathode size, average cathode efficiency 45 μ A/lumen, and cathode dark current at 22°C, 100×10^{-15} A.

It is very desirable that the photo sensitivity of the cathode area should be homogeneous and the transit time of the electrons in the tube is small. The noise should be as small as possible.

The calibration of the tube is carried out by using illumination by short light pulses of 2-3 nano-sec. For determination of dark current, a pulse height analyser is used after putting the photo-tube in a light tight box. These checks are described later in the chapter.

2.33 High voltage connection to the photo-tube:

Figure 2.4 shows the H.V. connections to the photo-tube; and the pre-amplifier circuit.

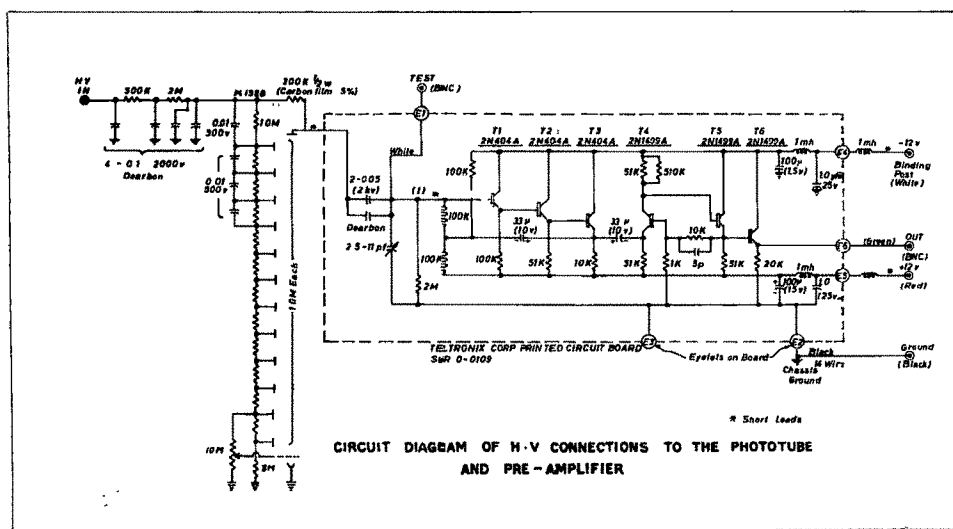


Fig.2.4

The dynodes are connected to a common voltage divider leading from a high voltage regulated power supply. A

filter network is used so that the ripple component is reduced, and the photo-tubes are decoupled. To decrease intermodulation it is essential that the AC return circuits of each of the photo-tube should be separate. By proper voltage distribution arrangement, each dynode is successively kept at a higher relative potential than the previous. The voltage difference at the first dynode is larger compared to the others so that the electrons emitted from the photo-cathode undergo larger acceleration. The later dynodes need a bypass capacitor because the secondary current gets larger, and can fluctuate the potential at the dynode.

2.34 H.V. Power Supply:

Figure 2.5 shows the circuit diagram of the H.V. supply that gives the required voltages to the anode and dynodes of the photo-tubes.

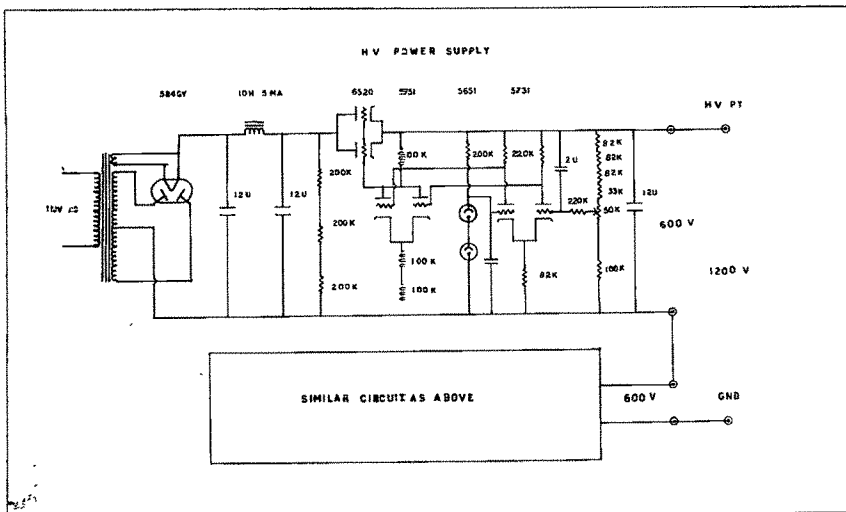


Fig.2.5

It is composed of two independent power supplies giving regulated output of about 600V each. The outputs are connected in series so that the common point of the upper power supply is at a floating potential. This requires the return circuit of that supply to be insulated. The arrangement minimises insulation problems because the voltage for a single unit is not large. The stabilizing circuits are conventional ones; using reference voltage from a gas tube and a series tube for regulation. A bleeder network is connected across the H.V. output so that suitable voltages can be used according to the individual characteristics of the photo-tube.

2.4 Amplifiers:

2.41 Pre-amplifier:

The circuit diagram is shown in Fig.2.4. It takes the output of the photo-tube and feeds it further to the main amplifier. The following are the criteria of operation of a pre-amplifier:

- (1) Matched impedance with the photo-tube,
- (2) Low noise level,
- (3) Stable operation,
- (4) Proper decoupling arrangement,
- (5) Small leads to reduce stray capacitances.

The output impedance of a photo-tube is very high.

To match this, a cascade of successive emitter followers is built using three 2N404A transistors, so that the input of one is looking into the output of the other. The input impedance offered by T1 is large where the output impedance of T3 is small, so that it can be matched properly with the amplifier stage having a gain of 10. The input and output of this amplifier are both emitter coupled. The feedback is large, so the operation of the amplifier is stable and the amplification factor depends upon the ratio of the feedback loop (Suga et al 1961). The voltage supply is $\pm 12V$.

A printed circuit board of the above circuit arrangement is mounted just beneath the photo-tube and very short leads are used from the input of the amplifier to the anode of the photo-tube.

2.42 Main amplifier:

The output of the pre-amplifier is connected to a 93 ohm termination line through a coaxial cable of the same impedance. The arrangement is shown in Fig.2.6.

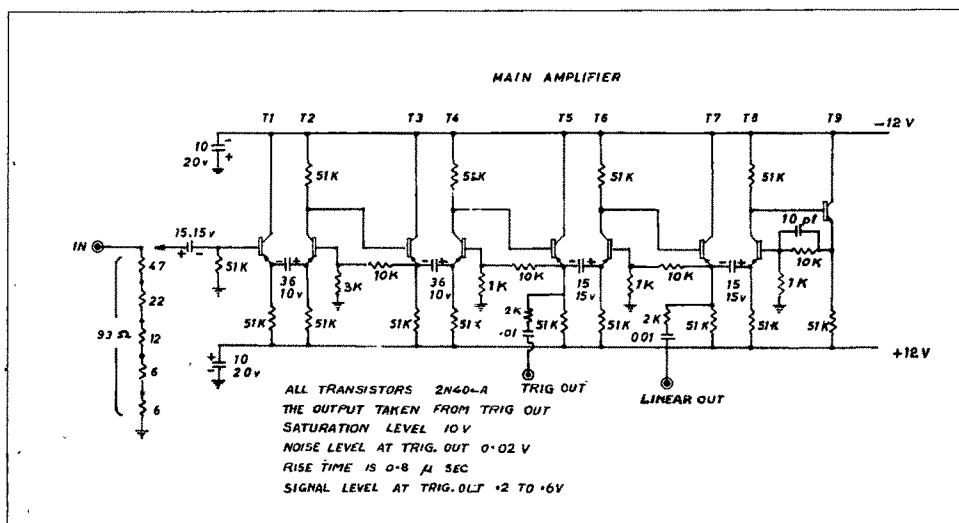


FIG. 2-6

Two amplifier loops having a total gain of 30 are used upto the stage of 'trigger out', of the BASJE. The general signal level at the 'trigger out' is 0.2 to 0.6 volts, with the noise level of about 0.1 to 0.2 V. The output has been taken at 'trigger out' and not from linear out because the BASJE circuits associated at 'linear out' tend to lower the pulse height, at particular intervals, which introduces pulse height variations that can be harmful to continuous recording.

2.43 Discriminator, pulse shaper, mixer and driver:

As shown in fig.2.7, the circuits are designed to amplify the pulses to a level that is suitable for discrimination after which there are fed to a pulse shaping circuit.

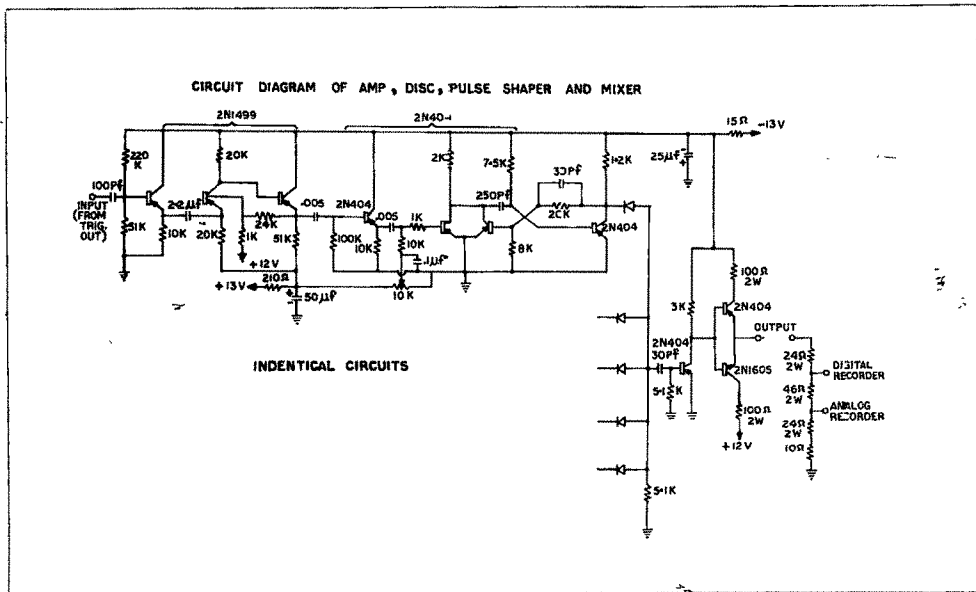


Fig.2.7

The outputs of 5 shaping circuits are then mixed and a driving circuit is used to transfer the resulting output to a pre-scaler.

It is necessary to amplify pulses taken from 'trigger out' so that the integral curve of the pulse height versus counts has a flat portion over a sufficiently large range. If the amplification is too small, the range will be too compressed and a slight fluctuation in the discriminator voltage will result in a large change in the counting rate. But, if the amplification is too large, it will saturate the noise pulses and discrimination process will become difficult and unreliable.

After an emitter follower, an amplifier stage is put with a gain of 24 so that the range of the flat part of the integral spectrum is from 2 to 4 volts. Saturation of the pulses occurs at about 10V. The differential spectrum typical of the 15 stages is shown separately in another section and will be discussed in detail there. Pulse height analysis is carried out at the pre-amplifier, main amplifier and input to the discriminator. This is helpful not only in finding out the point where the discriminator level can be fixed, but also to keep track of the stability and general behaviour of the circuits.

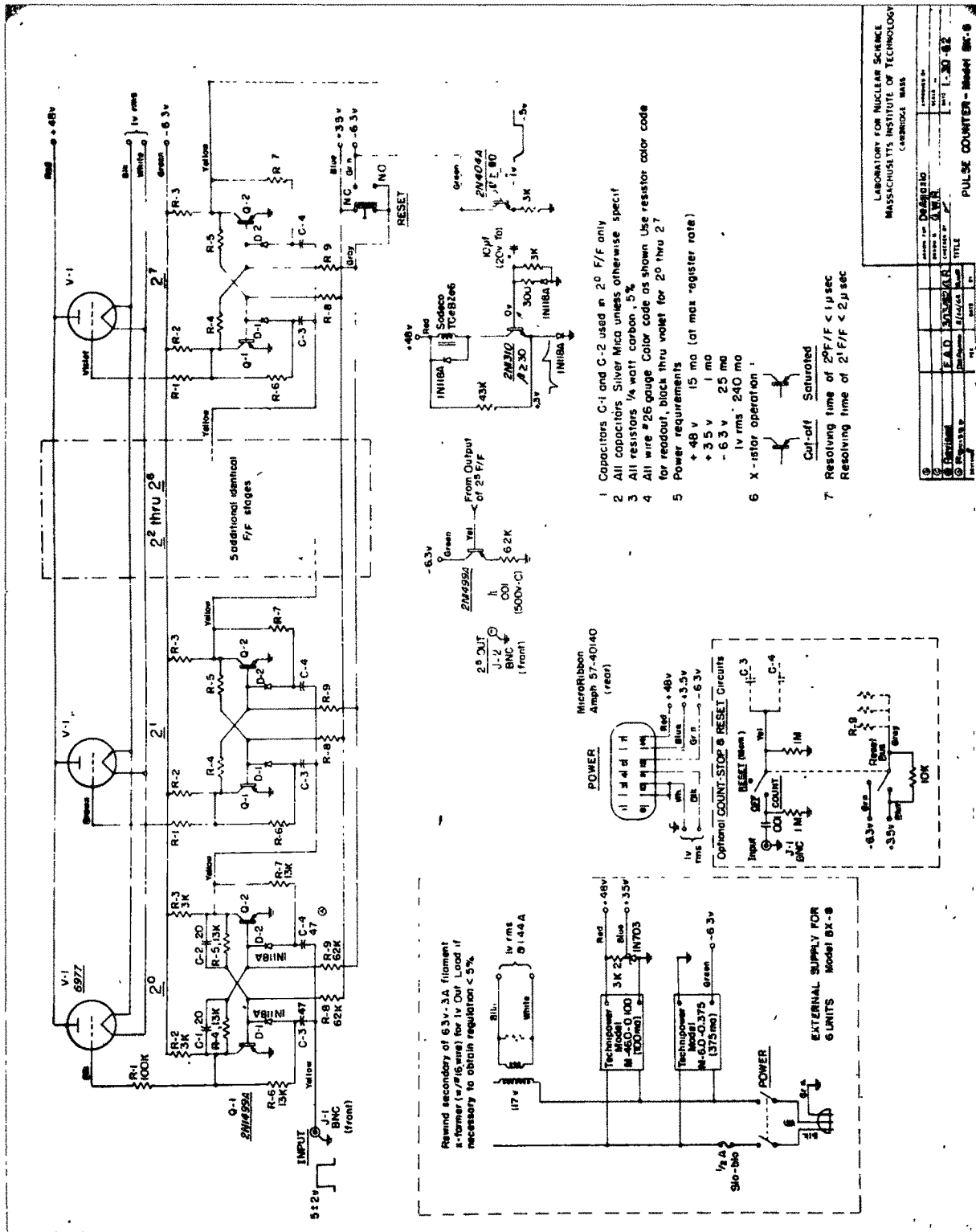
The discriminator circuit is designed in such a way that it is combined with the pulse shaper circuit. Two

transistors are connected in parallel in the emitter and collector. To one of them the discriminator circuit is connected, while the other, forms the part of the pulse shaper. With a slider arrangement, voltage can be varied so that the required level of discrimination can be set, and the circuit will trigger only when the pulse is higher than the predetermined voltage set by the potential divider. This circuit has all the advantages of stability and simplicity, and is specially designed for this unit. This has been subjected to various tests and the details will be described elsewhere in this chapter.

Pulse characteristics at the input and output of the cable from the driver stage to the Pre-scaler are given in the following table.

Table 2.1

Channel No.	Point	Pulse height volts	Rise time μ -sec.	Duration μ -sec.	Fall time μ -sec.
I	Input	8	0.2	1.0	0.4
	Output	6	0.2	1.0	0.4
II	Input	8	0.15	1.2	0.7
	Output	6	0.15	1.2	0.7
III	Input	8	0.2	1.0	0.5
	Output	6	0.2	1.0	0.5



- 1 Capacitors C-1 and C-2 used in 2⁰ F/F only
- 2 All capacitors Silver Mica unless otherwise specified
- 3 All resistors 1/4 watt carbon, 5%
- 4 All wire #26 gauge Color code as shown Use resistor color code for readout, black thru violet for 2⁰ thru 2⁷
- 5 Power requirements
 - + 48 v 15 ma (at max register rate)
 - + 3.5 v 1 ma
 - 6.3 v 25 ma
 - lv rms 240 ma
- 6 X -istor operation
 - Cut-off Saturated
- 7 Resolving time of 2⁰F/F < 1 μsec
Resolving time of 2¹F/F < 2 μsec

LABORATORY FOR NUCLEAR SCIENCE MASSACHUSETTS INSTITUTE OF TECHNOLOGY CAMBRIDGE, MASS.	
DATE	1. 30 62
REVISION	
DESIGNED BY	F. D. SUTHERLAND
CHECKED BY	
TITLE	PULSE COUNTER - Model BX-9

FIG. 2-8

Regulated power supplies are used for the DC voltage + 12 volts for transistor operation and for discriminator. Each channel has its own decoupling circuits.

2.5 Counting circuits:

2.51 Pre-Scaler:

The main purpose of a pre-scaler is to slow down the counting rate so that the decades can hold the total counts within their range, for the specified duration of recording interval, and there should be no over flow. Another important specification is that the resolving time should be as small as possible i.e. it should be able to distinguish between two pulses even if they are very close to one-another.

Figure 2.8 describes the circuit of the pre-scaler. The basic F/F circuit uses fast transistors 2 N1499 A. There are eight stages and each is supplied with arrangements for a visual display of its condition. The input accepts about 5V positive pulse and the output is given as a 6V negative pulse. Eight stages are used and the whole arrangement is put on a printed circuit board.

An additional feature that makes the scaler more versatile is to route the output circuit, through a rotary switch to different stages, so that the required number of stages can be used depending upon the counting interval.

The resolving time, as mentioned previously, is very

DIGIT	CONDITION ON BI-STABLE OUTPUTS								LEADS CONNECTED FOR AND CIRCUIT
	1	2	4	2'	$\bar{1}$	$\bar{2}$	$\bar{4}$	$\bar{2}'$	
0	0	0	0	0	1	1	1	1	$\bar{1}, \bar{2}, \bar{4}$
1	1	0	0	0	0	1	1	1	1, $\bar{2}, \bar{4}$
2	0	1	0	0	1	0	1	1	$\bar{1}, \bar{2}, \bar{4}$
3	1	1	0	0	0	0	1	1	1, $\bar{2}, \bar{4}$
4	0	0	1	0	1	1	0	1	$\bar{1}, \bar{2}, \bar{4}$
5	1	0	1	0	0	1	0	1	1, $\bar{2}, \bar{4}$
6	0	1	1	0	1	0	0	1	$\bar{1}, \bar{2}, \bar{4}, \bar{2}'$
7	1	1	1	0	0	0	0	1	1, $\bar{2}, \bar{4}, \bar{2}'$
8	0	1	1	1	1	0	0	0	$\bar{1}, \bar{2}'$
9	1	1	1	1	0	0	0	0	1, $\bar{2}'$

FIG 2.9a

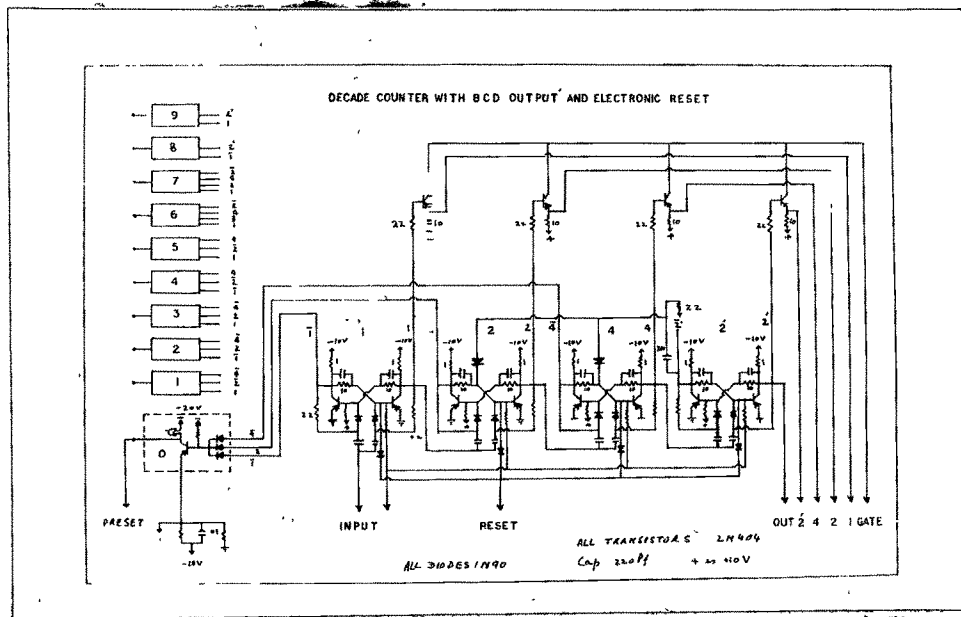


FIG. 2.9b

important, because in case of the slow counter there will be loss of counts. Using a double pulse generator the resolving time of the first stage is determined to be 0.5μ sec. for each channel. As the counting rate for each channel is approximately 5000 per sec., the probability of loss of counts is less than a fraction of a percent.

Similar units are built for each of the channel, with independent inputs and outputs.

2.52 Count decades:

Commercially manufactured R.I.D.L. decade modules are used. Each channel has 4 decades for count storage, that provide for a total count accumulation of 10^4 . Input pulse requirement is 10v positive and resolving time of 1.5μ sec.

It is composed of a standard instrument case containing a power supply and can be fitted into a 19" Relay Rack. Each module fitted into the case, draws power from it. The module contains 4 reading decades and one count control circuit board. In a single decade board four binaries are used. Each binary output is coded as 1.2.4.2, designated serially. This coding system is called B C D, shown in figure 2.9 a.

To decode these, logic circuits are used and the output assumes decimal form. Throughout the whole unit the same coding system is used.

BLOCK DIAGRAM OF
CLOCK CALENDAR

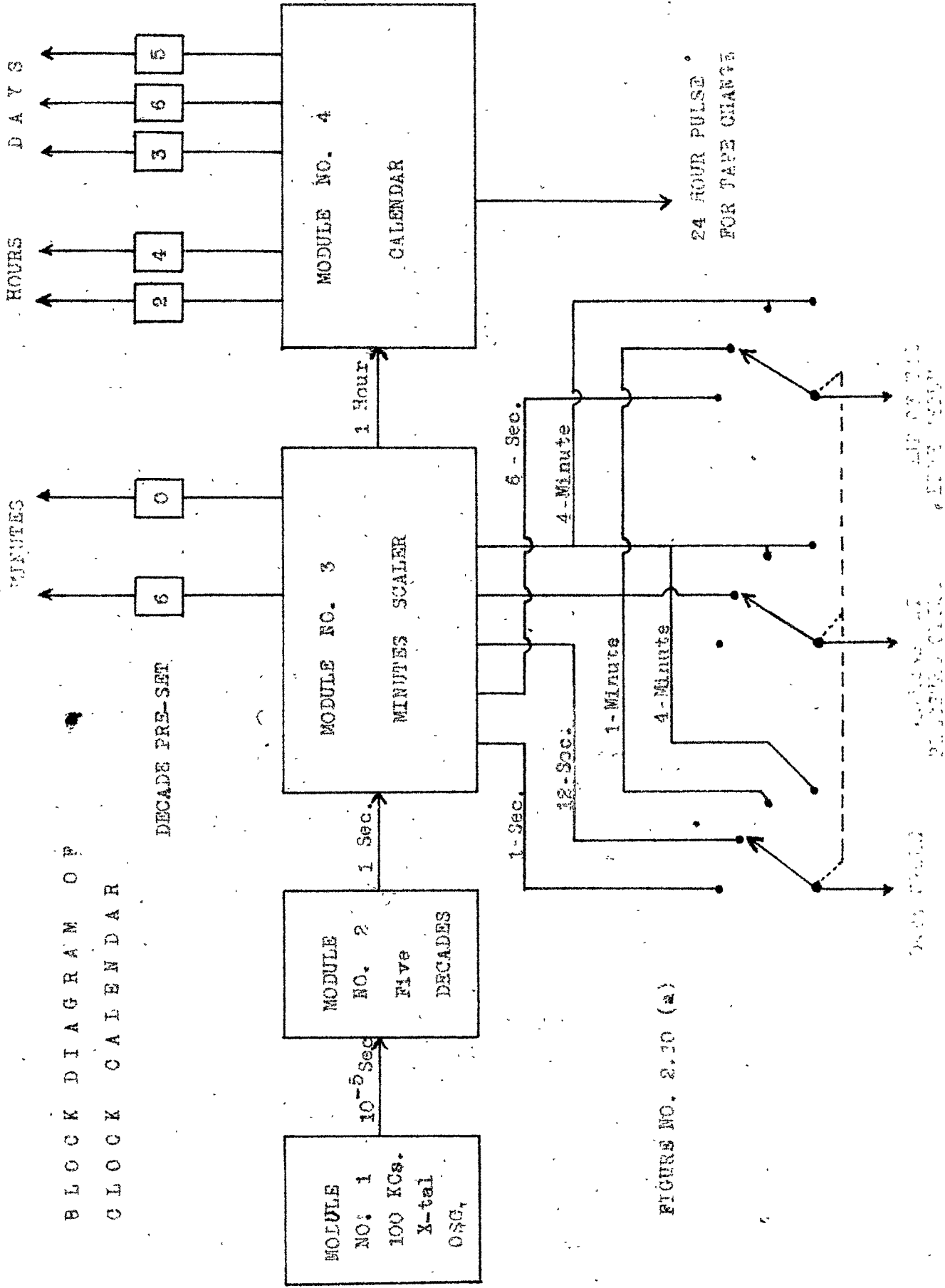


FIGURE NO. 2.10 (a)

: 60 :

A modification is carried out to put an electronic reset for the decade, as shown in figure 2.9 b.

This is designed in such a way that at the end of the count cycle, a pulse resets the decade and the new cycle starts.

As can be seen that the pre-scaler gives a negative pulse whereas the decades need a positive pulse, so a pulse inverting circuit is put in the control circuit board of the decade.

2.6 Electronic clock calendar:

Its purpose is two-fold. Firstly, to supply a pulse that initiates the recording cycle, and secondly, it provides in B C D code the time reference of the recording cycle, indicated in minutes, hours and days. A block diagram of the clock is shown in Fig.2.10 (a), indicating the modules that comprise the clock, punching cycles and form of BCD output for address punch out.

The clock is made up of four modules comprising of oscillator, scaler, minutes scaler and calendar. The first module contains an oscillator of frequency 100 kcs that uses a highly stable crystal specially cut so as to have a stability of .005% from 0 to 50°C. The transistor used is a silicon one, so that the oscillation frequency should remain stable. A buffer amplifier is used to give a

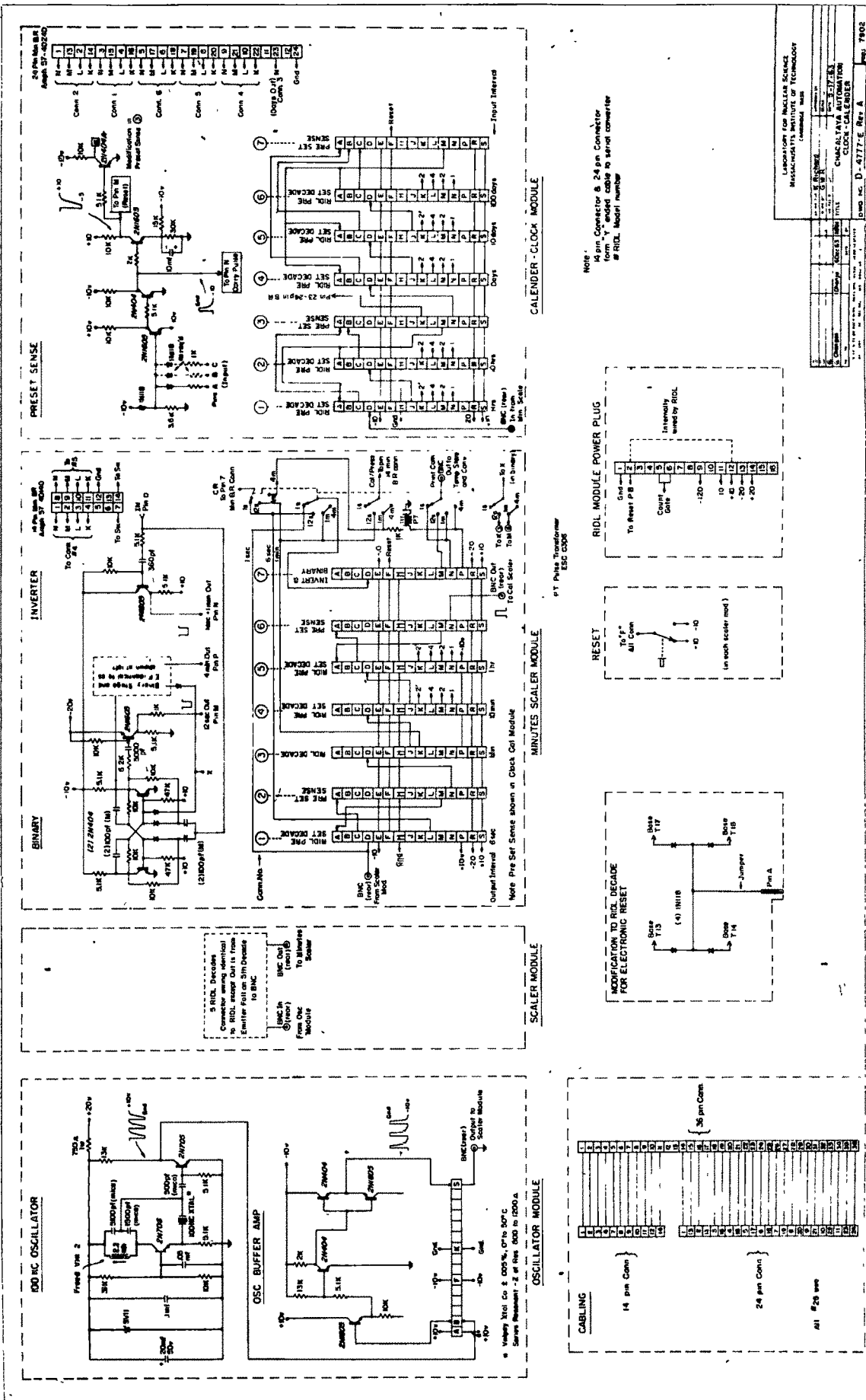


FIG. 2-10 b

LABORATORY FOR NUCLEAR SCIENCE
 Massachusetts Institute of Technology
 Cambridge, Massachusetts
 CHACALAYA AUTOMATIC
 CLOCK-CALENDER
 Dwg No. D-4177-E, Rev. A
 May, 1962

positive pulse to the next stage. The details can be followed from the circuit diagram shown in figure 2.10 (b).

The second module contains 5 RIDL decades and the output of the previous stage is fed to the first decade. It can easily be seen that the output of the last decade will be a pulse every second.

The third module is the most important one, and contains circuits that give initiating pulse for the recording cycle. The first printed circuit board contains a RIDL pre-set decade. With the help of a star wheel fixed at the top of the decade, a pre-set number can be set. When the decade, during the process of counting approaches this number, a pre-set pulse is given out. This is fed to a 'pre-set sense', that gives a pulse for resetting the decade and a carry pulse to trigger the next decade. The RIDL decade, modified for an electronic reset arrangement, receives the reset pulse and starts again for the next cycle. The pre-set is at 6, so that the carry pulse fed to the next stage is at 6 second interval. The decade marked 3 will give an output pulse at 1 minute interval. So, now we have 1 sec., 6 sec., and 1 minute pulses. To have initiating pulse every 1 sec., 12 sec., 1 minute and 4 minute, a switching arrangement is used. It has 4 positions and at each one of the positions, will give the required pulse interval.

For 12 second initiating pulse, a binary is used with 6 second pulse as input, and for 4 minute, a double binary is used with input pulse of 1 minute. For calendar or pressure inclusion, the relay operation requires a positive pulse at 1 minute interval, for 12 second recording cycle, and a 4 minute interval pulse, for 1 minute recording cycle. For each cycle of data punching 13 codes are required, also 7 codes for address, 4 codes for pressure and 1 each for the func. codes. These should not exceed 80 upto the 'end of the line cycle'.

The details are given in the following table:

Table No.2.2

Summary of recording intervals

Data interval	Address	End of the line	Total codes	
			without pressure	with pressure
1 Sec.	-	6 Sec.	78	-
12 Sec.	1 mt.	1 mt.	73	77
1 mt.	4 mt.	4 mt.	60	64
4 mt.	4 mt.	4 mt.	21	25

The fourth decade is pre-set at 10, so that its output pulse is at every 10 minute interval. It gives a BCD code output for the purpose of punching minutes. The next

decade is pre-set at 6, giving a pulse at one hour interval. Hence 0-59 mts. can be punched.

An hour's pulse forms the input of the fourth module. Pre-set decades marked 1 and 2 count hours and ten hours. The first is reset at 4 and the second at 2. The common 'pre-set sense' is connected to the pre-set output of both, and at 24, it resets both the decades and gives a carry pulse to a set of three pre-set decades that count days, 10 days and 100 days respectively. There is a common pre-set sense for **these** decades and if these are set at 365, these will operate upto this number and then are re-set, thereby a year can be counted. The BCD code output of the pre-set decades is fed to the serial converter and punched and typed in the proper sequence of data recording.

2.61 DC/DC Converter:

The mountain stations, in general, suffer from frequent power stoppages. But, for an electronic clock it is very essential that it should operate even during power failures.

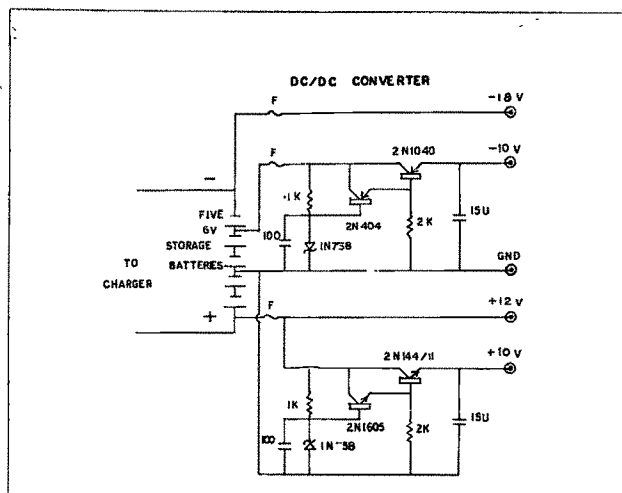


Fig.2.11 DC/DC Converter for clock calendar.

The arrangement shown in figure 2.11, uses a bank of 5 secondary batteries arranged in such a way that it gives + 12v on one side and - 12 and - 18 volt on the other side. Using a reference of zener diode, 1N758 that gives 10v, and a series transistor controlled by a D.C. coupled amplifier, stabilized output of +10v and -10v is got. It may be noted that only -10, and +10, need to be regulated; -20v supply having a current consumption of 440 ma is used only for display bulbs in the RIDL decades. The +20v is required only for the oscillator supply and that too is dropped to +10v. So +12v is found to be sufficient for the purpose. As the crystal oscillator operates at 10v, regulated by a zener, the arrangement was found to be satisfactory. Tests carried out for the regulated $\pm 10v$, in the range of the current required for the calendar, are found to be satisfactory.

The batteries are kept in a floating charge condition by using a proper battery charger, put across the whole bank of batteries. The arrangement has all the advantages of simplicity and operational ease. No difficulty is experienced in the continuous operation of this unit. During major breakdown which at times may extend to about a week, the converter is switched off and restarted after the resumption of the power.

2.7 Integral circuits and Temporary Storage:

The major purpose of this stage is to store the information (which is transferred from the decades) during the recording cycle, until it is punched out. It has three printed circuit boards for a single channel. The two boards contain memory circuits that use Shockley diodes and can handle B C D information of 4 decades. The third circuit board receives an initiating pulse from the clock and generates two pulses, the first one reads the B C D information, and the other resets the decades. It also receives a pulse from the last stage of the ring counter in the serial converter, that interrupts the current to the Shockley diodes thereby resetting them. It occurs at the end of the recording cycle.

A Shockley diode is a four layer device with two terminals, Silicon doped with Boron and phosphorous. The diffusion process takes place at red heat and each layer

is about 0.0005 inch thick (Shockley and Gibbons 1958). The diode functions as two inter-connected diffused base transistors with outer-most layers as emitters. This forms a closed feedback loop, and is unstable if the gain around the loop is greater than unity. As the voltage is applied, the intervening layers oppose the flow of the current and no conduction takes place until the voltage is high enough to break the potential barrier. The current versus voltage graph is shown in Fig.2.12.

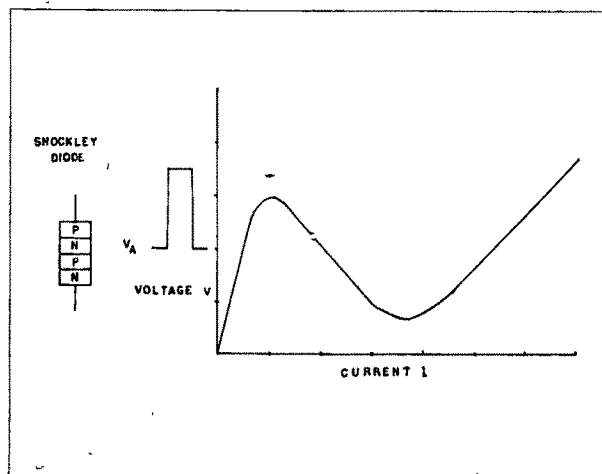
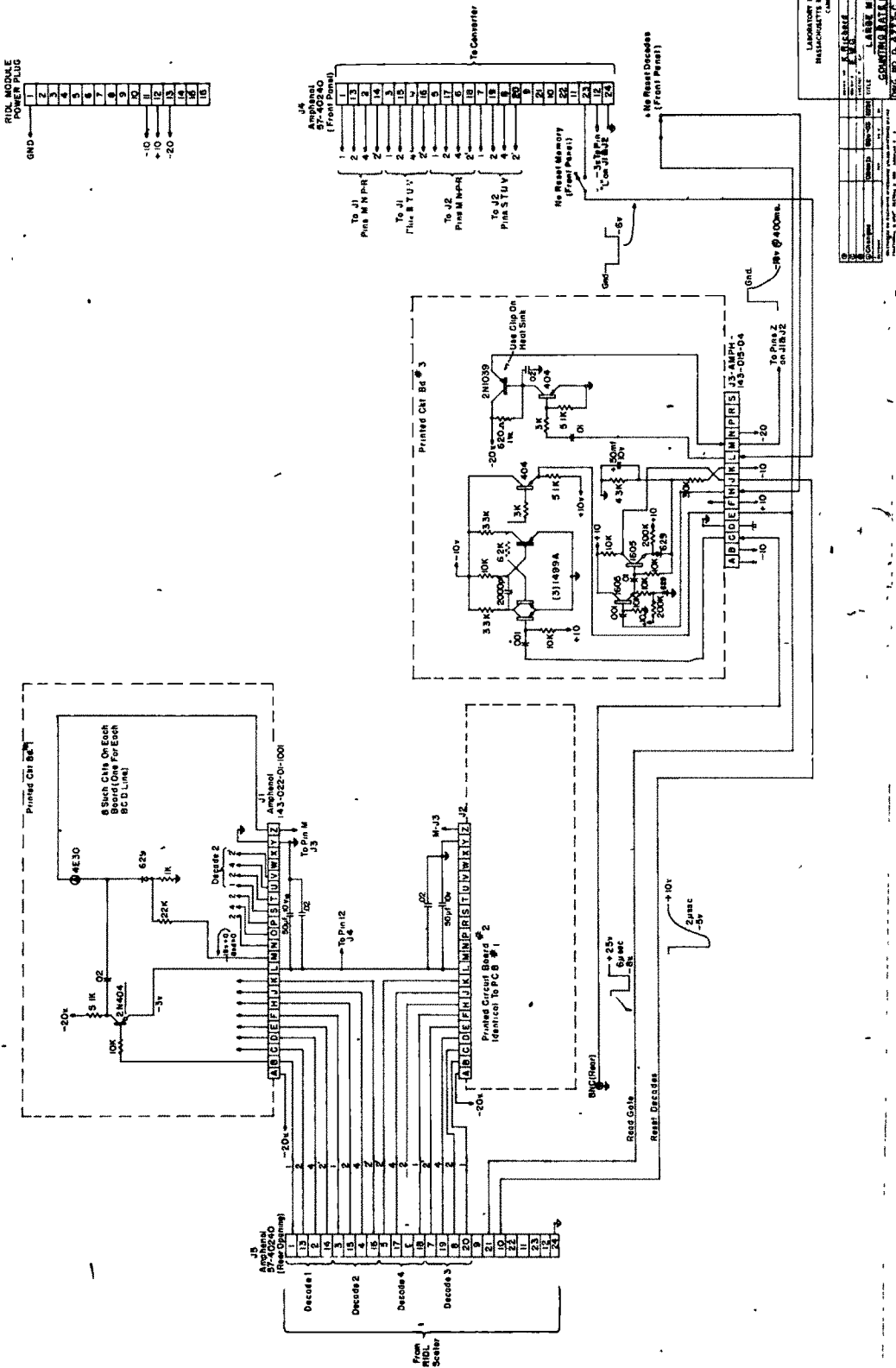


Fig.2.12 Current voltage graph of a Shockley diode.

It can be seen that a certain part of the curve has negative resistance. So, even if the voltage is lowered, large current will continue to flow, and for stopping the current, we will have to bring the voltage almost to zero. Its use as a storage component is made by keeping it at a voltage below the break down. As a pulse is fed, the voltage rises higher than the break down and the Shockley



LABORATORY FOR NUCLEAR SCIENCE
 MASSACHUSETTS INSTITUTE OF TECHNOLOGY
 Cambridge, Mass.

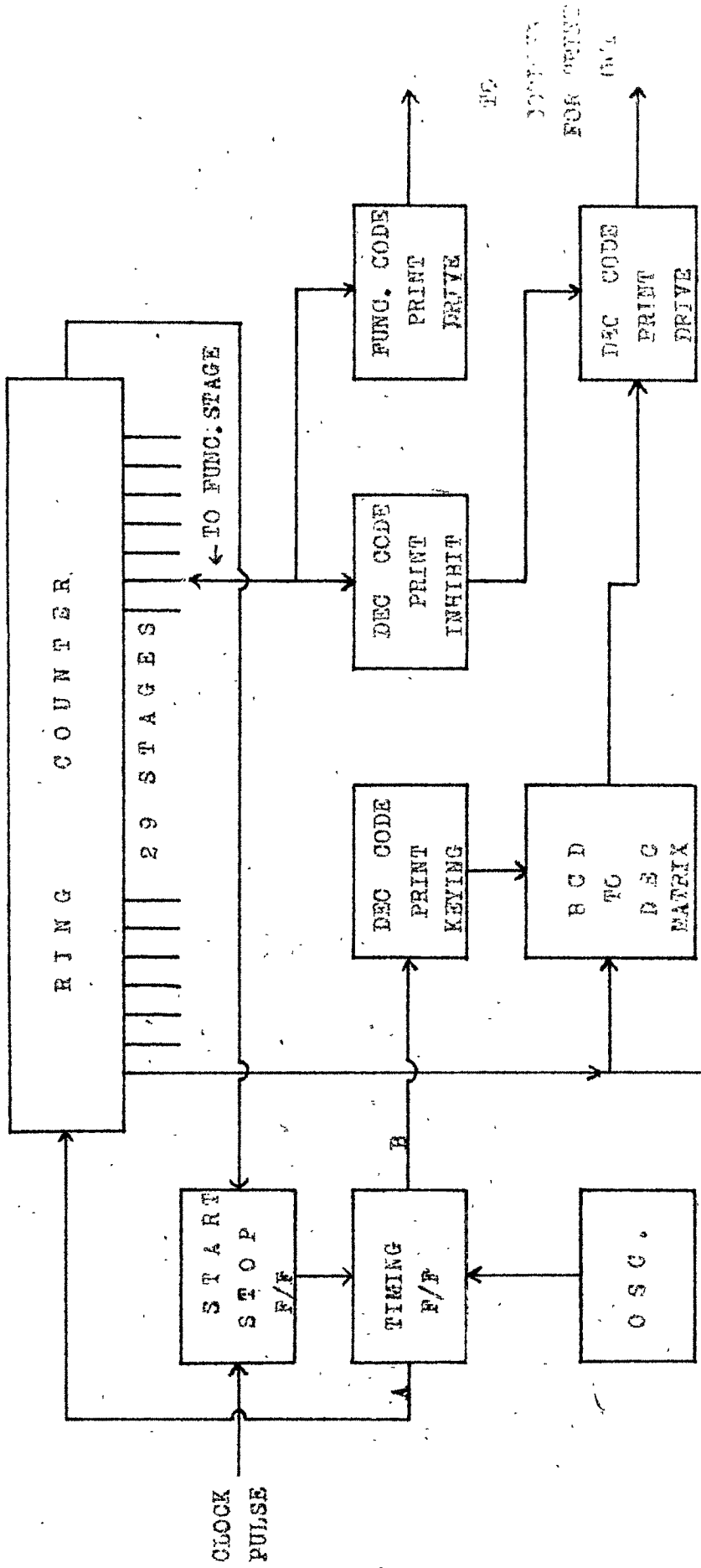
PROJECT NO. 68-2777-1-5
 FILE NO. 68-302
 TITLE LASER WEAPON DETECTOR
 AUTHOR J. M. GIBBS
 DATE 1968
 CONTROLLING AGENCY COMNAVSTAAL BILBAO

FIG. 2-13

diode starts conducting, and although the voltage has returned to be original value, it continues to conduct and will stop only if the voltage is brought to zero. Hence the conducting and non-conducting conditions of each of the BCD line of the decade can be transferred to the corresponding Shockley diodes.

Following the circuit diagram of the temporary storage shown in figure 2.13, an initiating pulse from the clock, every 12 second (or any other interval previously determined), activates a univibrator which through an emitter follower feeds a 6μ second pulse as a read gate to the decades. The 6μ second pulse activates the gated emitter followers of the BCD lines. The negative pulse from the emitter follower of each of the BCD line is fed to the temporary storage circuit consisting of an amplifier and a Shockley diode circuit. The breakdown voltage of the Shockley diode is $-30v$ and it is normally kept at $-20v$; so, with the addition of a negative pulse from the BCD line, the Shockley diode breaks down and it registers a conducting state. In case the BCD line is non-conducting, no over-riding pulse appears and the Shockley diode remains in the same non-conducting state. The trailing edge of the read pulse produces a 2μ second, $15v$ negative pulse. This is fed to the electronic reset circuits of the decades that are reset, and the decade starts counting for the next interval. So the dead time,

BLOCK DIAGRAM OF SERIAL CONVERTER



REF: 3995777A

FIG. 1

during which pulses are not recorded, is 2μ second. On board 3, there is another circuit that supplies $-20v$ to the Shockley diodes through a controlled series transistor. At the end of the recording cycle the last pulse from the ring counter in the serial converter is fed to an amplifier controlling the series transistor, which is turned non-conducting thereby stopping the voltage to the Shockley diodes so that these are reset and the memory is ready for the next cycle (Richard et al 1963).

2.8 Print-out circuits:

2.81 Serial converter:

The primary function of the serial converter is to read the BCD lines in the temporary storage and punch the information. Essentially it converts the parallel information into serial information. The major circuits that compose it are start-stop F/F, timing F/F, oscillator, ring counter, BCD to DEC matrix and other gating and drive circuits shown in the block diagram in figure 2.14.

For the start of a recording cycle proper clock pulse is fed to the start stop F/F, which is flipped over, thereby unclamping the timing F/F that starts giving pulses, at points (A) and (B), the interval depending upon the frequency of the relaxation oscillator. One side of the timing F/F supplies pulses to the ring counter and the other to the print keying connected to the 'BCD to DEC Matrix'. The

sequence of pulses involved in this operation is shown in figure 2.15.

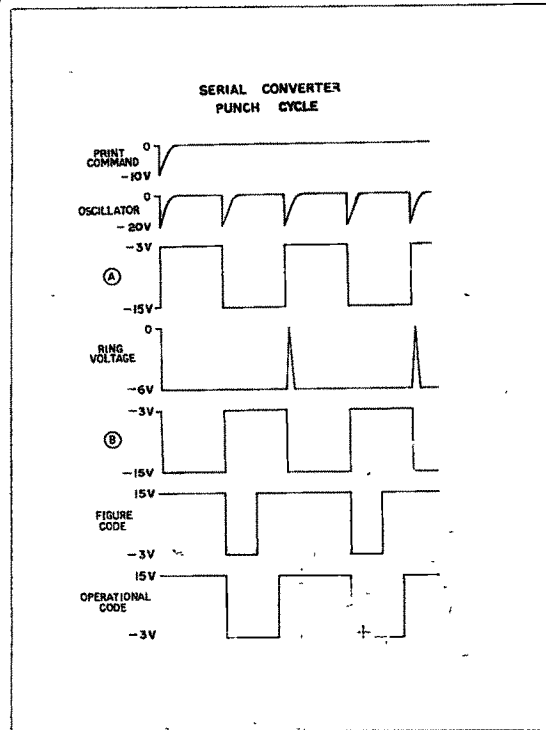


Fig.2.15

Feeding of ring counter pulses results in unclamping the BCD lines that change the condition of the respective F/F in the 'BCD to DEC Matrix' by a set pulse.

Following the circuit diagram of the serial converter shown in figure 2.16 we find that the logic circuits of the Matrix are constructed on the basis of the codes used in the decades. So, the BCD 4-line code gives a single pulse in decimal code. The duration of the print impulse will depend upon the timing of the print keying F/F. After it has

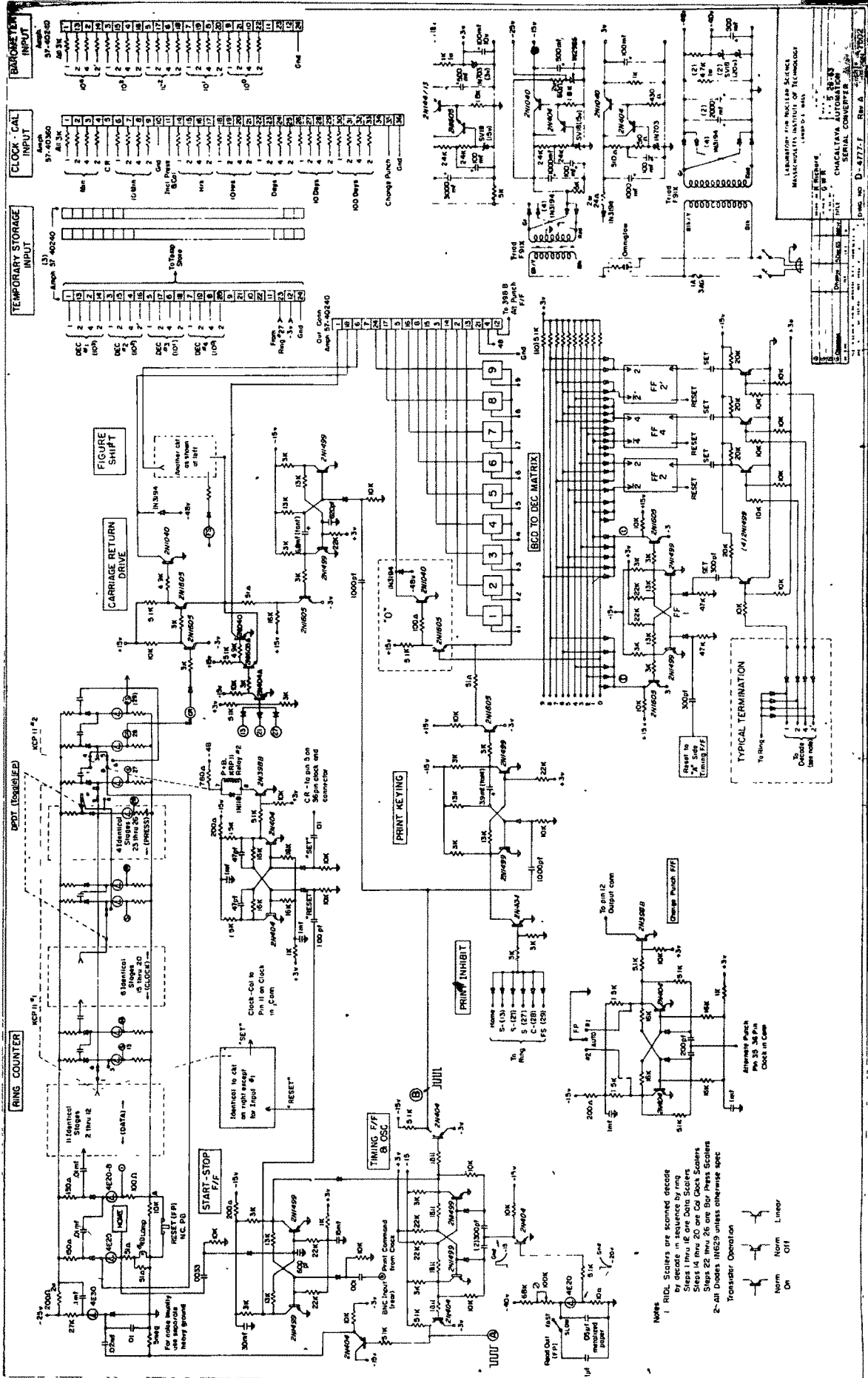


FIG. 2-16

RESEARCH LABORATORIES
MASSACHUSETTS INSTITUTE OF TECHNOLOGY
CAMBRIDGE, MASS.
SERIAL CONVERTER
CHALGATA AUTOMATOR
Rev. 5-58-53
Drawn: S. G. W. H.
Checked: S. G. W. H.
Date: 5-58-53
Draw No. D-4777-1 Rev. A

punched out the proper digit, the F/F of the matrix is reset. The next stage of the ring counter is triggered that unlocks the next BCD lines and again through the matrix the proper digit is punched. For the space and the functional characters the ring counter pulse is fed to a print inhibit circuit and this clamps the print keying F/F but sends in a proper printing impulse through another circuit. At the last step of the ring counter, a pulse is fed back to the home circuit which starts conducting, setting back the start/stop F/F, which clamps the timing F/F and so the whole cycle of operation is stopped. This last pulse from the ring counter is also fed to the temporary storage that resets the Shockley diodes.

The ring counter controls the basic sequence of the serial converter. Its design shown in circuit diagram in figure 2.16 incorporates Shockley diodes connected in such a way that each conducts one after the other.

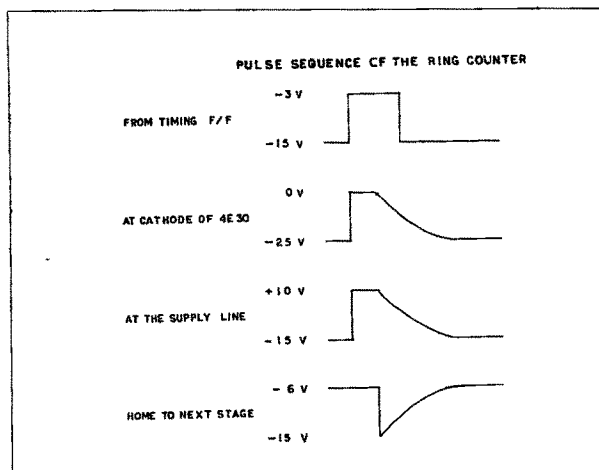
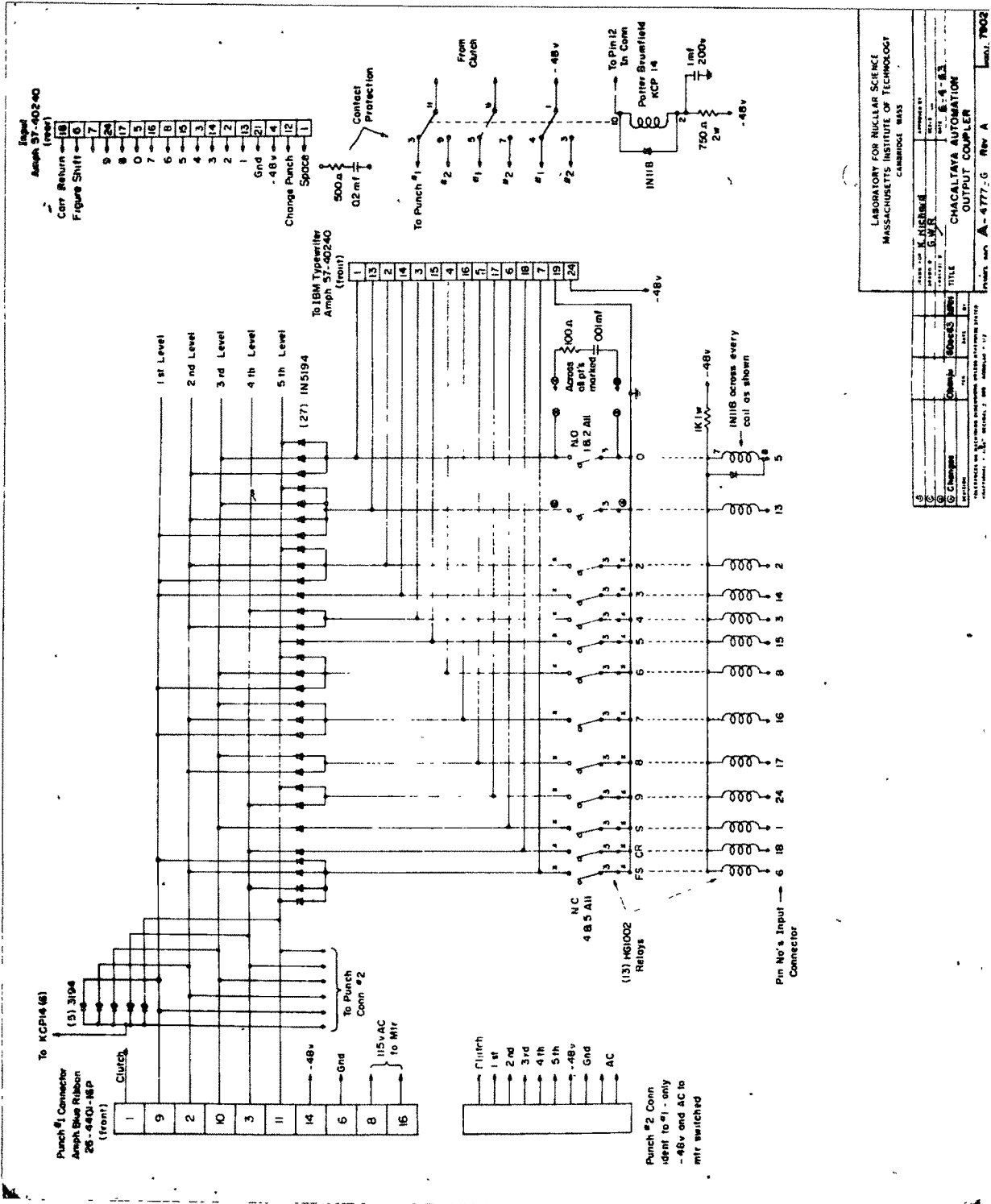


Fig. 2.17

Following the pulse sequence of the ring counter indicated in figure 2.17, the Shockley diode in the home position is normally on, and the current required for it passes through a resistance of 200 ohms, developing an effective voltage of 15v on the cathode line. This prevents the other Shockley diodes from breaking down and charges the 0.1 mfd. capacitor. The incoming positive pulse from the timing F/F breaks down 4E30 Shockley diode and discharges the capacitor through it. This results in sending a pulse of about 25v in the supply line, thereby driving the voltage on it to zero and stopping the current in the home stage. This stoppage of the current results in feeding an effective pulse of -9 volts to the next stage through a .01 mfd. capacitor, which results in breaking down the next stage before any other stage is able to do so. Similar situation repeats as the next pulse arrives from the timing F/F and then the next Shockley diode will start conducting, making the previous one off. So each stage conducts successively, the duration depends upon the timing pulses. During conduction of a Shockley diode, a 6v pulse develops across the 100 ohms resistance, that acts as a gate for the BCD lines. The pulse from the last stage triggers back the home position.

2.82 Printing of calendar and pressure:

For a 12 second punching cycle, the print out of calendar and pressure is required every minute. So, at



LABORATORY FOR NUCLEAR SCIENCE
 MASSACHUSETTS INSTITUTE OF TECHNOLOGY
 CAMBRIDGE, MASS.

9	NAME OF PROJECT	CHACALATA AUTOMATION
8	NAME OF INVESTIGATOR	G. CHACALATA
7	DATE	APR 1953
6	PROJECT NO.	6-4-83
5	TITLE	CHACALATA AUTOMATION
4	TYPE OF INSTRUMENT	OUTPUT COUPLER
3	REVISION	
2	DESIGNED BY	K. HICKS
1	APPROVED BY	

Product No. A-6777-G Rev A
 MODEL 7902

FIG. 2.18

this interval a pulse is fed to proper binaries that switch on relays and put in the sequence of the ring counter, additional number of stages, depending on the BCD lines to be read. With the help of a toggle switch the pressure 'read out', can be included or excluded. At the end of the cycle the F/F's are switched off to the original position. A similar relay arrangement is put for including functional codes in the punching cycle. The circuits are shown in figure 2.16.

2.83 Coupler:

The output of the serial converter is routed through a coupler and fed to the punchers and the typewriter. The coupler has 13 relays (HG 1002) that are energised according to the digit or the functional code to be punched. The circuit diagram of the coupler is given in figure 2.13.

Ten relays are used for the digits and three for the functional codes. For punching out information on 5 track paper tape, proper code is constructed for each of the digit and the functional code. As the punching cycle is very short, it is difficult to replace paper tape without stopping the puncher, so two tape punchers are used, each operating every 24 hours. The voltage supply to the clutch of the punchers is routed through a relay, that is operated by a F/F located in the serial converter, and triggered in either position, by a 24-hour pulse. The 48v required for

the tape puncher and for the typewriter solenoids is taken from the power supply in the serial converter module.

As HG 1002's are mercury relays, care should be taken that they are kept in the vertical position throughout their operation.

2.84 Punchers:

Motorized tape punchers are used for data recording. The paper tape used is "11/16 wide and punched in 5 track code. The operating speed is 20 codes per second but, in general, it is not operated at this high speed, because for 12-sec.interval operation there is enough time for the information to be punched, until the next cycle starts. The clutch is magnetically operated, has single revolution, and drives the cam shaft on the punch. The control impulse for clutch operation should have minimum duration of 15 milli-sec. The voltage required is 48v. There are individual magnets for each unit of the code and are selected according to the code formation. The control impulse duration is the same as for the clutch, and code magnets may be impulsed simultaneously at the start of each punching cycle. For tape supply a roll housing is mounted on the main cover. This can hold about 1000 ft.of paper tape, which lasts for 24 hours with 12-second interval recording.

2.85 Typewriter:

IBM input output writer model 87 is used. A

formaliner is fixed at the carriage of the typewriter with an endless sheet of paper. Decimal input and proper functional codes are fed from the coupler. For normal operation, a 25 milli-second pulse for typing key and 39 milli-second pulse for functional operation is required. The supply voltage is 48v. The output is parallel to the punched output, and is used for scanning and other test purposes.

2.9 Digital Servo-barometer:

Basically, it is a mercury barometer fitted with a float at the top of the mercury column, and a servo-coupled differential transformer that keeps itself locked to the float. The movement of the mercury column due to the variation of pressure, changes the float position, and thereby the differential transformer. This mechanical change is amplified with the help of precision gears and recorded by mechanical counters. Based on the above principle, an instrument manufactured by 'Exactel Company' is used. The data are reduced to the standard barometric conventions by incorporating compensatory devices. The general configuration of the instrument is shown in figure 2.19.

It indicates the mercury cistern, float and other mechanical parts. The cistern and the column are of high quality stainless steel and the mechanical construction is of very high accuracy. The instrument is capable

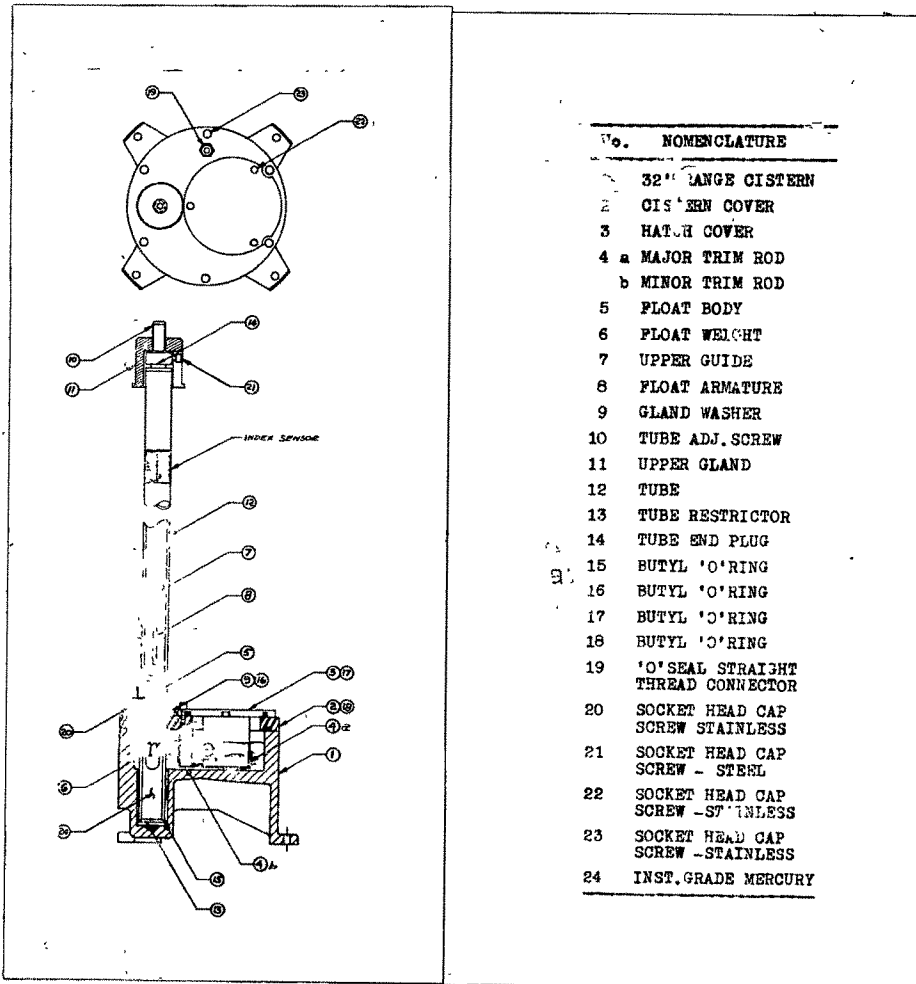


FIG. 2.19 : SERVO-BAROMETER CISTERN AND TUBE ASSEMBLY.

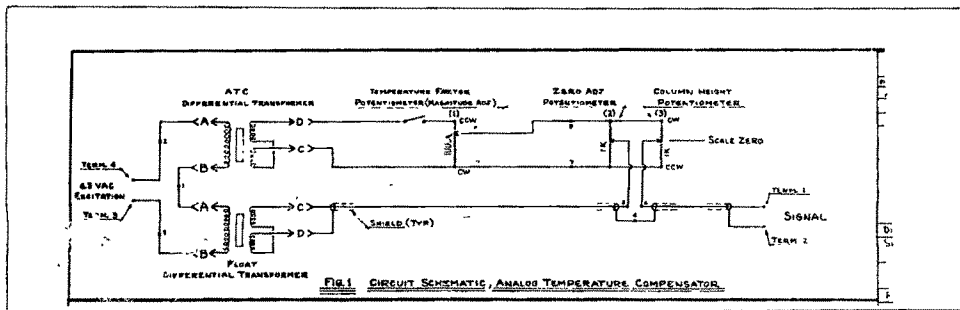


FIG. 2.20

of providing digitized pressure readings to an accuracy of a tenth of a millimeter.

In figure 2.20, the circuit diagram of the float differential transformer and the temperature compensating arrangements are shown. The different potentiometers indicated therein are used for the accurate adjustment of the value of the compensation. The compensation arrangement is automatic and is used to free the pressure readings from the effect of temperature changes. The temperature sensing device consists of a long aluminium tube with an invar rod drawn through its centre. The differential expansion produced by the temperature change is multiplied by a linkage. Normally, the differential transformer is servo-positioned to the electrical centre of the armature of the float. The output of the differential transformer of the temperature compensator displaces the balanced position by an amount required for temperature correction. This is checked in detail to ensure proper behaviour in the temperature range encountered. The room temperature is normally maintained at $60^{\circ} \pm 4^{\circ}\text{F}$ and so it is checked in the range of 48 to 68°F . The values of the correction so obtained are compared against the calibrated values of the instrument, as shown in figure 2.20. The inaccuracy is found to be within the error specified.

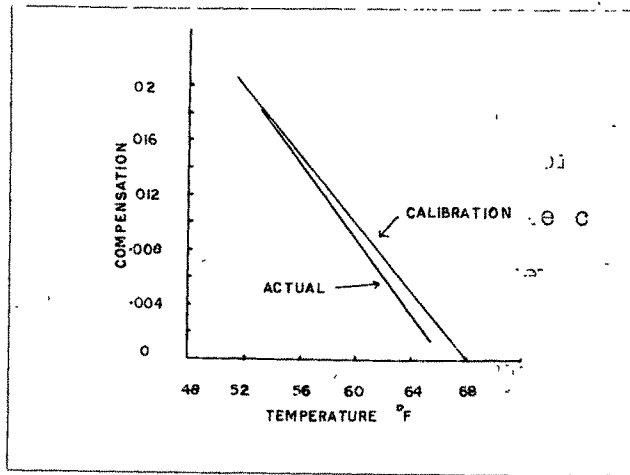


Fig.2.21 Graphs showing temperature compensation checks for servo-barometer.

2.91 DEC to BCD converter:

The Digicon counter in the servo-barometer gives mechanical contact decimal output. For the read out system described previously, BCD form is needed. The author designed the necessary circuit arrangement for it, and also an electronic locking arrangement, described in Fig.2.22.

At the start of the pressure punching cycle, the pulses generated at the successive points form stage 23 to 26 of the ring counter (shown in figure 2.16 of the serial converter), are serially routed through a DEC to BCD matrix, giving BCD output depending upon the contact position at the Digicon decimal counter. The first pulse at the ring counter stage (23) locks the Digicon counter electromagnetically and the last pulse at stage (29) release it, so that during pressure read out proper contacts are maintained.

2.10 Tests and Checks:

2.101 Stability of the discriminator:

As the function of a discriminator is to eliminate noise, it is essential that the biasing voltage should remain constant, and the discriminator response should be linear in the range of the noise level. The method adopted for checking comprises of feeding a pulse of known amplitude at the input of the discriminator and keeping its voltage level low so that an output pulse is observed; but, as the discriminator level is increased the output pulse disappears at some point. Different discriminator voltages are noted to correspond to different amplitudes of input pulses. In the range of the input pulse of 0.1 to 0.7v, corresponding discriminator voltage change is noted for each 0.1v step.

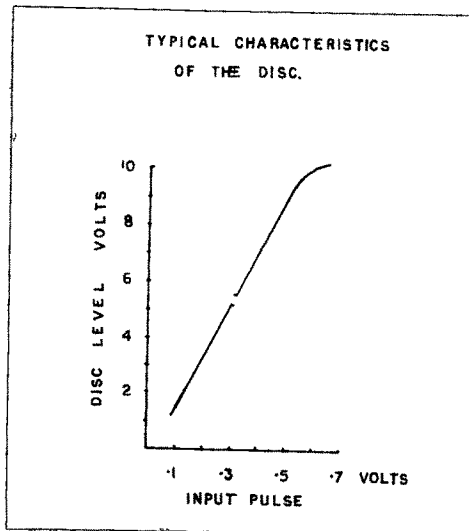


Fig.2.23 Graph indicating pulse height V/S discriminator voltage.
A typical graph is shown in the above figure.

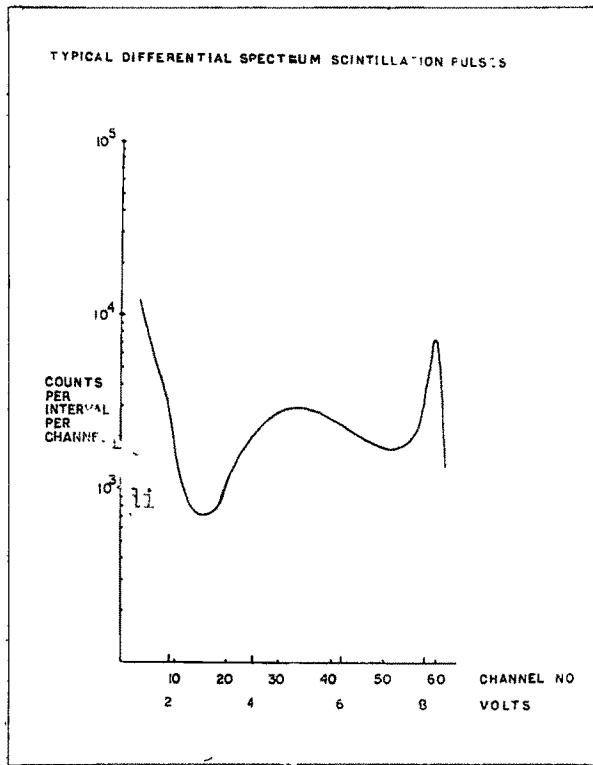


FIG. 2.24

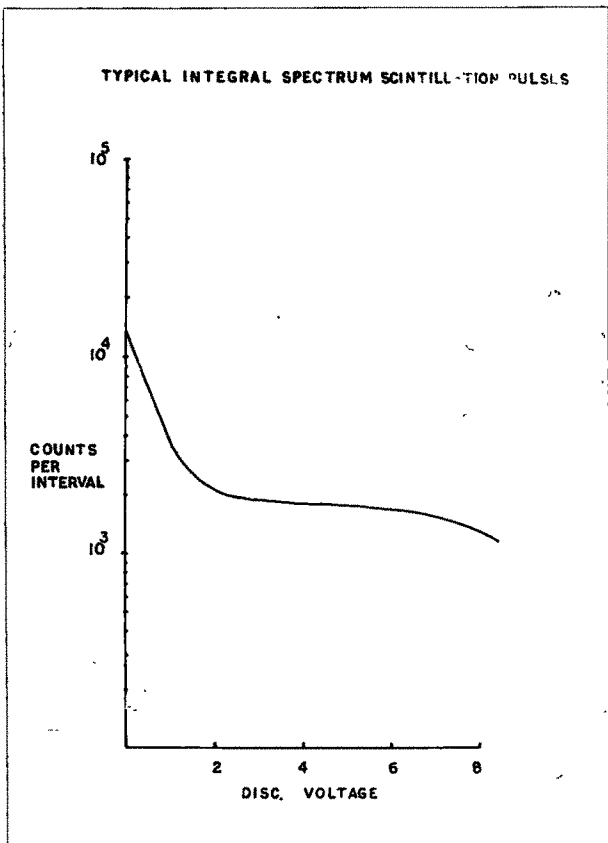


FIG. 2.25

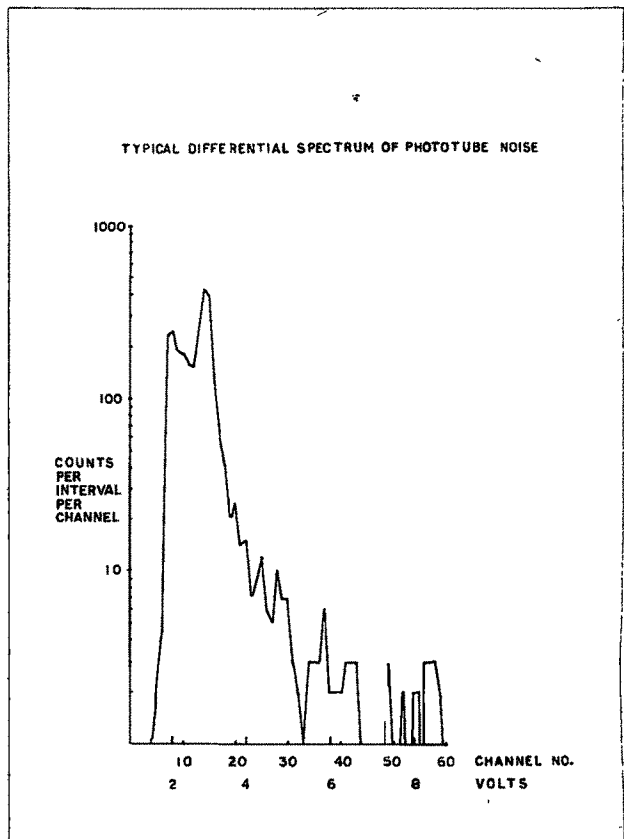


FIG. 2.26

Using this method all the 15 discriminator circuits are checked. Linearity in the 0.1 to 0.5v range of input pulse amplitude is observed, and the discriminator voltage required is in the range of 2 to 10v. For checking stability, the same performance criterion is maintained.

• 2.102 Pulse Height Analyser checks:

The number of photons observed in a scintillator are proportional to the energy of the particle actually expended in the scintillator. The pulse height output given by the photo-tube is proportional to the photon energy striking the photo-cathode. The output pulses show a certain spectrum. The differential spectrum is investigated by using a pulse height analyser. With the photo-tube looking into the scintillators, input to the analyser is taken from a point at the end of the amplifier system. A typical graph of one of the 15 detectors is shown in figure 2.24.

The graph indicates the counts per interval per channel for the range of 2 to 8v of pulse height. At low voltage of the pulse height the counts are large due to the noise. A minimum is observed at about 3 volts after which there is an increase in counts with a maximum at about 5 volts. Another point of maximum is observed at about 8v due to the saturation characteristics of the amplifier system.

Integral spectra are taken by recording total counts at regular steps of discriminator voltage. A typical plot of the integral spectrum is shown in figure 2.25.

The steep rise in the graph at lower discriminator voltage is due to the contribution of noise pulses. A flat part in the curve is observed from about 3 to 6 volts, where the counts remain the same inspite of the variation in discriminator voltage.

In order to estimate the overall noise characteristics of a detector system, it is essential to know the dark current of the photo-tube. For the determination of the differential spectrum of the dark current, the photo-tube is taken away from the scintillator and sealed in a light tight container. The output pulses are fed to the pulse height analyser. A typical differential spectrum is shown in figure 2.26. The spectrum is seen to be very steep towards higher pulse heights. Hence by fixing a higher discriminator voltage the noise can be greatly reduced.

Now, with these three sets of graphs it is easy to ascertain the level of discriminator voltage to be fixed for eliminating noise. It is observed that in some photo-tubes, the contribution of the dark current is rather high. The reason for this is that some leakage is taking place at the anode due to high voltage. This is removed by isolating the anode from the dynodes at the base of the photo-tube.

The discriminator level is fixed by taking into consideration the flat part of the integral curve and the amount of noise present at that level, so that it is compromised between the noise content and the slope of the integral curve.

The combined calibration chart is given in Table 2.3, which shows, the range of the integral curve's flat part, and the point where the discriminator level is fixed.

Table 2.3

Chart showing discriminator levels for each scintillator

Det. No.	Minima. Diff. Spect. (Volts)	Integ. Spect. (Volts) range, flat part.	Slope (% per volt)	Disc. level adjusted (Volts)	Remarks
1.	3.5	3.0-5.0	4.0	4.0	
2.	3.4	2.0-4.5	5.0	4.0	
3.	4.0	2.5-4.5	6.0	4.0	
4.	3.0	2.5-4.5	6.0	3.5	
5.	3.0	2.0-4.0	5.0	3.4	
6.	3.4	3.0-5.0	6.5	4.0	
7.	3.5	2.5-5.0	5.0	4.1	
8.	3.5	2.0-4.5	3.5	3.7	
9.	3.4	2.5-5.0	4.0	4.0	
10.	3.2	2.5-4.5	5.0	4.0	
11.	4.6	3.0-6.0	3.0	5.0	
12.	3.0	2.0-4.0	5.5	3.6	
13.	3.3	2.5-4.5	5.0	3.7	
14.	3.4	2.5-4.5	6.0	4.0	
15.	3.5	3.0-5.0	3.0	4.0	

The noise level is kept below 0.01% for the discriminator level adjusted for each of the detectors.

2.103 Temperature Checks:

In order to avoid any temperature changes in the scintillators, the cave is kept at a constant temperature of 15°C maintained to within $\pm 1^{\circ}\text{C}$. In the electronic centre where the amplifier and discriminator circuits modules are kept temperature of $20 \pm 2^{\circ}\text{C}$ is maintained. The specified temperatures are monitored at regular intervals.

C H A P T E R III

METHOD OF ANALYSIS

Part A Treatment of data:

3A.1 Introduction

The recording of cosmic ray intensity forms a time series, indicating the number of particles in successive intervals. The interval of recording is chosen after taking into account the nature of variations and their statistical properties. For any variation pattern to be perceptible, it must show above the statistical fluctuations. The time series are regarded as stationary if the probability distribution depends only upon the time difference and not on the time itself; and if the time series do not contain any time source variations. Stationary time series do not imply that the sample remains the same at all times but have a mean and variance that remains constant. A time series often involves different frequencies, and it is our endeavour to identify the prominent frequencies. But before subjecting the data to any kind of analysis, it is important to see that the data are self consistent.

3A.2 Format and duration of the data:

The data have been recorded every 12 second, and the time every 1 minute together with pressure recordings. A sample of the data recorded on a typewriter, operating

parallel to paper tape punchers, is shown below.

COSMOPOLITAN

CALIF

CHANNEL
I II III

128313851384	136212801385	137813731376	138013751380	138513771370	3621431	4086
138713821370	139713851372	138813601376	138113771374	138313751376	3721431	4086
138413741379	137613911379	138713811382	139613761366	138113761368	3821431	4086
138313711372	138713781376	137813791378	137413761367	138613871364	3921431	4086
137713751389	137413801377	137213771379	137913831372	139513741390	4021431	4086
138313851382	138113681388	138613661382	138413751389	138313731367	4121431	4086

1st 2nd 3rd 4th 5th 111. 111.

10 SECOND INTERVALS OF A MINUTE.

DATE: 11. 11. 11. HOURS 11. DAY NO.

PRESS: 11. 11. 11.

Each of the line contains data over a period of 1 minute.

The data punched on 5 track paper tape are converted into IBM cards by using a tape to card converter, D.S.W. 870. These cards form the basis of all further processing. The information on the punched cards is compared with that of the typewriter, so as to detect any errors in the process of tape to card conversion.

The recording of the data was started on April 15, 1964 and was discontinued on June 27, 1966. The durations of the recorded data for this period are indicated in the following table.

Table No. 3.1

From	To	Number of days	Interval of recording	Pressure recording.	Remarks
15-4-64	5- 5-64	21	12 seconds	No	
13-5-64	15- 6-64	34	-do-	-do-	
22-6-64	26- 9-64	97	-do-	-do-	
10-10-64	29-12-64	81	-do-	-do-	
8-6-65	4-10-65	119	-do-	Yes	Pressure recording started on 20-8-65
21-11-65	27- 1-66	67	-do-	-do-	
18-2-66	21- 4-66	63	-do-	-do-	
29-4-66	27- 6-66	60	-do-	-do-	

The detectors, when being checked and calibrated for the Air Shower Experiment (BASJE) of which they formed a part, could not provide any data during these periods. No data could be recorded on the days of power failures or instrument breakdowns.

3A.3 Self consistency of the data:

The detectors are divided in three independent sections and their recordings form three sets of time series. For any physical phenomenon to be genuine, it must show in all the three series. We shall describe a method used for the determination of such a consistency.

Let the series be represented as :

$$x_1 , x_2 \dots\dots\dots x_n \quad (3.1)$$

$$y_1 , y_2 \dots\dots\dots y_n \quad (3.2)$$

$$z_1 , z_2 \dots\dots\dots z_n \quad (3.3)$$

A new series is found by dividing series 3.1 by 3.2.

$$a_1 = x_1/y_1$$

$$a_2 = x_2/y_2$$

.....

$$a_n = x_n/y_n$$

If the same physical phenomenon is affecting both the series (3.1 and 3.2), then the new series,

$$a_1 , a_2 \dots\dots\dots a_n \quad (3.4)$$

should have constant values. But this may not be so due to certain factors such as difference in the detectors and in the electronic circuits incorporated with them. The variance σ^2 of the series 3.4 is dependent upon the variance σ_1^2 (of series 3.1) and σ_2^2 (of series 3.2). Assuming a normal distribution for the series 3.4, the probability that value a_i exceeds the average value by $\pm 2 \sigma_4$ on either side, is 4.5% . Consequently, if 94.5% of the values are within the limit of $\pm 2 \sigma_4$, the data represented by the series 3.1 and 3.2 are considered self consistent.

In a similar way two more series are generated; first one, by taking ratios of the series 3.2 and 3.3, given by,

$$b_1, b_2 \dots \dots \dots b_n \quad (3.5)$$

and the second series, by taking ratios of the series 3.3 and 3.1, given by,

$$c_1, c_2 \dots \dots \dots c_n \quad (3.6)$$

The process similar to the one applied to the series 3.4, are also applied to the above two series (3.5 and 3.6). If 94.5% of the values are found to be within $\pm 2\sigma$ limits, the data represented by the series 3.2 and 3.3 are considered self consistent.

It may be noted that in the intercomparison performed above, each of the series gets checked twice. Any inconsistency in one of the series will show up at two places.

For all further analysis the simultaneous values of the three series are combined together.

3A.4 Data used for Power Spectrum Analysis:

The analysis have been performed on the data extending from November 21, 1965 to June 27, 1966. This duration has an advantage of having pressure data as well. Only for about 5% of the days the cosmic ray data are rejected for the above duration due to the inconsistency in one of the channels.

The data have been subjected to an additional scrutiny for continuity. Wherever large discontinuities occur, the series is terminated at that point. For any particular set subjected to the analysis, not more than 5% of the data points are by interpolation.

Part B Power Spectrum Analysis:

3B.1 Introductory remarks:

Our chief concern here is to determine frequencies that make substantial contribution in a time series representing cosmic ray fluctuations and their power. Conventional methods of finding frequencies employ Fourier analysis. But, where random changes of phase exist, this method fails because it can be shown that as the length of the record tends to infinity, the corresponding estimate of the Fourier transform of the time series for any frequency approaches zero. A different method can be used here by taking the mean square, which under certain conditions tends to a finite value.

A series comprising of n data points having dt as the interval between the adjacent points is the basis for computing m number of values of power density for non-zero frequencies in a spectral window ranging from $1/2m dt$ to $1/2 dt$. Since we are interested in investigating short periods of the order of a few minutes, we shall fix the

frequency range of the spectral window such that it contains the required periods. Hence, m is fixed by the discrimination required in the final spectrum. The value of dt also determines the frequency resolution of the linearly spaced frequencies in the spectral window. The value of n is determined by the physical requirements of the analysis and the degree of accuracy required for the spectral density estimates. The estimates are computed by taking mean lagged products of the n data points up-to m number of lags. This forms into a sort of auto-correlation function which is then subjected to Fourier transform.

Details about the choice of the constants are discussed later in this chapter.

3B.11 Auto-covariance function:

In most cases the signals and noises may be represented or approximated to a stationary series, having Gaussian distribution with zero averages. Then, their relevant statistical properties are contained in the auto-covariance function. Following the method outlined by Blackman and Tukey (1959), general formulas representing auto-covariance function can be derived as follows:

Let a time series be represented by,

$$X(t_1), X(t_2) \dots \dots \dots X(t_n)$$

$$\text{average is defined as } \overline{X(t_i)} = \text{ave } X(t_i)$$

$$\begin{aligned} \text{and covariance } C_{ij} &= \left\{ X(t_i), X(t_j) \right\} \\ &= \text{ave} \left\{ X(t_i) - \bar{X}(t_i) \right\} \left\{ X(t_j) - \bar{X}(t_j) \right\} \end{aligned}$$

If the average is zero,

$$\text{then } C_{ij} = \text{ave} \left\{ X(t_i) \cdot X(t_j) \right\}$$

As the series is supposed to be stationary, so it is unaffected by the translations of time at the origin. The covariance depends only upon the time separation given by $(t_i - t_j)$.

$$\text{So, } C_{ij} = C(t_i - t_j).$$

Thus the noise is completely specified by a single function of a single variable particularly $C(0)$, the variance (for zero average, the average square of $X(t)$).

In the case of auto-covariance $C(\tau)$ we specify the lag to which the process has to be carried out.

$$\text{So, } C(\tau) = \lim_{T \rightarrow \infty} \frac{1}{T} \int_{-T/2}^{+T/2} x(t) \cdot x(t + \tau) dt,$$

is the auto-covariance function, for lag τ . It can also be called mean lagged product.

$$\text{Hence, } C(\tau) = \text{ave} \left[x(t) \cdot x(t + \tau) \right]$$

As, there is direct relationship of the joint probability distribution to the auto-covariance function, the stationary time series can be expressed in terms of serial correlation coefficients.

3B.12 Fourier Transform:

The power spectrum $P(f)$ is the Fourier transform of the auto-covariance function.

$$\text{Therefore } P(f) = \int_{-\infty}^{+\infty} C(\tau) \cdot e^{-2\pi i f \tau} d\tau$$

The function of frequency $P(f)$ describes the power spectrum of the time series. If we suppose $x(t)$ as a voltage across (or a current through) a pure resistance of one Ohm, then the time averaged power dissipation in the resistance is represented by the variance of $x(t)$ between the frequency range f and $f+df$.

The relation of the auto-covariance function as the Fourier transform of the power spectrum can also be used to express power spectrum as the Fourier transform of the auto-covariance.

Expressed in discrete cosine form

$$P(f) = \int_{-\infty}^{+\infty} C(\tau) \cdot \cos 2\pi f \tau d\tau$$

$$C(\tau) = \int_{-\infty}^{+\infty} P(f) \cdot \cos 2\pi f \tau df$$

The general power spectrum response curve is shown in figure 3.1.

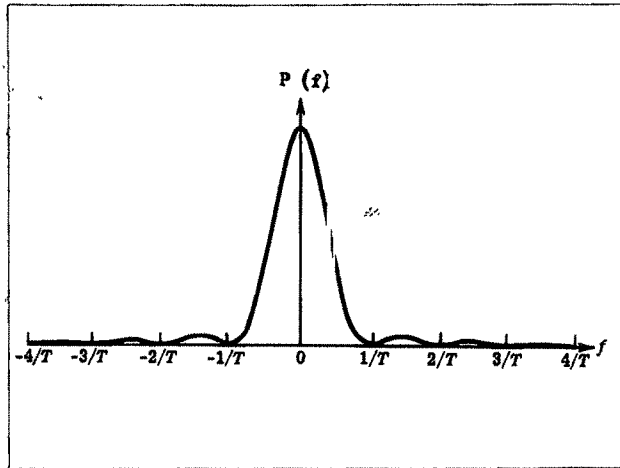


Fig.3.1

3B.13 Numerical formulas:

If there are n data points of dt time interval between the adjacent values, the mean lagged product C_r with lag interval of $d\tau = h dt$, can be computed as follows:

$$C_r = \frac{1}{n-hr} \sum_{q=0}^{q=n-hr} X_q \cdot X_{q+hr}$$

The value of $r=0, 1, \dots, m$ and $m \leq \frac{n}{h}$ where m is the maximum lag. It is usual to use lags not longer than about 20% of the length of the record;

The raw spectral density (V_r) can be computed according to the formula.

$$V_r = d\tau \left[C_0 + 2 \sum_{q=1}^{q=m-1} C_q \cdot \cos \frac{qr\pi}{m} + C_m \cos r\pi \right]$$

To this we can apply Hanning filter to get U_r , the smoothed spectral estimates,

$$U_r = \frac{1}{4} V_{r-1} + \frac{1}{2} V_r + \frac{1}{4} V_{r+1}$$

or Hamming filter,

$$U_r = 0.23 V_{r-1} + 0.54 V_r + 0.23 V_{r+1}$$

Estimates with subscript 0 will apply in the range just above the zero frequency and with subscript r , for a frequency of $\frac{r}{2m \cdot d \tau}$, upto $\frac{1}{2d\tau}$, 0.5 cycle per observation. By multiplying it with the appropriate values, the frequencies can be expressed in the desired units.

3B.2 Aliasing:

A time series with a certain basic time interval has a sampling frequency (F_s). If the terminating frequency (F_t) of the spectral window does not fold into the sampling frequency (F_s), then certain spectral intensity will lie from F_t to F_s . The frequencies upto F_t are all distinguishable but the higher ones are not, never the less, these will contribute some power. If the folding frequency (F_t), is the principal alias and is not able to fold itself upto the sampling frequency, then in terms of the discreteness of the data, all the values will not be read. Such a situation is made clear by figure 3.2, which shows how equally spaced time samples from any cosine wave could have come from each of the many other cosine waves.

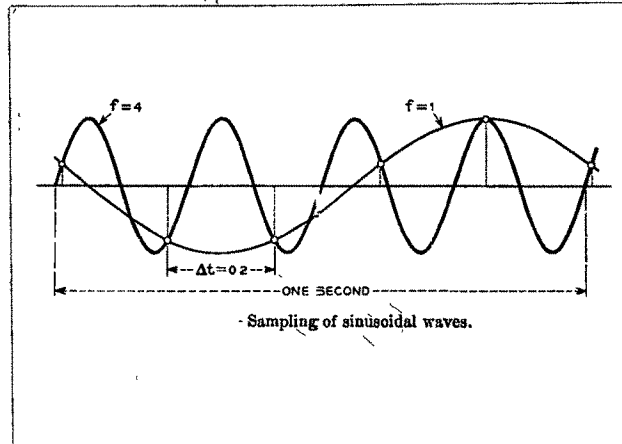


Fig.3.2

This may lead us into false information.

The methods of aliasing can be considered in terms of the proper folding of the frequency so that the power between F_t and F_s is accounted for. The sampling frequency can be decreased so that the terminating frequency folds itself into that, this will give us better estimates of the elementary frequency bands.

3B.3 Filters

3B.31 General digital filters:

In some cases it may be very evident that a certain range of frequencies or a frequency is largely present in the data. These frequencies may not be of immediate interest and so should be eliminated before the data are subjected

to power spectrum analyses. In case it is a low frequency, a high pass filter should be used and if the main contamination is in the H.F. the filter should be low pass. We shall first consider a low pass filter.

If X_1, X_2, \dots, X_n are the observed values then the new series

X'_1, X'_2, \dots, X'_n is obtained by applying the formula,

$$X'_i = \sum_{j=-m}^{+m} W_j \cdot X_{i+m+j}$$

where W_j are the filtering weights, and the number of observations involved in the filtering process are $2m + 1$. So, the application of a filter results in the reduction to $N-2m$ values from the original data having N values.

A high pass filter is derived by the numerical differentiation of the low pass filter. A filtered series is represented by

$$\ddot{X}'_i = X_{i+m} - \sum_{j=-m}^{+m} W_j \cdot X_{i+m+j}$$

A very effective high pass filter results from the choice of

$$W_j = \frac{1 + \cos \frac{j \pi}{m}}{2m}$$

The cut off frequency of the filter is given by $\frac{1}{m \Delta t}$, so the value of m is determined by the cut off frequency required.

The response of the filter is given by

$$A = [1 + Q(f)]^2$$

where $Q(f) = Q_0(f) + Q_0 \frac{1}{2}(f + f') + \frac{1}{2} Q_0 (f - f')$

$$Q_0(f) = \frac{\text{Sin } 2\pi f_m dt}{2\pi f_m dt}$$

$$f' = \frac{1}{m dt}$$

The response curve of an equally weighted running mean type of filter function is shown in figure 3.3. By using proper weights the negative response found at some frequencies can be avoided.

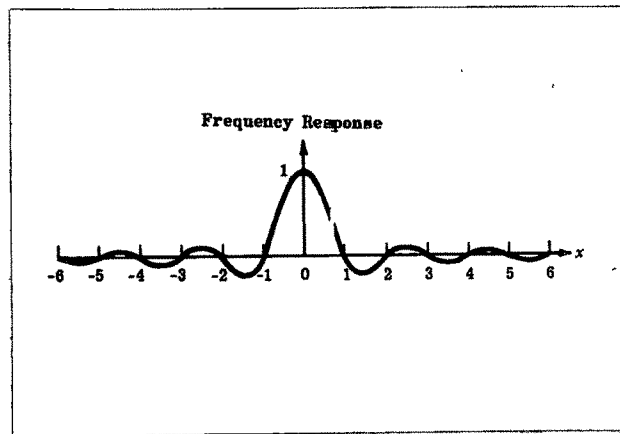


Fig. 3.3

3B.32 Hanning and Hamming filter:

The data subjected to P.S.A. (Power Spectrum Analysis) have discrete time interval and only a limited length can be used. This will introduce a frequency resolution that can be improved only to a limited extent.

The question of choosing the lag window, so that the power should concentrate exactly at the frequency present in the sample becomes difficult, because the power may not concentrate at the main lobe. One of the methods to correct this is to make the main lobe flat. This will decrease the adjacent frequency resolution, but the power estimate becomes better.

A lag window, called the hanning filter is,

$$D_1(dt) = \begin{cases} (1 + \cos \frac{\pi dt}{T_m}) & \text{for } dt < T_m \\ 0 & \text{for } dt > T_m \end{cases}$$

Another lag window, called hamming filter is,

$$D_2(dt) = \begin{cases} 0.54 + 0.46 \cos \frac{\pi dt}{T_m} & \text{for } dt < T_m \\ 0 & \text{for } dt > T_m \end{cases}$$

The general characteristics of both the filters are the same except for their effects on the side lobes.

3B.4 Pre-whitening

In considering the spectral windows, we assume that the power spectrum has no peaks vastly higher than the general level of the curve. This assumption is necessary because the function does not vanish outside a small interval. So, if we have a large peak of $D(f)$ near one of the value of f_1 , it will contribute a small fraction of itself at some other point f_2 . If this value out-weights the power

at f_2 , then the power spectrum will not be representative of the actual values at each frequency but will be contaminated by the contribution from other frequencies. So, in case, large values of power are concentrated in the L.F. side of the power spectrum it will tend to seep through to the higher frequencies. For the estimation of the different characteristics of the pre-whitening it may be fruitful to determine the slope and the general shape of the power spectrum expressed in octave intervals. It may be determined in a preliminary check, if large peaks occur at L.F. side of the spectrum or not. In case the slope is very small i.e. the distribution of power density is almost linear and no large peaks occur on the L.F. end, the application of pre-whitening may not be necessary.

In case pre-whitening has to be performed, we have only to find where the power is expected to be large. As most of the noise is in the low frequencies the following scheme can be used. The data are modified by the formula,

$$X_{r-1} = X_r - \lambda X_{r-1} \quad (r=1,2 \dots\dots n);$$

where λ is usually taken as 0.7 and n denotes the number of data points.

The multiplier for the above process is,

$$1 + \lambda^2 - 2 \lambda \cos 2 \pi f dt.$$

by which the values of refined spectral density should be

multiplied to compensate for the pre-whitening process carried out on the initial time series.

3B.5 Chi-square test

The power densities at different frequencies derived from the recorded data, need to be estimated for their reliability. For this, we will need their variance and covariance. But the estimates of power are derived from the auto-covariance which in turn is dependent upon the lag function. So, the determination of variance and covariance from this function becomes difficult and intricate. By taking a less rigorous treatment it has been shown by Blackman and Tukey, that the accuracy of the spectral density estimates depends upon the ratio of the number of data points to the number of lag points. The actual value approximately follows Chi-square distribution with $2(\frac{n}{m} - \frac{1}{3})$ degrees of freedom. We do not know the probability distribution of the power density but its variance, we may suppose that it behaves like n^2 on $\frac{n}{m}$ degrees of freedom. This fits the physical view that we have m results from n observations. Once the degrees of freedom of the distribution is known we can find the confidence limits in the usual way. If we merely want to know that a peak in our results is significant or not, we test against the hypothesis that the population power spectrum does not have a peak there (Swinnerton-Dyer 1963).

3B.6 Superposing of power density estimates:

A method for increasing the reliability estimates of the spectral density is by superposing one set of values upon another set. This results in increasing the degrees of freedom of the superposed set, and so the peaks show greater reliability. This method can also be used for finding out the persistency in the occurrence of the frequencies by superposing large number of samples and estimating the reliability of the resultant peaks in the spectral densities.

3B.7 Choice of the constants for the spectral analysis:

The discrete time interval between the adjacent values of the data determines the sampling frequency F_s , and thereby the highest terminal frequency F_t , which is the upper limit for a spectral window. From physical considerations and computational aspects the required value of n is chosen. The resolution in the spectral window is dependent upon the value of the lag m to which the autocovariance function is calculated. Larger the value of the lag, finer is the frequency resolution; but the reverse is true for the statistical accuracy of the power density estimates. The table 3.2 indicates some of these aspects for data intervals of 12 seconds, 1 minute and 5 minutes.

Table No. 3.2

(Interval)	Sampl- ing fre- quency.	Termi- nal fre- quency.	No.of data points.	Lag.	Frequency resolution.	Degrees of free- dom.
dt	F_s	F_t	n	m	r	k
12 Second	300 CPH	150 CPH	900	30	5.0 CPH	59
				60	2.5 CPH	29
				75	2.0 CPH	23
1 Minute	60 CPH	30 CPH	180	30	1.0 CPH	11
				60	0.5 CPH	5
				75	0.4 CPH	4
5 Minutes	12 CPH	6 CPH	72	12	0.5 CPH	11
				24	0.25CPH	5
				30	0.2 CPH	4

It is clear from the above table that a compromise has to be made in the choice of the constants. For a power density estimate to be more reliable, it should have large degrees of freedom, but this will tend to decrease the frequency resolution.

The chief interest of the present investigations being periods of the order of a few minutes, a spectral window of 1 to 30 CPH is chosen. For this, with dt of 1 minute, lag, m of 30 is required. The duration of a single sample subjected to spectrum analysis is three hours i.e. 180 data points. This gives about 11 degrees of freedom for the reliability estimates of the spectral

density. The choice of a three hourly interval is convenient for comparing the average spectral density estimates for this interval, with other physical parameters such as k_p .

A Fortran programme for computing spectral density and incorporating the above mentioned features is written for IBM 1620 computer. The values of dt , h , m , and n could be varied by the use of a control card. The value h is introduced to take into account 'aliasing'.

The spectrum analysis is performed in two parts. In the first one, the deviations from the average are computed. The process of per-whitening is not applied because in the range of 1 to 30 CPH the slope of the spectral density is found to be about 0.2 db per octave, which means that the spectrum is almost flat. No filter is applied because in the processes of computing derivations the low frequencies mostly due to diurnal and semi-diurnal variations will be automatically filtered out. The output of the first part of the programme is fed to the second one, the output of which gives auto-covariance, raw spectral density and refined spectral density. So, for each three hourly interval of data we get 31 values of spectral density estimates for frequencies from 0 to 30 CPH.

The computer programmes are given in the appendix.

3B.8 Method of epochs:

In inter-related physical phenomena, any change in one parameter may have corresponding consequences in another. A method of study formulated for finding consistency or any other physical effect in a certain parameter may be considered in terms of finding epochs from another corresponding parameter. In the present study neutron monitor data of Deep River and k_p index are used for fixing epochs that are representative of certain interplanetary conditions. The spectral density estimates during the days of similar epochs are superposed. The resultant spectral density estimates are indicative of the behaviour of the spectral frequencies in the different physical conditions represented by the epochs.

C H A P T E R I V

RESULTS OF THE ANALYSIS

4.1 Variability of spectral estimates:

The spectral window used in the present study is from 1 to 30 cycles per hour, having a resolution of 1 CPH (cycle per hour). A single sample subjected to spectral analysis has 180 data points with one minute interval between the successive points. The 1 to 6 CPH range is investigated separately, with a resolution of 0.2 CPH. For this a single sample has 72 data points of 5 minutes interval between successive points.

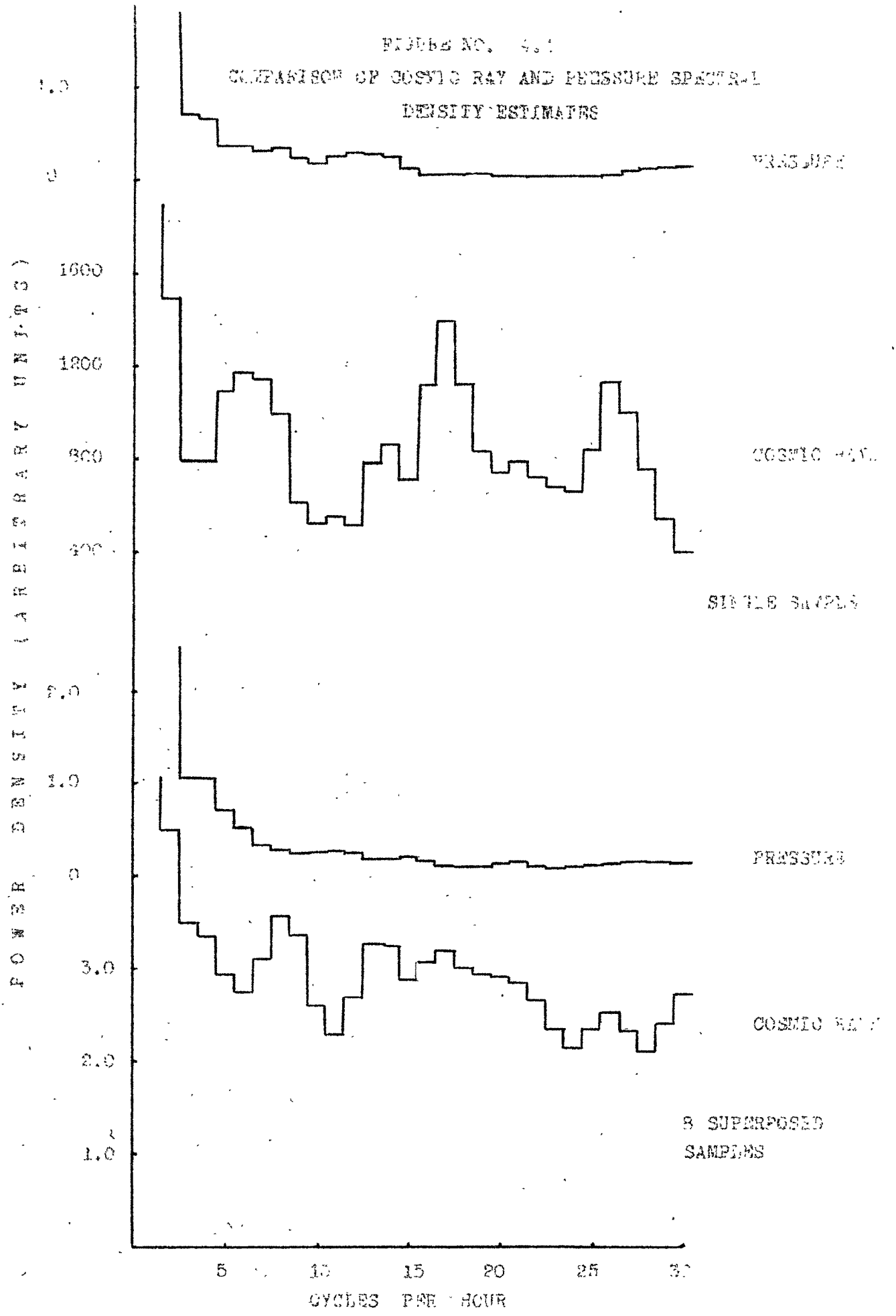
For each three hourly sample, the spectral constants are the same and so are the degrees of freedom. Hence, the power estimates of a particular frequency in different samples can be intercompared. Parameters specifying other phenomena, for the sample interval, can be used for correlation.

The study of the gross characteristics for 6-30 CPH range is carried out by averaging the power density estimates. The choice of proper epochs representing different geophysical factors and the knowledge of the average spectral power for these epochs can give us information regarding the effect of these geophysical factors upon the cosmic ray frequencies lying in the 6-30 CPH range.

The results presented here are based on the analysis

FIGURE NO. 4.1

COMPARISON OF COSMIC RAY AND PRESSURE SPECTRAL
DENSITY ESTIMATES



conducted on the basic 12 second interval data from November 21, 1965 to June 15, 1966.

4.2 Pressure variations in the frequency range of 1 to 30 CPH and their effect on cosmic rays:

Using one minute pressure recordings of the digital Servobarometer, power spectrum analysis is performed for three hourly intervals with a spectral window of 1 - 30 CPH. Simultaneous cosmic ray data of the same intervals are subjected to a similar analysis. It is found that neither for a single sample nor for 8 superposed samples, there are prominent peaks in the pressure estimates. The spectral estimates for single sample as well as for eight superposed samples of pressure and cosmic rays are shown in Figure 4.1.

As no pressure peaks occur in the spectral range of 1 to 30 CPH, the peaks observed in the spectral density estimates for cosmic rays should be attributed to the phenomenon other than the pressure variations. As such, there is no need to apply pressure correction to the cosmic ray data.

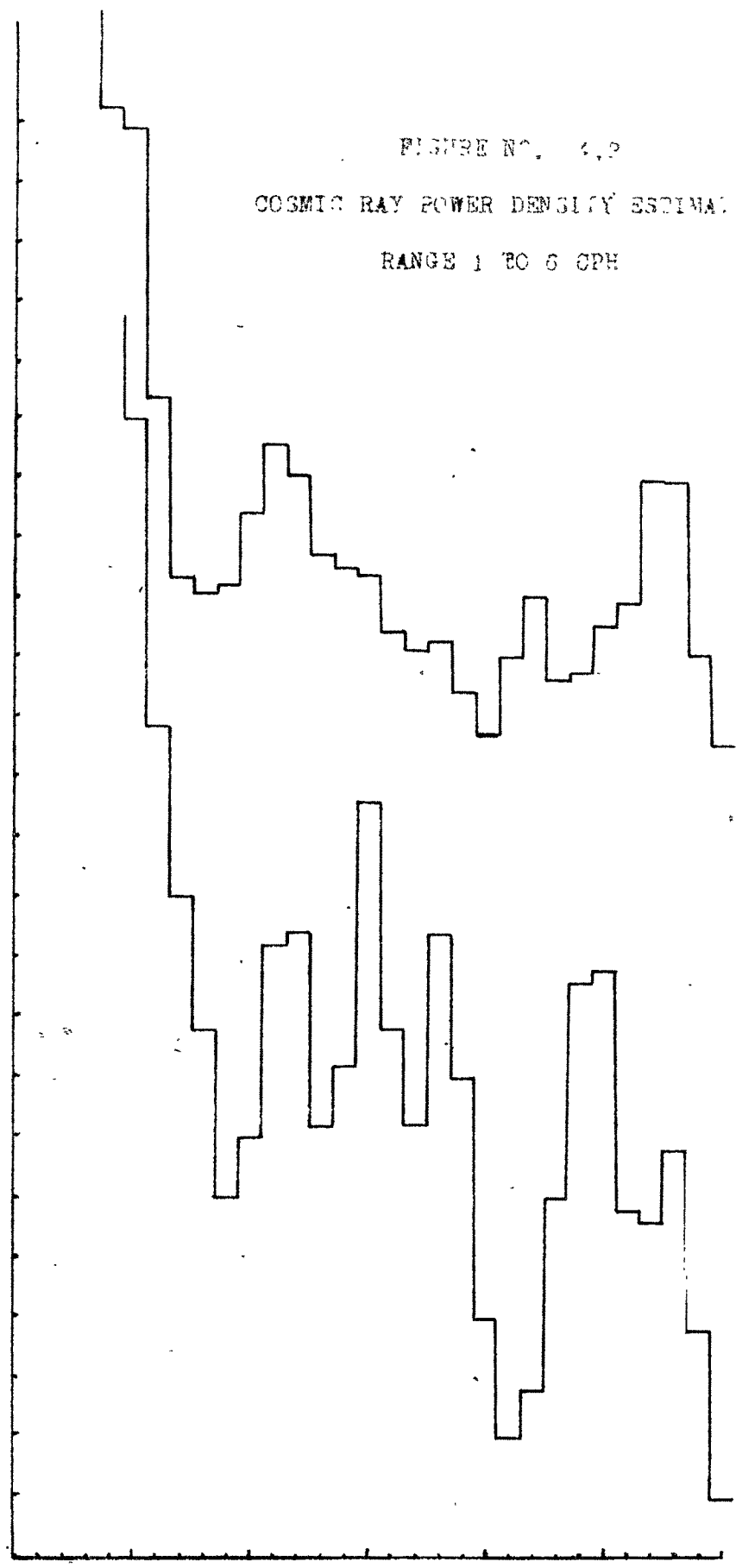
4.3 Search for persistent frequencies:

The frequencies in the range of 1-6 CPH are investigated with a resolution of 0.2 CPH. Six hourly intervals having 72 data points with a basic difference of 5 minutes between the successive points, are subjected to P.S.A. Peaks are observed around 3 and 5 CPH. As four samples

FIGURE NO. 4.2
COSMIC RAY POWER DENSITY ESTIMATES
RANGE 1 TO 6 CPH

POWER DENSITY (ARBITRARY UNITS)

5.0
4.0
3.0
2.0
1.0
0.0
1.0
2.0
3.0
4.0
5.0
6.0



EVER
SAY DES
AT TPOSED

STAMP
GAMER

CYCLES PER HOUR

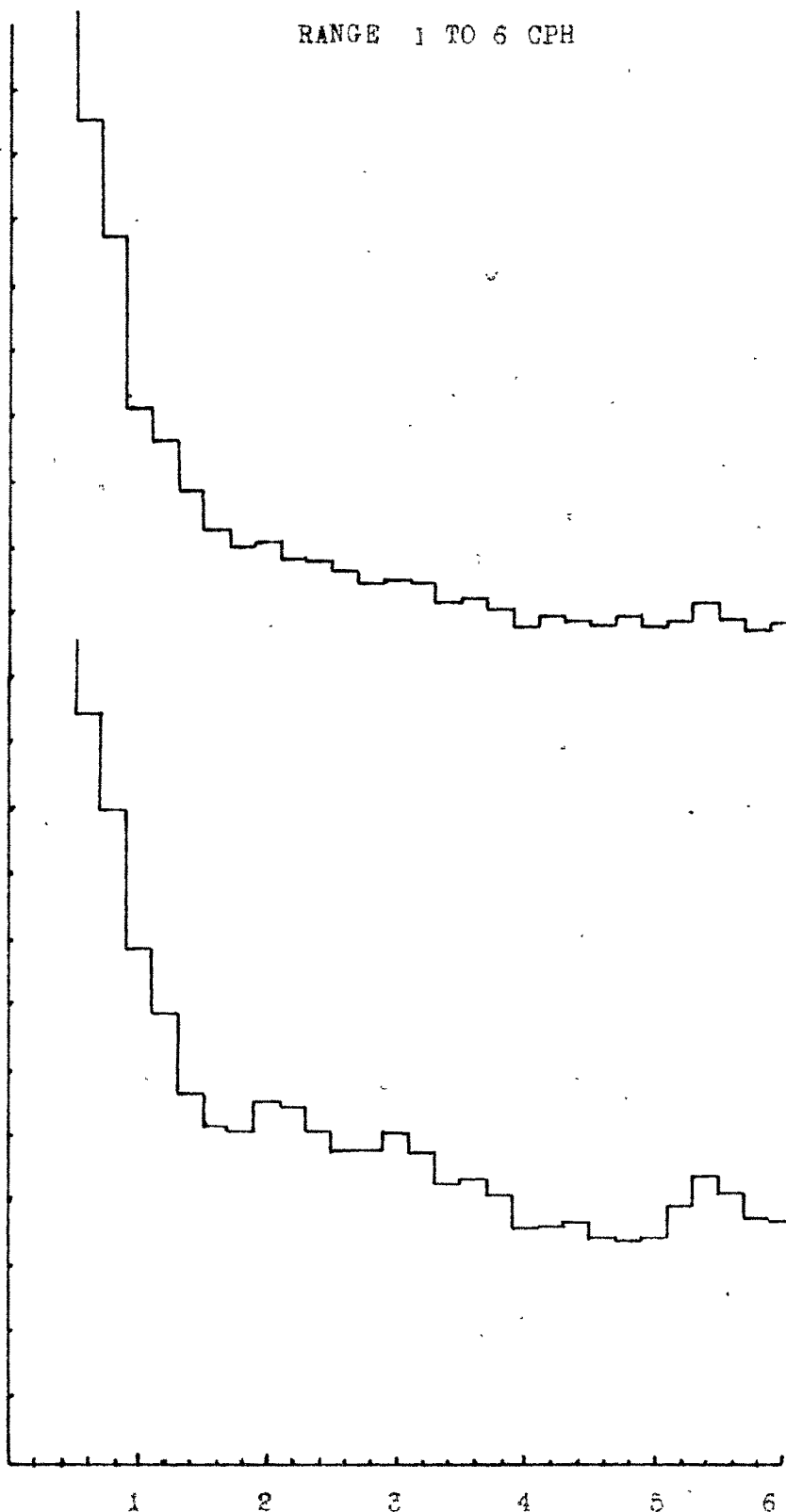
FIGURE NO. 4.3

COSMIC RAY POWER DENSITY ESTIMATES

RANGE 1 TO 6 CPH

POWER DENSITY (ARBITRARY UNITS)

5.0
4.0
3.0
2.0
1.0
5.0
4.0
3.0
2.0
1.0



109
SAMPLES
SUPERPOSED

48
SAMPLES
SUPERPOSED

CYCLES PER HOUR

comprising a day are superposed, the peaks are observed more or less at the same frequencies, as shown in Figure 4.2. As more and more samples are superposed, the spectral activity is smeared out. This is shown in figure 4.3. No peaks in the spectral density estimates are found to be significant for 48 samples from day No.414 to 427, and for 109 samples from day No.359 to day No.427. No particular selection criteria are fixed for superposing the samples.

Hence in the range of 1-6 CPH, frequencies at 3 and 5 CPH are found to be prominent for a single 6 hourly sample, but over an extended period, these tend to cancel out. So there are no preferred frequencies in this frequency range over an extended period of time.

The investigations are extended to the range of 1 to 30 CPH, using samples of 3 hourly interval, and 1 CPH frequency resolution. Figure 4.4 shows the superposed spectral estimates of 487 three hourly samples indicated by the lower-most graph. No particular selection rule is applied for the choice of the samples, and they are taken from the continuous data from day No.325 to 439. Only those samples are rejected where one of the channels is not working properly or certain discontinuities have occurred in the data. Each sample has 11 degrees of freedom, thereby making 5357 for the superposed graph.

FIGURE NO. 4.4

COSMIC RAY POWER DENSITY ESTIMATES 1970-1971

- (1) 487 SAMPLES SUPERPOSED
- (2) 547 SAMPLES SUPERPOSED
- (3) 1034 SAMPLES SUPERPOSED (1+2)

POWER DENSITY PER CYCLE OBSERVATION

780
760
740
720
700
680
730
710
690
740
720
700
680

5 10 15 20 25 30

CYCLES PER HOUR

16
27

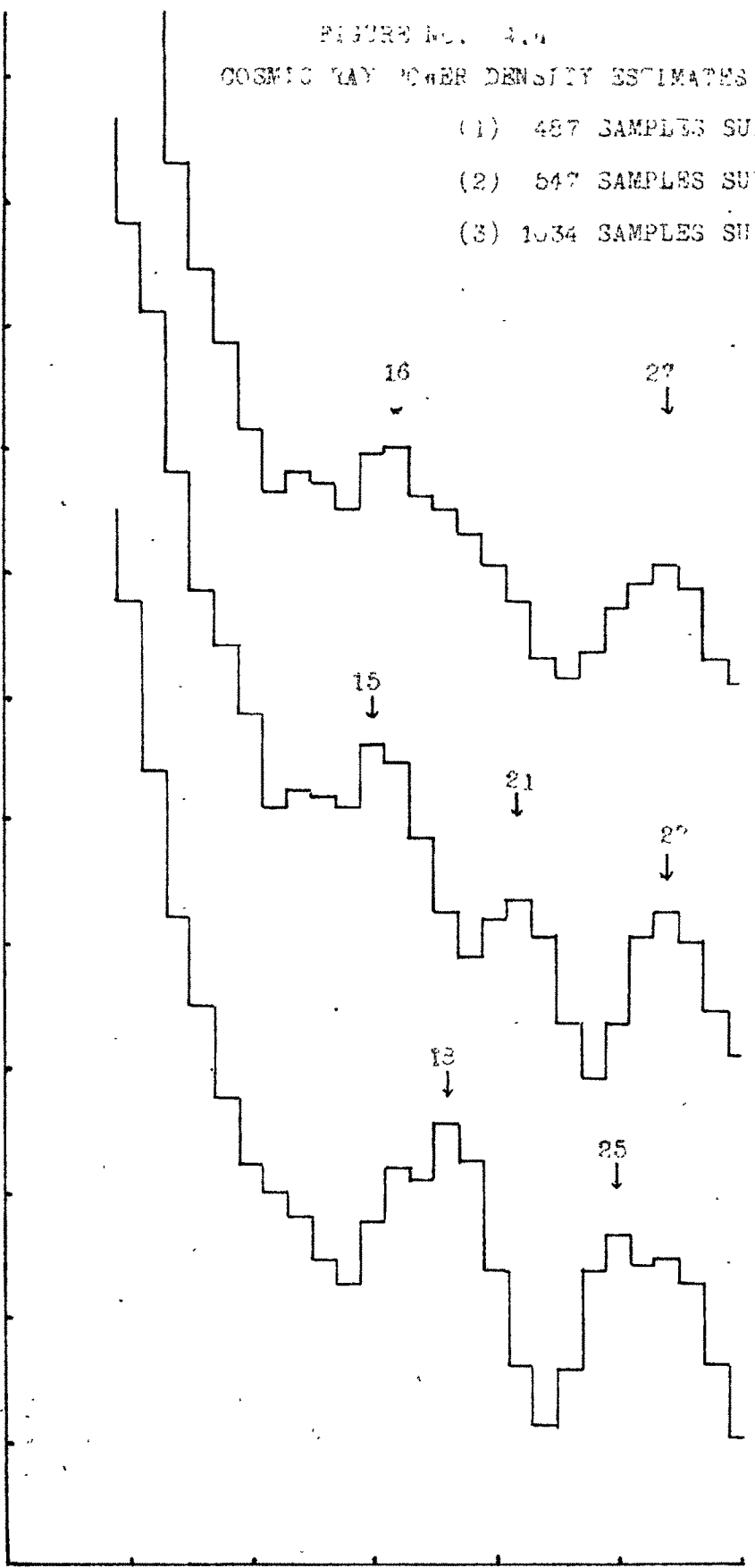
15
21
27

13
25

(3)
99%
CONFIDENCE
LIMITS

(2)
99%
CONFIDENCE
LIMITS

(1)
99%
CONFIDENCE
LIMITS



Applying the significance test, we find that 18 CPH group (200 sec.period) and 25 CPH group (144 sec.period) are significant at 99% level. The 18 CPH group has alongside another frequency of 16 CPH. and 25 CPH group has 27 CPH, which are equally significant.

The spectral estimates for 547 samples from day No. 440 to 531 are superposed and the graph shown in figure 4.4. Peaks, significant to the same level are observed at 15, 21 and 27 CPH. The frequencies in the present case are slightly different from the previous graph of 487 superposed samples.

Extending the above results, the operation of superposition is completed for the total number of samples. Figure 4.4 shows the spectral estimates for 1034 samples from day No.325 to 531. Significant peaks are observed at 16 and 27 CPH.

Since certain frequencies are found to be persistent over long periods of time, it may be of interest to investigate if these have certain preferred directions. The time dependence of a frequency is found by obtaining eight sets of spectral density estimates having superposed three hourly samples of similar timing, that are spaced as 0-3, 3-6, 6-9, 9-12, 12-15, 15-18, 18-21, 21-24 hours. The eight values of the spectral density estimates so obtained for a particular frequency are subjected to harmonic analysis after finding the deviations from the mean of the eight

values. Thus, the amplitude (r_1) of the diurnal wave and its direction (ϕ_1) of maxima for the particular frequency are calculated. The values of r_1 and ϕ_1 are considered for the prominent frequencies, and are shown in table No.4.1.

Table No.4.1

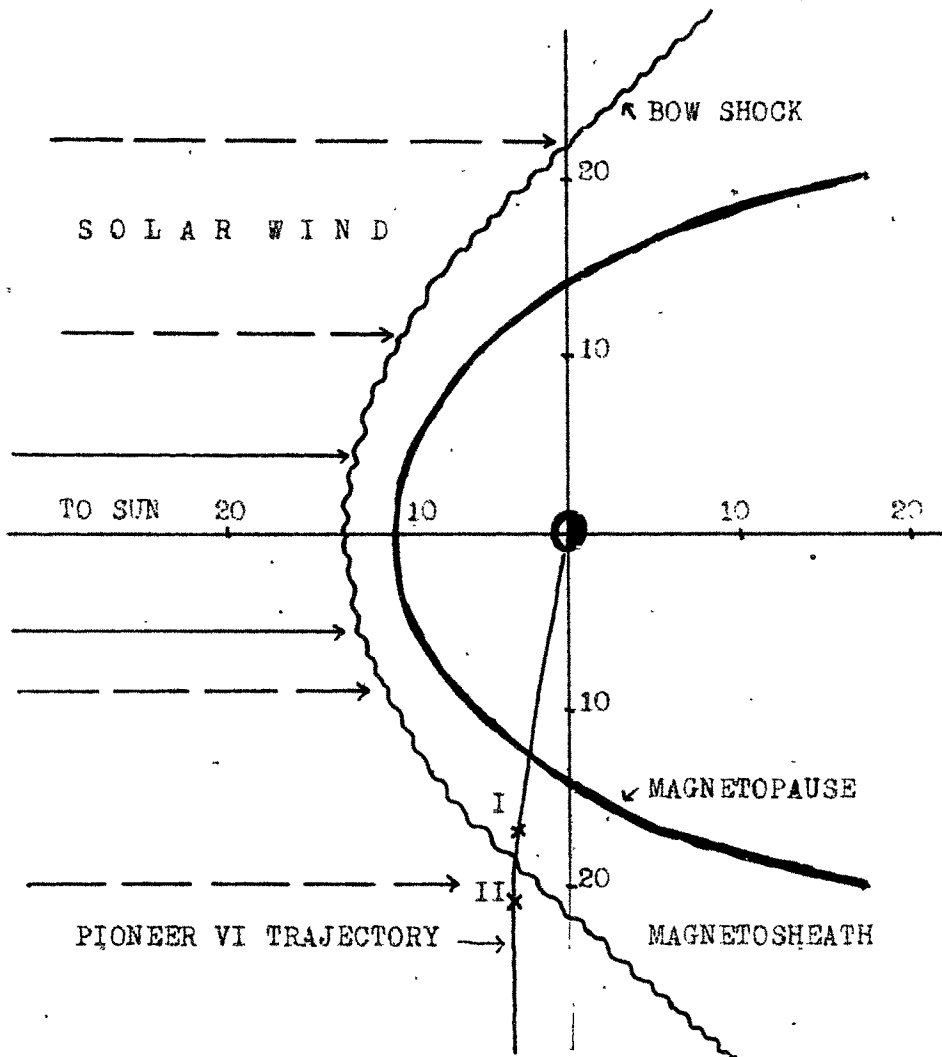
No. of Samples	Prominent frequencies	Amplitude in %	r_1 in%	ϕ_1 (local time)
487 (day 325 to 439)	18 CPH	.035 \pm .0005	3.3 \pm .6	39 ^o
	25 CPH	.035 \pm .0005	3.5 \pm .6	42 ^o
547 (day 440 to 531)	15 CPH	.035 \pm .0005	7.2 \pm .6	280 ^o
	21 CPH	.035 \pm .0005	1.0 \pm .6	356 ^o
	27 CPH	.035 \pm .0005	4.4 \pm .6	297 ^o
1034 (combina- tion of the above two) (day 325 to 531)	16 CPH	.035 \pm .00036	2.0 \pm .4	247 ^o
	27 CPH	.035 \pm .00036	1.0 \pm .4	236 ^o

It can be seen that the directions are not consistent for both the sets.

4.4. Comparison of cosmic ray frequencies with the frequencies found in magnetic field measurements by Pioneer VI, Range 1-30 CPH:

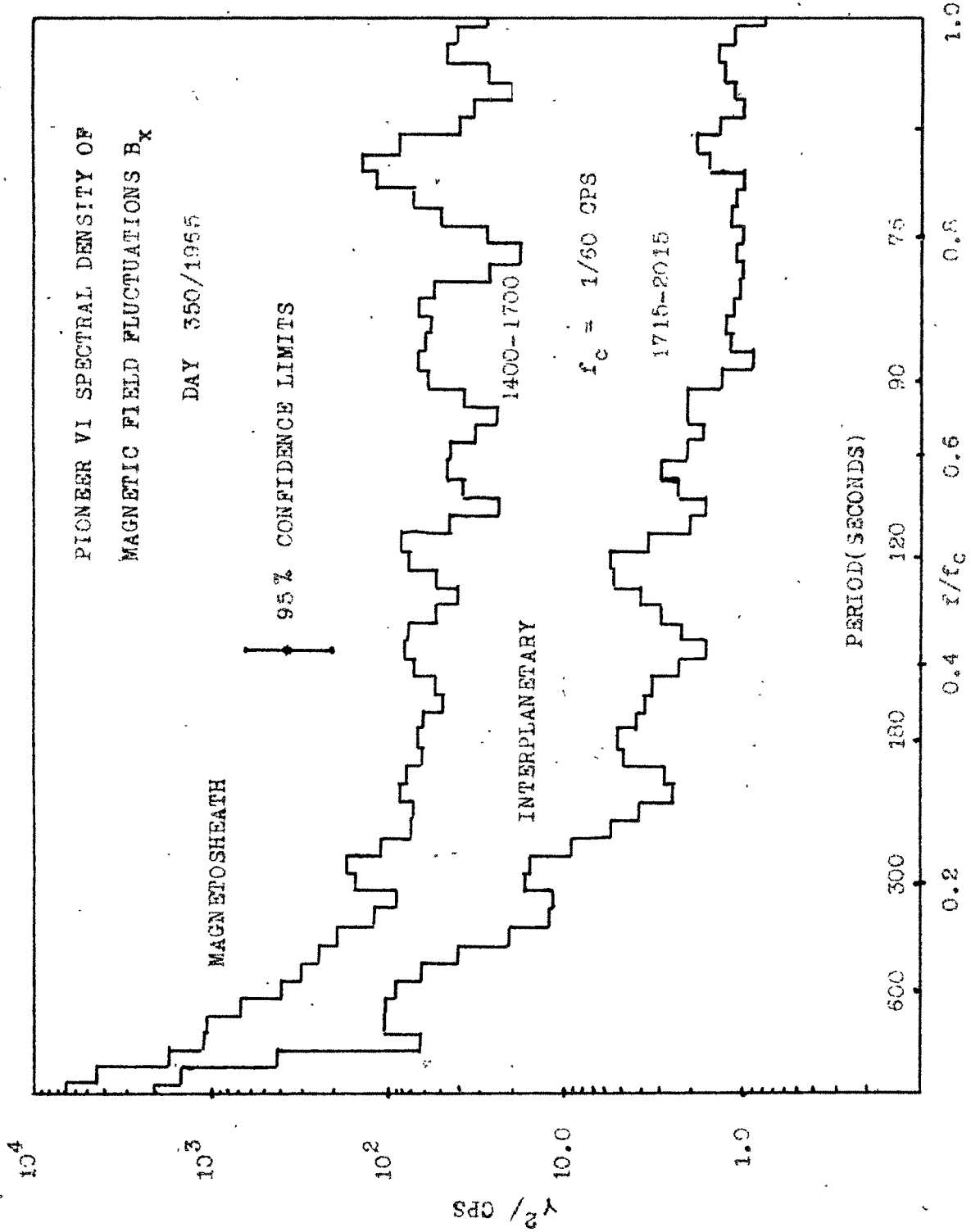
Ness et al (1966) have detected certain frequencies in the magnetic field fluctuations in the magnetosheath

FIGURE NO. 4.5



POSITION OF PIONEER VI DURING THE TIME OF MAGNETIC
FIELD MEASUREMENTS (REPORTED BY NESS ET AL 1963)

FIGURE NO. 4.6

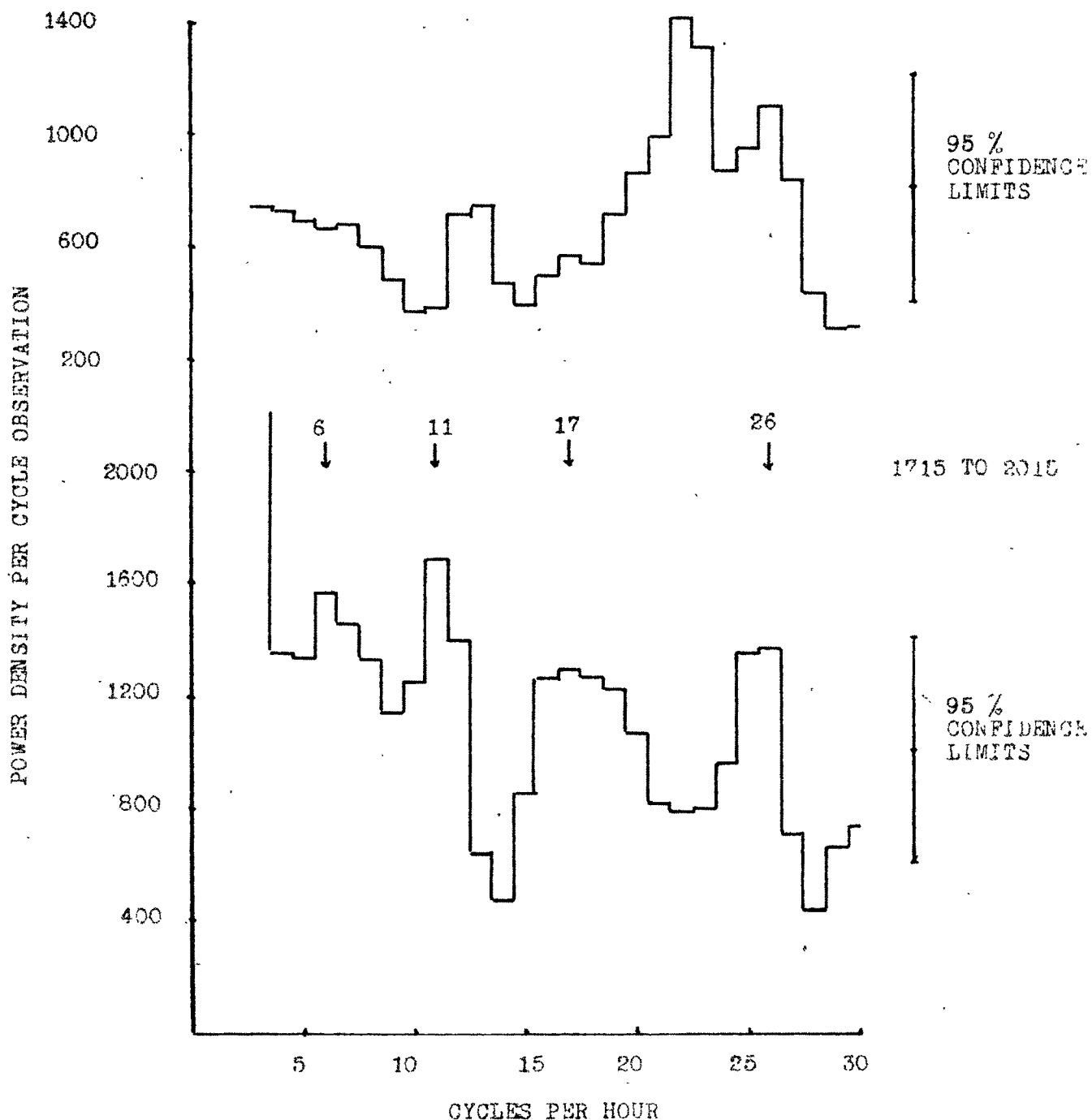


(FROM NESS ET AL 1956)

FIGURE NO. 4.7

SPECTRAL DENSITY OF COSMIC RAY FLUCTUATIONS FOR THE SAME
THREE HOURLY PERIODS FOR WHICH SPECTRAL DENSITY OF MAGNETIC
FIELD FLUCTUATIONS IS REPORTED BY NESS ET AL.

DAY NO. 350
DEC 16, 1965
1400 TO 1700



and in the interplanetary space recorded by Pioneer VI during its outward journey. The position of the satellite during the time of measurements is shown in Figure 4.5.

During the interval 1400 to 1700 hour, the satellite was inside the magnetosheath indicated by position I in the diagram, and during 1715 to 2015 hours (position II) it was outside the bow shock, in the interplanetary space.

The data of the magnetic measurements for the three hourly intervals have been subject^{ed} to power spectrum analysis by Ness et al (1966) and the two graphs of the spectral density estimates are shown in figure 4.6 (from Ness et al 1966).

For the same three hourly intervals from 1400 to 1700 hours, and 1715 to 2015 hours U.T. on December 16, 1965, day No.350, the cosmic ray data are also subjected to power spectrum analysis and spectral densities are calculated. The spectral density estimates for 1715 to 2015 hour sample are plotted in Figure 4.7. and are shown in the lower graph. In the graph statistically significant spectral peaks are observed at 6, 11, 17 and 26 cycles per hour. For the sample, 1400 to 1700 hour, shown in the upper graph in the same figure, significant frequencies are at 13, 22 and 26 CPH. The significance level and the amplitude for each prominent cosmic ray frequency are given in the following table.

Fig.No. 4.8 Comparison of spectral density peaks of cosmic rays for a three hourly sample from 1400 to 1700 hours Dec.16, 1965, with the spectral density peaks of the magnetosheath field fluctuations for the simultaneous period.

Fig.No. 4.9 Comparison of spectral density peaks of cosmic rays for a three hourly sample from 1715 to 2015 hours Dec.16, 1965, with the spectral density peaks of the interplanetary field fluctuations for the simultaneous period.

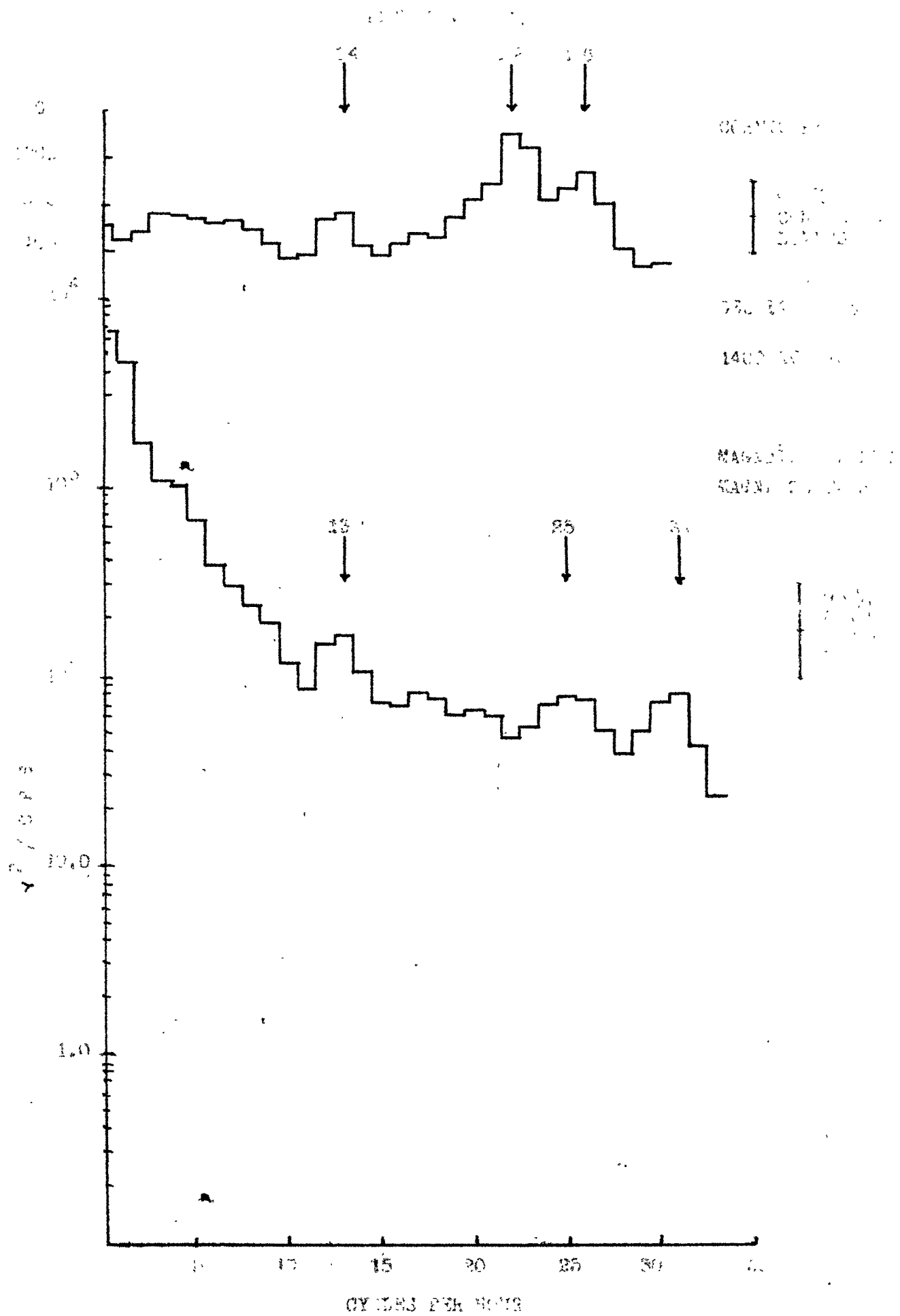
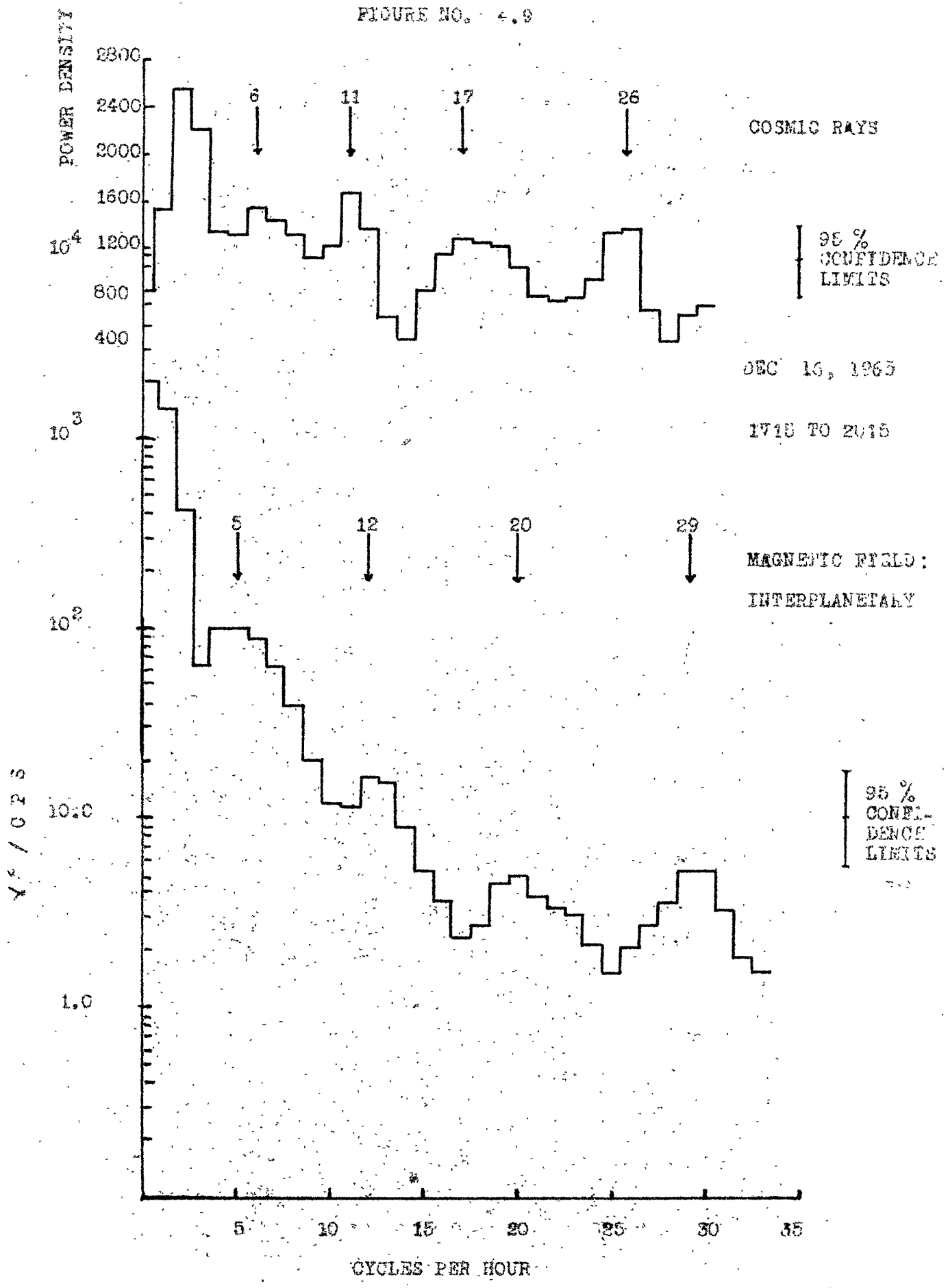


FIGURE NO. 4.9



COSMIC RAYS

95 %
CONFIDENCE
LIMITS

DEC 16, 1965

1715 TO 2015

MAGNETIC FIELD:
INTERPLANETARY

95 %
CONFIDENCE
LIMITS

Table No. 4.2

<u>Interval</u>	<u>Prominent frequencies</u>	<u>Significance level %</u>	<u>Amplitude %</u>
1715 to 2015	6 CPH	90	.051 ± .01
	11 CPH	90	.052 ± .01
	17 CPH	95	.047 ± .01
	26 CPH	95	.048 ± .01
1400 to 1700	13 CPH	90	.035 ± .01
	22 CPH	95	.049 ± .01
	26 CPH	95	.043 ± .01

Figure 4.8 shows the comparison of the spectral density estimates of cosmic ray intensity and the simultaneous spectral estimates of the magnetosheath field measurements for the interval from 1400 to 1700 hours. Figure 4.9 shows, similarly, cosmic ray spectral estimates and simultaneous spectral estimates of the interplanetary field measurements for the interval from 1715 to 2015 hours. It can be seen that cosmic rays as well as the interplanetary and magnetosheath magnetic fields have prominent frequencies in the same range, which are statistically significant.

4.5 Behaviour of cosmic ray frequencies in different interplanetary conditions

4.5.1 Condition of increase and decrease of cosmic ray intensity:

A histogram can be drawn of the percentage changes of the daily mean intensity of Deep River neutron monitor.

FIGURE NO. 4.10
 INTENSITY PLOT, DEEP RIVER NEUTRON MONITOR RECORDINGS FROM NOV. 1965 TO JUNE 1966
 (DAILY MEAN INTENSITY)

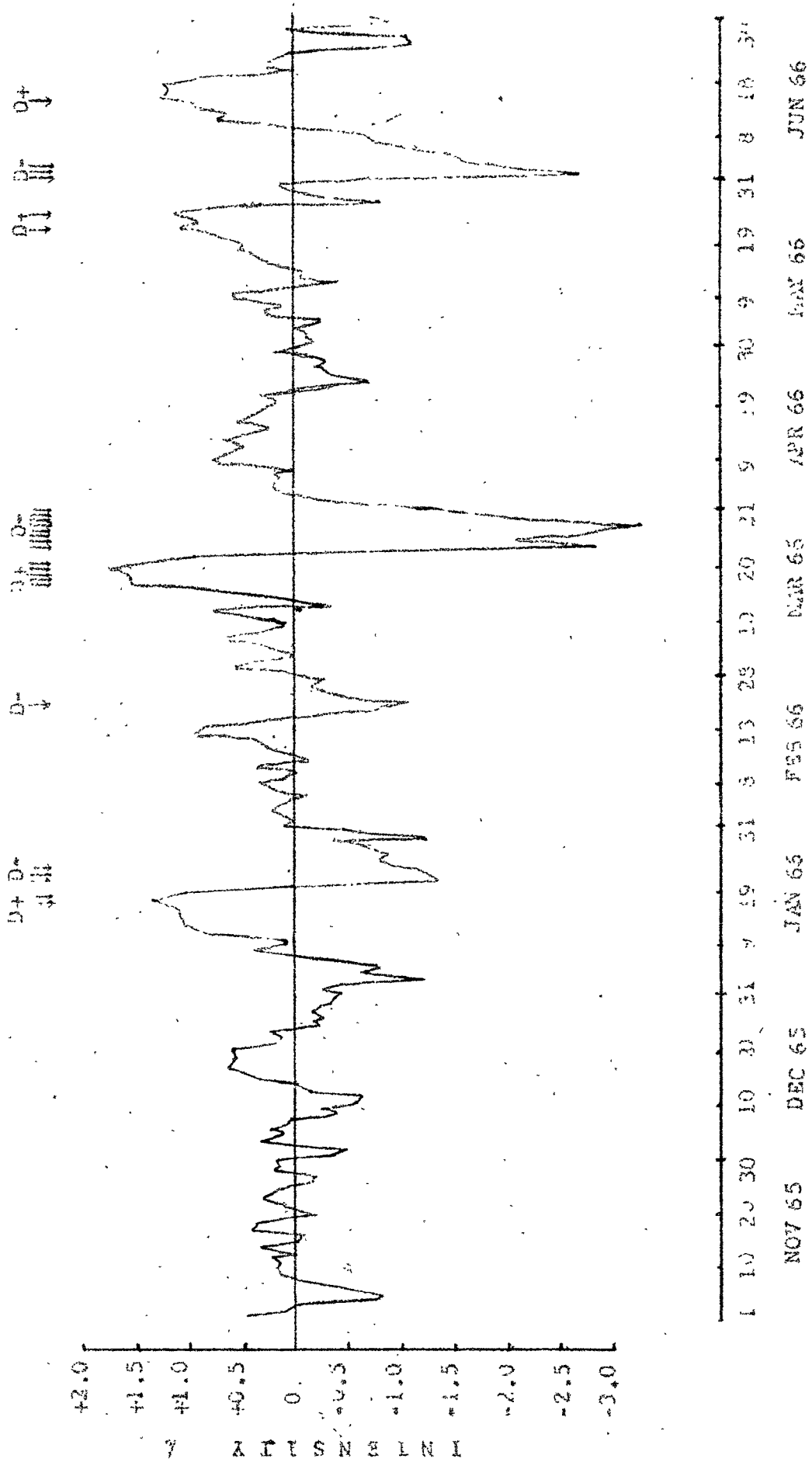
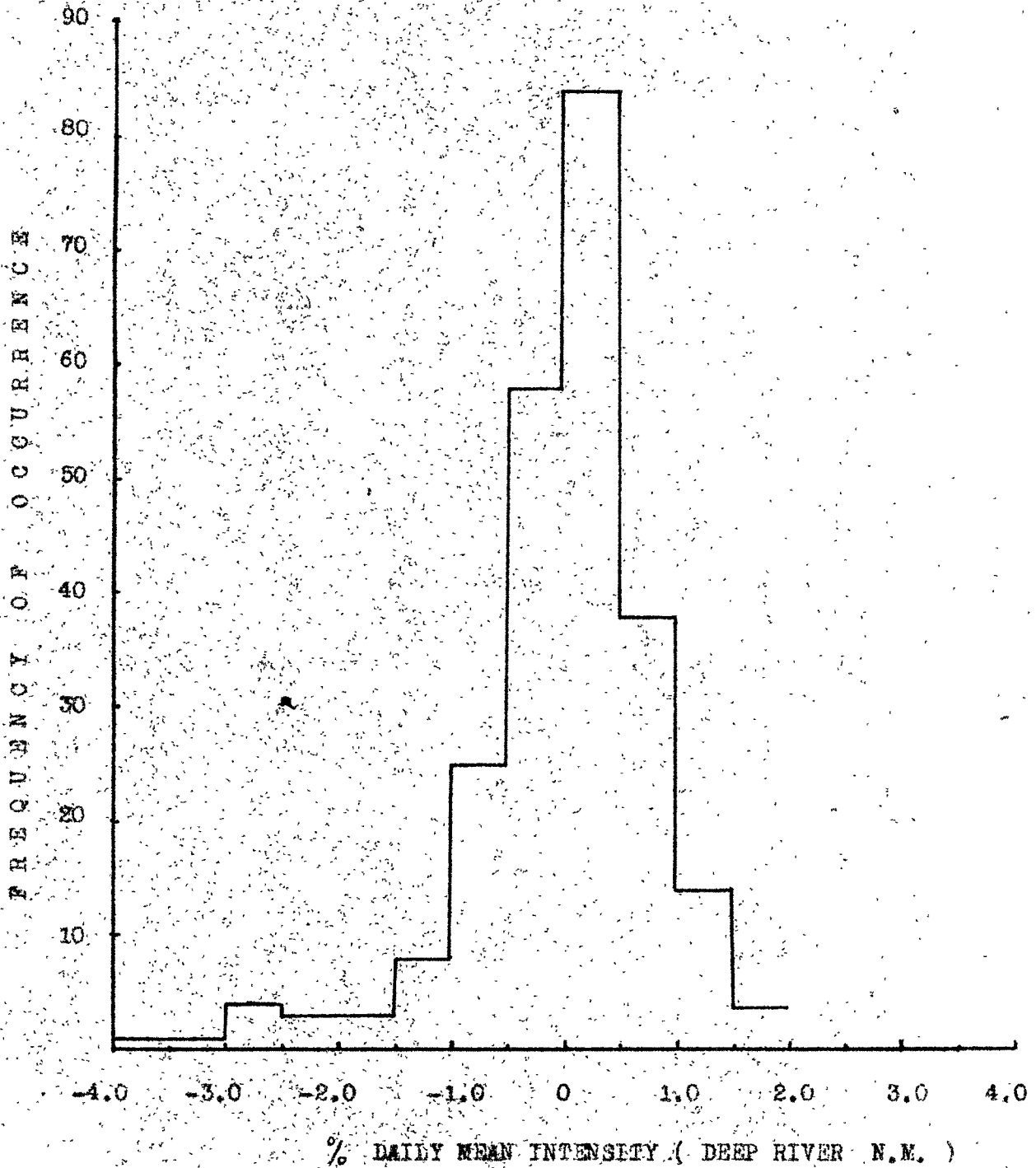


FIGURE NO. 4.11

HISTOGRAM SHOWING THE DISTRIBUTION OF THE PERCENTAGE CHANGES OF THE DAILY MEAN INTENSITY OF DEEP RIVER NEUTRON MONITOR FROM NOV. 1965 TO JUNE 1966 (PLOTTED IN FIGURE 4.10).



The data used for this purpose extends from November 1965 to June 1966. The plot of the intensity is shown in Figure 4.10 and the distribution in figure 4.11. The following six epochs are fixed according to the criteria given below:

Daily mean intensity range from:

(1)	-1.0 or lower	designated as	Disturbed Day	D(-)
(2)	-0.5 to -1.0	" "	Semi-disturbed Day	SD(-)
(3)	0 to -0.5	" "	Quiet Day	Q(-)
(4)	0 to 0.5	" "	" "	Q(+)
(5)	0.5 to 1.0	" "	Semi-disturbed Day	SD(+)
(6)	1.0 or higher	" "	Disturbed Day	D(+)

The days for epochs D(-) and D(+) are indicated in Figure 4.10.

The spectral estimates of the three hourly samples in the days of the particular epoch are superposed. The three graphs for the particular negative epochs are shown in Figure 4.12. Similar graphs for positive epochs are shown in Figure 4.13.

From the superposed spectral power estimates for each of the epochs, average power for the frequencies from 6 to 30 CPH is calculated. This can be a good indicator of the general behaviour of the frequencies in the said epoch.

In the following table are shown the average power for 6-30 CPH for each of the six epochs, the prominent

FIGURE NO. 4.12

SUPERPOSED SPECTRAL DENSITY ESTIMATES (COSMIC RAYS)
FOR THE THREE NEGATIVE INTENSITY CHANGE EPOCHS.

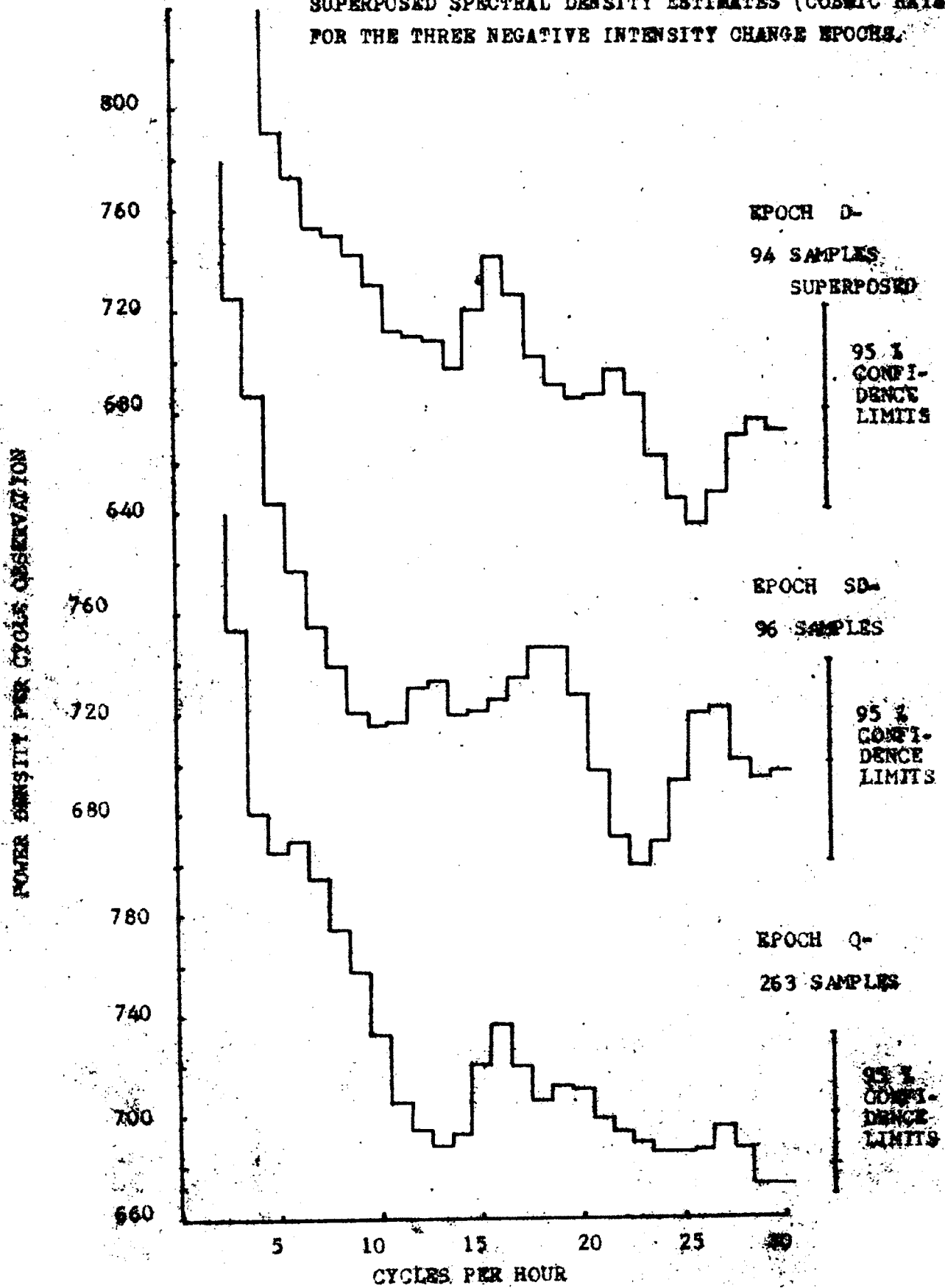


FIGURE NO. 4.13

SUPERPOSED SPECTRAL DENSITY ESTIMATES (COSMIC RAYS)
FOR THE THREE POSITIVE INTENSITY CHANGE EPOCHS

820

780

740

700

660

620

800

760

720

680

640

780

740

700

660

EPOCH D+

75 SAMPLES

SUPERPOSED

95 %
CONFIDENCE
LIMITS

EPOCH SD+

214 SAMPLES

95 %
CONFIDENCE
LIMITS

EPOCH Q+

292 SAMPLES

95 %
CONFIDENCE
LIMITS

5

10

15

20

25

30

CYCLES PER HOUR

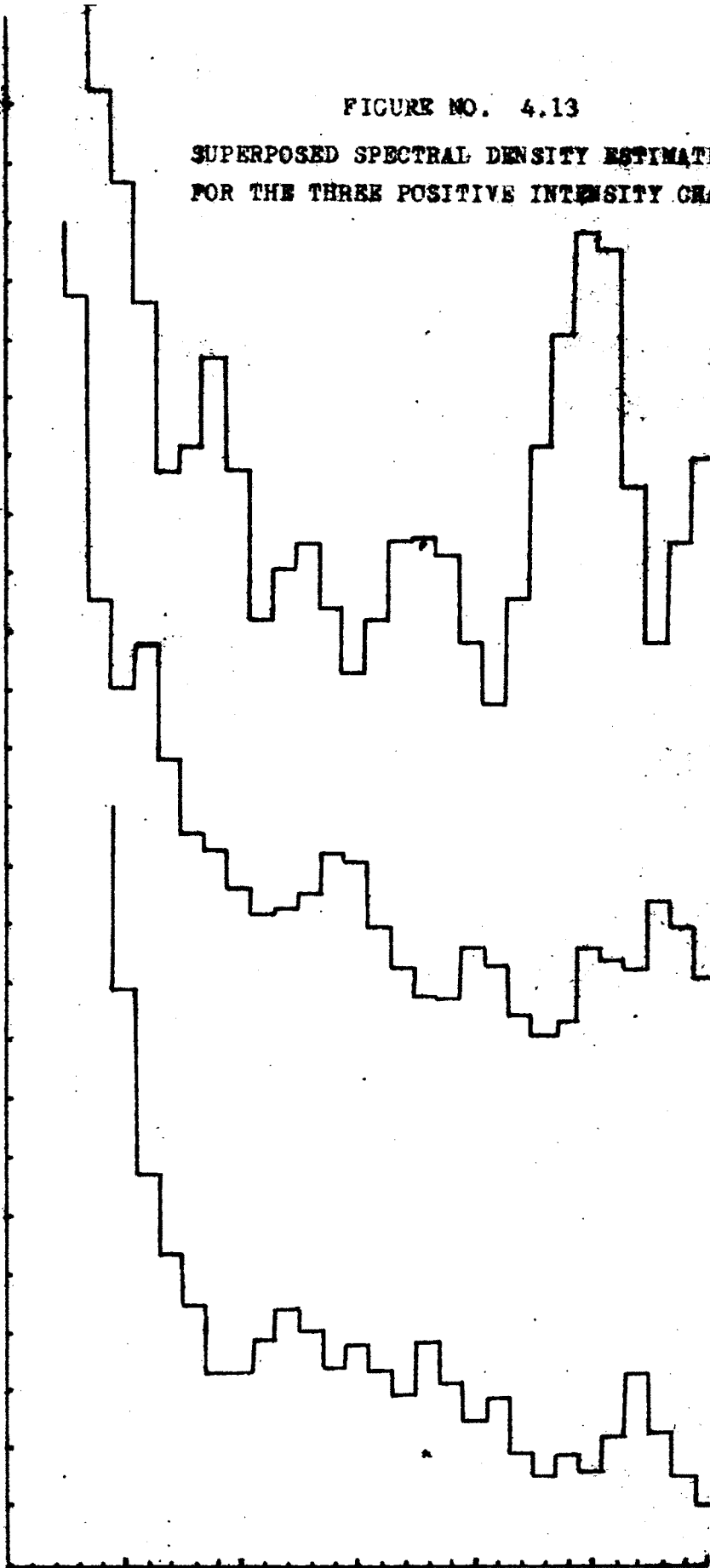
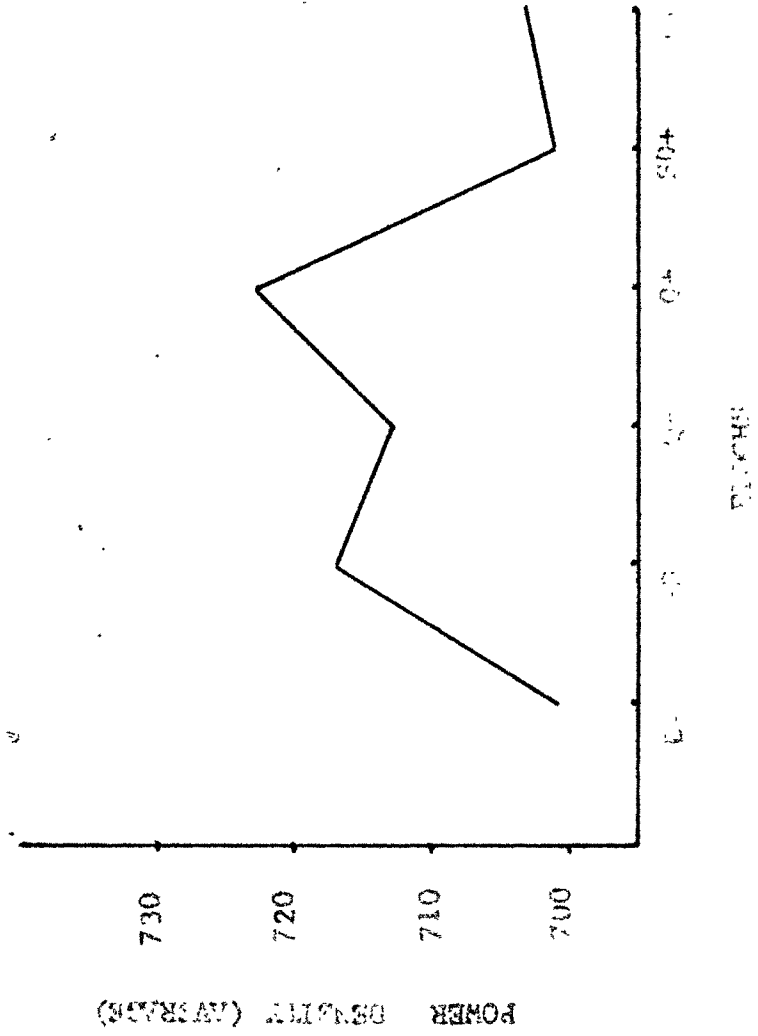


FIGURE NO. 14

AVERAGE POWER CHARACTERISTICS OF 6 TO 30 CPH
FOR DIFFERENT INTENSITY CHANGE EPOCHS
(COSMIC RAYS)



frequencies together with their significance levels and the amplitudes.

Table No. 4.3a

Epoch	No. of samples	Average power	A^2 / cycle obs.	Prominent Freq.	Signifi- cance %	Amplitude in %
			6-30	CPH		
D(-)	94	701		16 CPH	95	.035 ± .0010
SD(-)	96	717		18 CPH	95	.034 ± .0010
				27 CPH	95	.034 ± .0010
Q(-)	343	713		16 CPH	90	.034 ± .0006
Q(+)	292	723		27 CPH	90	.034 ± .0005
SD(+)	214	701		6 CPH	90	.036 ± .0007
				14 CPH	90	.034 ± .0007
D(+)	75	703		9 CPH	90	.035 ± .0012
				13 CPH	90	.035 ± .0012
				18 CPH	95	.030 ± .0012
				25 CPH	99	.036 ± .0012

In the epochs D(-) and D(+), although, the average power is almost the same, the spectral frequencies in D(+) are much more prominent than in D(-).

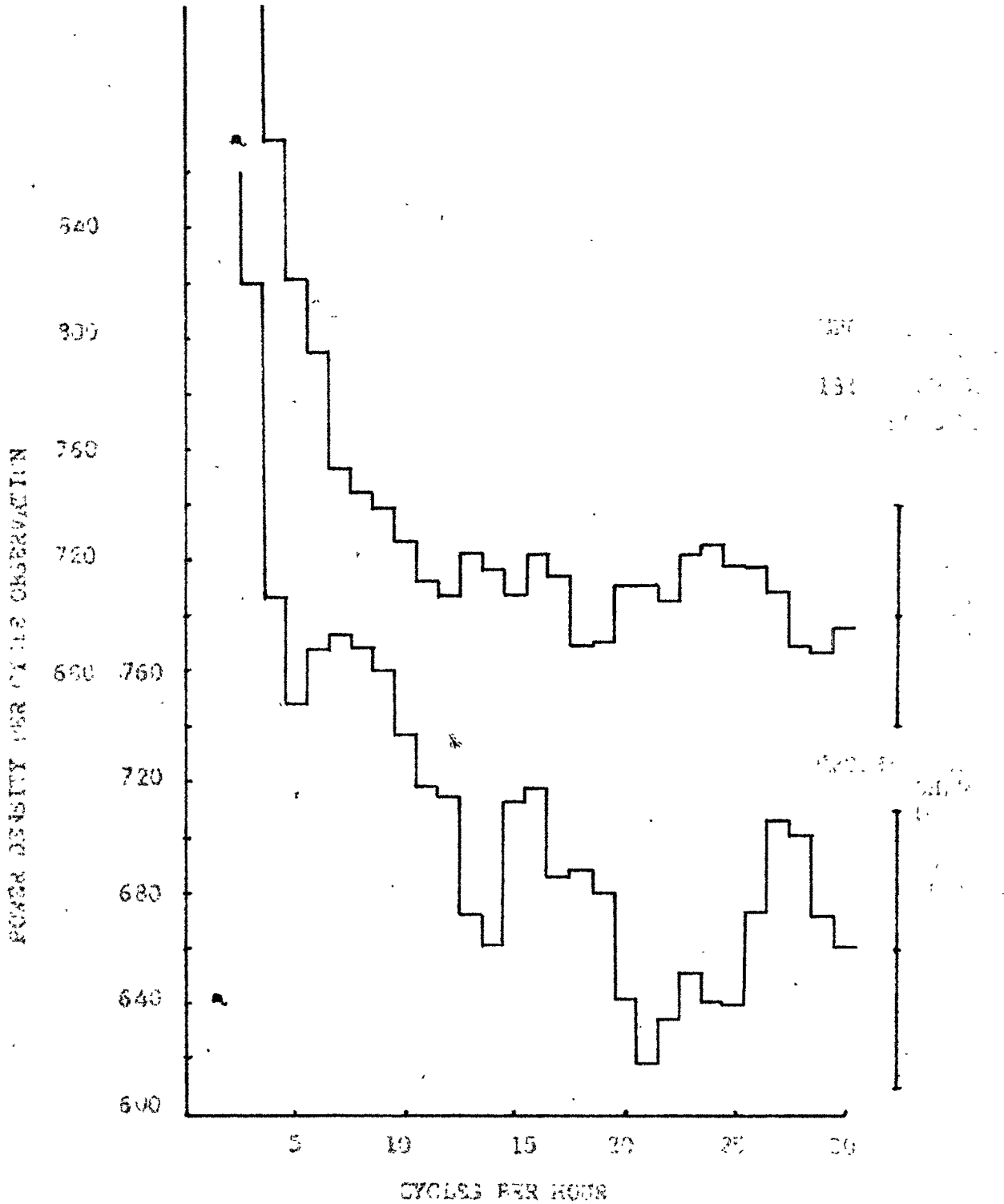
The average characteristics for the epochs for 6-30 CPH range of frequencies are shown in figure 4.14. It can be seen that the average power for the frequency range 6-30 CPH is lower for epochs of large intensity compared with epochs of low intensity.

4.52 Fast and slow changes in interplanetary conditions:

The fast change epoch day is the one when the change

FIGURE NO 4.15

SUPERPOSED SPECTRAL DENSITY ESTIMATES (COSMIC RAYS)
FOR FAST CHANGE AND SLOW CHANGE EPOCHS.



of intensity δ I is greater than or equal to -0.5% . For slow change epoch, over three successive days a cumulative change of $\pm 0.5\%$ or more has occurred but not more than $\pm 0.5\%$ for any particular day.

To determine the nature of short period variations during the epochs, Deep River Neutron Monitor daily averaged values from November 1965 to June 1966 are taken and two epochs are fixed incorporating the above mentioned criteria.

The days of the fast change epoch are grouped together and the spectral density estimates of the three hourly samples for these days are superposed. Similarly, the spectral estimates lying in slow change epoch are also superposed. The two graphs are shown in Figure 4.15. The average power in the range of 6-30 CPH is calculated for the two type of epochs. This together with the prominent frequencies, and their characteristics are given in the following table:

Table No. 4.3 b

Epoch	No. of samples	Ave. Power 6-30 CPH $A^2/Cy. Obs.$	Prominent frequency	Confidence level %	Amplitude in %
Fast change	104	693	15 CPH	95	.0340 \pm .001
			16 CPH	95	.0345 \pm .001
			27 CPH	95	.0342 \pm .001
			28 CPH	95	.0340 \pm .001
Slow change	181	718	none		

Prominent frequencies are observed in the fast change condition. In the slow change condition the average power is high and since all frequencies are active no peaks stand out over the background.

4.53 Forbush decrease:

We investigate here the behaviour of the spectral density estimates during a Forbush decrease. We would be interested in finding out the prominent frequencies during pre-onset, onset and post-onset phases of a Forbush decrease and also the effect of these phases on the average power density from 6 to 30 CPH. For this purpose three Forbush decreases are selected. Their characteristics are given in the following table.

Table No. 4.4

<u>Sr.No.</u>	<u>Date of occurrence</u>	<u>Day No.</u>	<u>Time of onset</u>	<u>Intensity decrease at Deep River N.M.</u>
1	23 Mar., 66	447	9 hours	5 per cent
2	26 May, 66	511	20 hours	2 per cent
3	31 May, 66	516	20 hours	3 per cent

The third Forbush decrease of 31 May, 66 occurred during the recovery phase of the Forbush decrease of 26 May, 66.

Taking an epoch of six samples from the time of onset of the Forbush decrease, the spectral density

FIGURE NO. 4:16a

SUPERPOSED SPECTRAL DENSITY ESTIMATES (COSMIC RAYS)
FOR THE DIFFERENT PHASES OF:
FORBUSH DECREASE OF MARCH 23, 1966

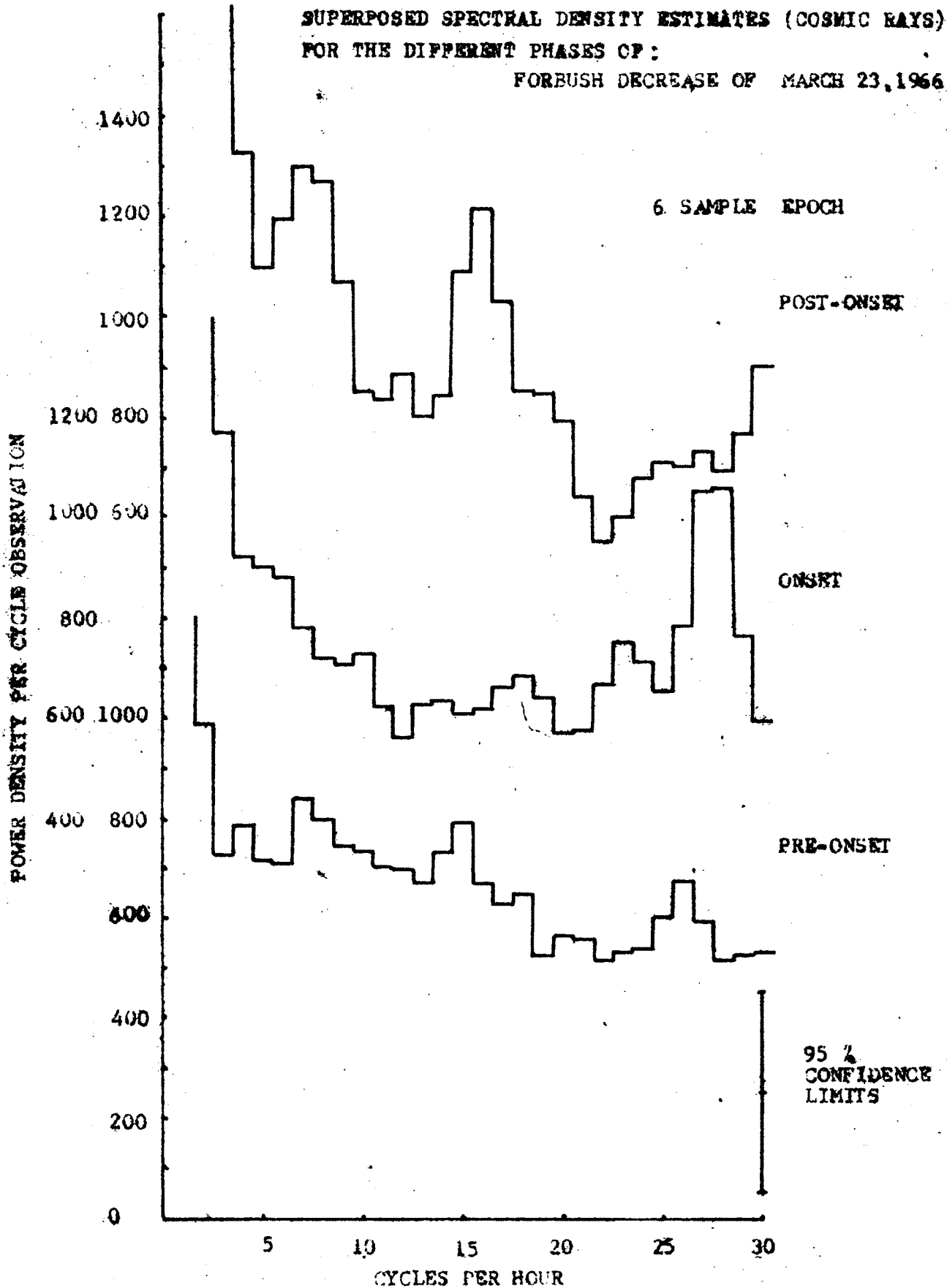


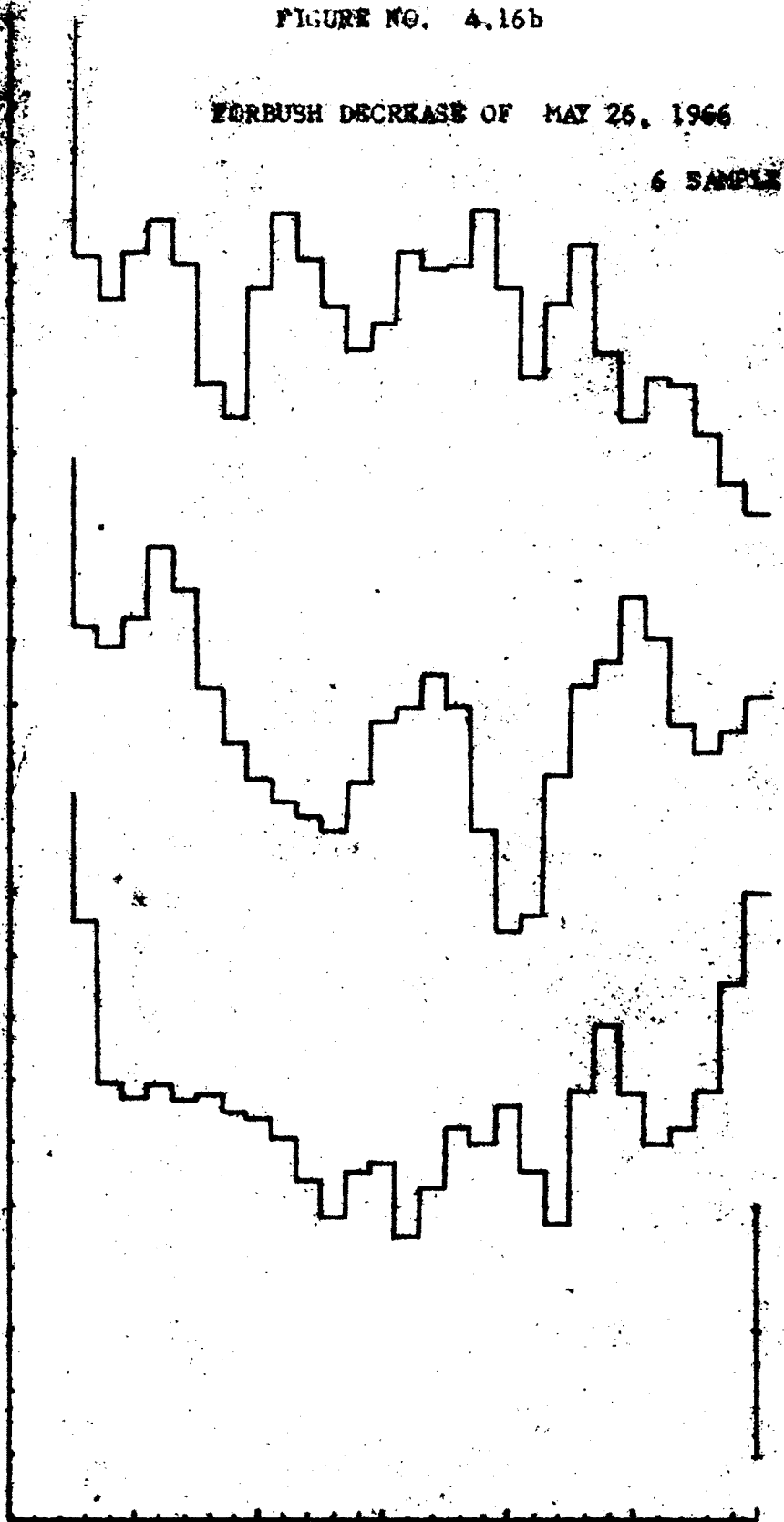
FIGURE NO. 4.16b

FORBUSH DECREASE OF MAY 26, 1966

6 SAMPLE EPOCH

POWER DENSITY PER CYCLE OBSERVATION

1000
800
600
400
200
0



POST-ONSET

ONSET

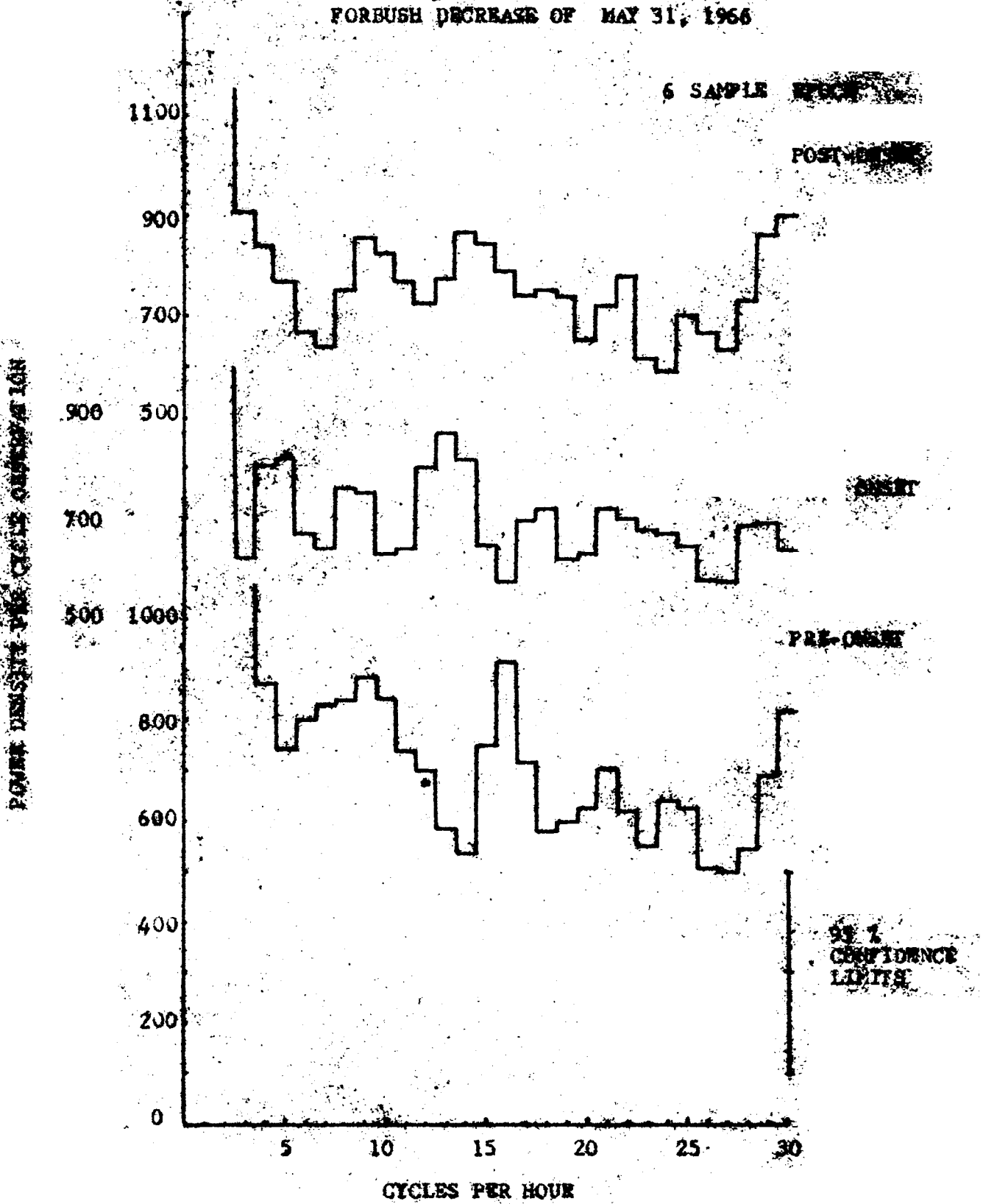
PRE-ONSET

95%
CONFIDENCE
LIMITS

CYCLES PER HOUR

FIGURE NO. 4.16c

FORBUSH DECREASE OF MAY 31, 1968



estimates for each sample are superposed. The process of superposition is also carried out for the six samples in the pre-onset phase and for the six samples in the post-onset phase as well. The resultant graphs for the three Forbush decreases are shown in Figure 4.16(a, b, c.).

To ascertain the general characteristics for the frequency range of 6 to 30 CPH during a Forbush decrease, the average power for each case is calculated.

The following table shows the average power and the prominent frequencies in the onset epoch for each of the Forbush decrease. For the broad peaks the frequency range is indicated within which the frequencies are significant to the same extent.

Table No. 4.5

Desig.	Date of occurrence	Ave. power 6-30 CPH \bar{A}^2 /cy.obs.	Prominent frequencies	Confidence limits%	Amplitude %
FD-1	23 Mar., 66	705	28(27-28)CPH	95	.06±.004
FD-2	26 May, 66	656	17(15-18)CPH	95	.07±.004
			25(23-27)CPH	95	.08±.004
FD-3	31 May, 66	681	13(12-13)CPH	90	.065±.004

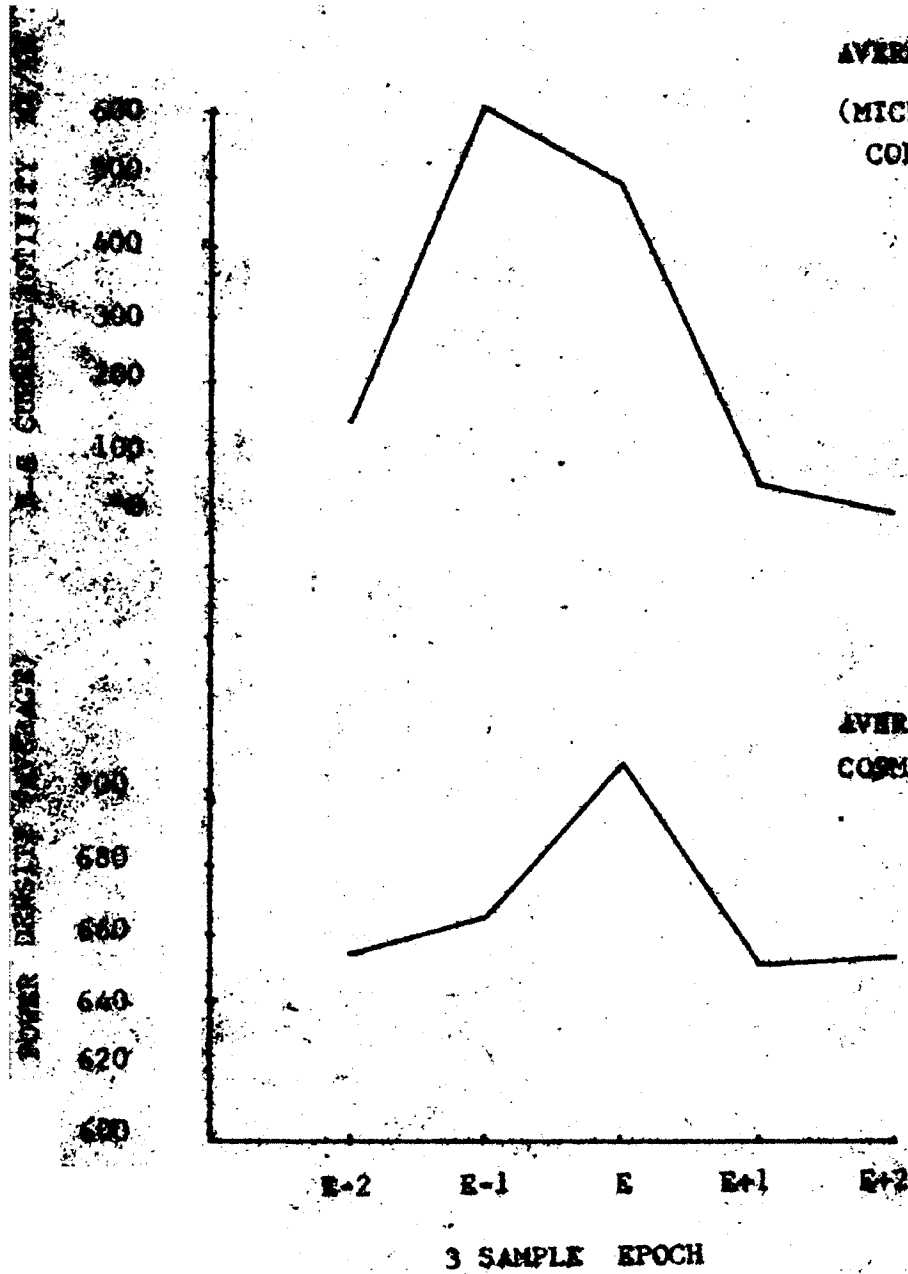
In comparing the prominent frequencies in the onset epochs for the three Forbush decreases, we find that for FD-1 which has the largest decrease, only one sharp peak is at 27-28 CPH, and FD-3 has a peak at 13 CPH.

FIGURE NO. 4.17

AVERAGE CHARACTERISTICS OF FORESHOCK DECREASE

AVERAGE TELLURIC CURRENT
(MICROPULSATIONS) ACTIVITY
COLLEGE, ALASKA

AVERAGE POWER 6 To 30 CPS
COSMIC RAYS



In considering the presence of the prominent frequencies in pre-onset, onset and post-onset phases for each of the Forbush decreases, we indicate in the following table the frequencies that are prominent to 95% confidence limits.

Table No. 4.6

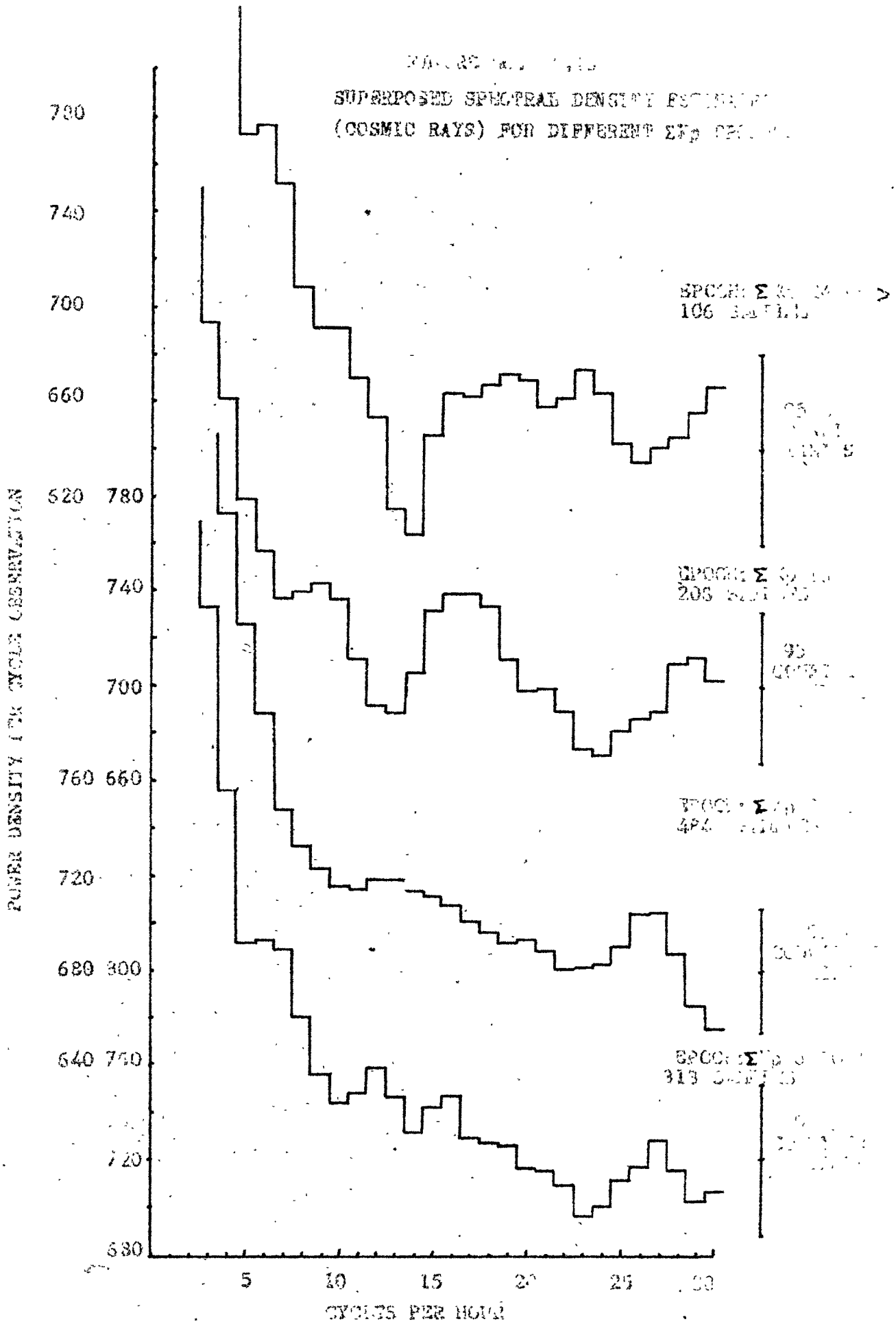
<u>Forbush decrease</u>	<u>P r o m i n e n t F r e q u e n c i e s</u>		
	<u>Pre-onset</u>	<u>onset</u>	<u>Post-onset</u>
FD-1	none	27-28 CPH	7, 16 CPH
FD-2	24 CPH	15-18 CPH 23-17 CPH	none
FD-3	16 CPH	13 CPH	none

From the above table we find that a large Forbush decrease tends to favour certain frequencies even after the onset, whereas for less intense Forbush decreases the frequencies are prominent in the onset epoch and not after that.

The average power for the frequency range from 6 to 30 CPH for three sample epochs of the three Forbush decreases is plotted in Figure 4.17. We find that the average power at the beginning and at the end epochs is less than the average power for the onset epoch. Hence there is an increase in the average power during the onset of a Forbush decrease.

The variations in the earth's magnetic field induce

FIGURE 1
 SUPERPOSED SPECTRAL DENSITY ESTIMATES
 (COSMIC RAYS) FOR DIFFERENT EMP OBSERVATIONS

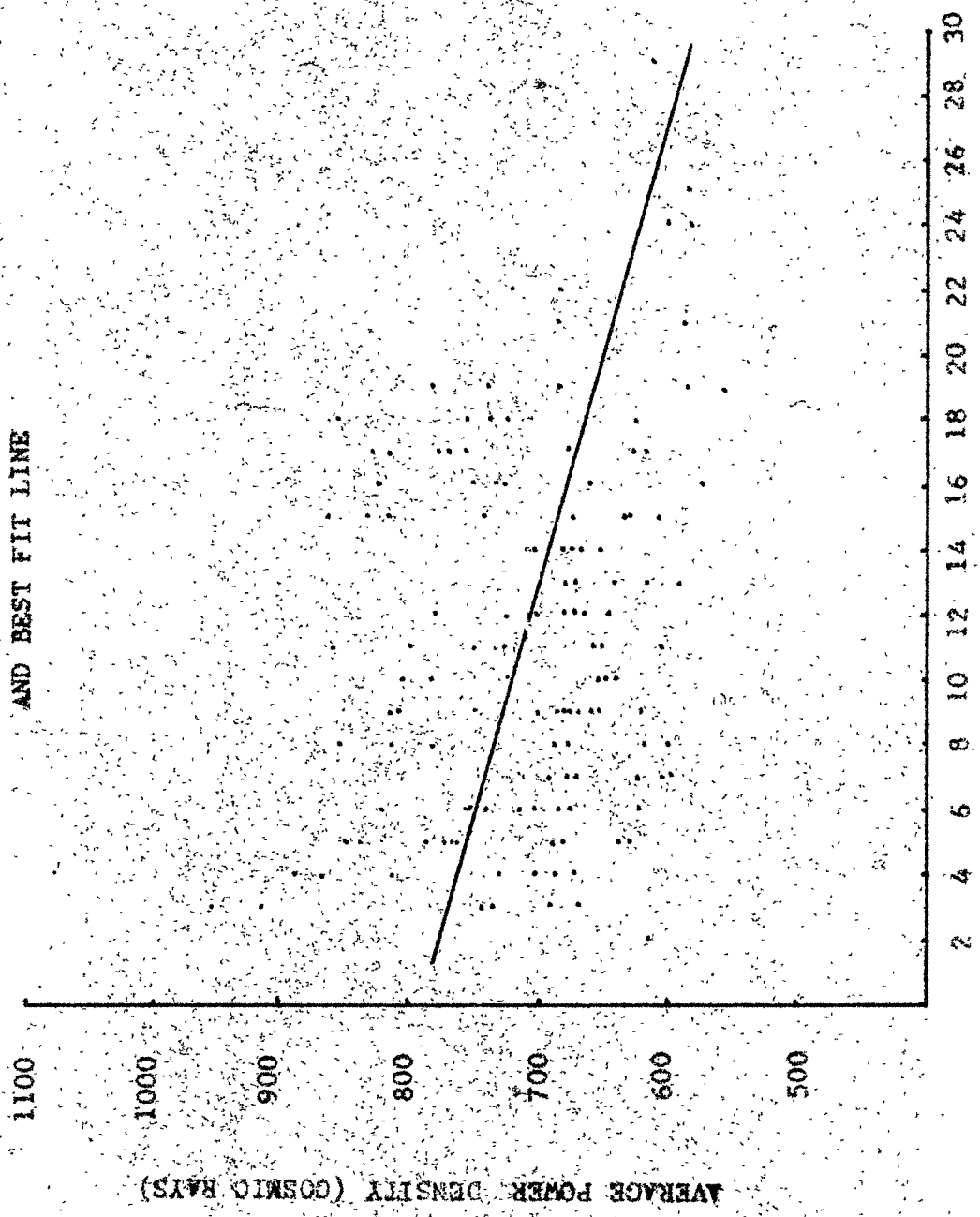


currents in the earth. Hence the Telluric currents records provide very good indication of the micropulsation activity. Taking the hourly amplitude of the N-S Telluric currents recorded at College, Alaska (Hessler 1966), the average is found out for the duration of the three samples epochs of the Forbush decreases. The plots in figure 4.17 show the strength of the current for different epochs of each of the Forbush decrease. In comparing these graphs with the ones of the average power of the cosmic ray frequencies from 6 to 30 CPH, we find that the micropulsation activity follows almost a similar pattern as that of the cosmic ray frequencies, i.e. there is a rise in the activity during a Forbush decrease.

4.6 Behaviour of cosmic ray frequencies in different ΣKp epochs:

Using daily ΣKp as an epoch parameter, days are grouped according to four classifications; the days that have ΣKp from 0 to 7, 8 to 15, 16 to 23, and 24 or higher. The spectral density estimates of the samples in the epoch days are superposed. The four graphs of the superposed estimates of each frequency are shown in Figure 4.18. The prominent frequencies in each of the epoch are shown in the following table.

SCATTER PLOT OF AVERAGE POWER 6 TO 30 CPH AND ΣKp ,
AND BEST FIT LINE



Σ Kp

Table No. 4.7

Epoch ΣKp	No. of samp- les	Average power 6 to 30 CPH	Prominent frequency	Significa- nce level %	Amplitude %
C to 7	213	736 $A^2/Cy.Obs.$	27 CPH	90	.035 \pm .0007
8 to 15	484	705 "	26 CPH 27 CPH	95	.050 \pm .0006
16 to 23	208	711 "	9 CPH 16 CPH 17 CPH 28 CPH	90 95 95	.035 \pm .0007 .050 \pm .0007 .034 \pm .0007
24 or higher	106	688	16 CPH 19 CPH 23 CPH	95	.090 \pm .001

It is observed that for the epochs with low ΣKp , 27 CPH is the only frequency that is found to be prominent; for medium $\Sigma Kp(16-23)$ prominent peaks are at 9, 16, 17 and 28 CPH. In the case of high $\Sigma Kp(>24)$ we find that frequencies from 16 to 23 CPH are prominent. Hence, there is a tendency for the peaks to be prominent during high ΣKp . In compiling the average power of the frequencies from 6 to 30 CPH, we find that the value of the power is high for the low ΣKp when compared to the average power for the high ΣKp . This is made clear in Figure 4.19 which shows a scatter plot of average power (6-30 CPH) and ΣKp . The best fit line indicates decrease in power with increase in ΣKp .

CHAPTER V

CONCLUSIONS:

In explaining the observed cosmic ray fluctuations of the order of a few minutes period, we note that the non-existence of any barometric pressure fluctuations in the frequency range under study makes it possible to conclude that the frequencies observed in the secondary cosmic rays are not due to atmospheric pressure oscillations.

The most significant evidence concerns the broadly similar fluctuations in the interplanetary magnetic field and the cosmic ray intensity when they have been simultaneously measured. Same is the case for the fluctuations of the field in the magnetosheath and the cosmic ray intensity. Though it is clear from figures 4.9 and 4.8 in Chapter IV that the correspondence for each pair of observations is not exact, the frequencies 5-6 and 11-12 GPH appear predominantly in interplanetary field and cosmic ray intensity and 13-14 GPH and 25-26 GPH are common for magnetosheath field and cosmic rays.

To explain the average amplitude of the observed cosmic ray oscillations through changes in the cut-off rigidity, we need a change of about .03% in the dipole magnetic moment. This is explained in Appendix II. The detection of geomagnetic micropulsation of the PJ 4 and PC 5 type corresponding

to the frequency range being studied in our cosmic ray investigation is consistent with the suggestion that the cosmic ray fluctuations are produced by the change of geomagnetic cut-off. Indeed, Kato (1967) has observed magneto-hydrodynamic waves of this frequency range at the geomagnetic equator. Although the H.M. waves get damped close to the earth, their amplitude in the upper part of the magnetosphere can be quite high.

According to the suggestion of Patel (1967), the magnetic moment changes could be produced by the bulk motion of the magnetosphere as described by Brice (1967). This would mean that there should be a marked local time dependence with a maximum oscillations observed when the earth is in the 15 hour direction. We have seen in Table 4.1 that there is no significant local time dependence when we consider the total data. While the hypothesis of Patel cannot be completely excluded, a direct interaction of the plasma wind with the magnetosphere is the more likely candidate to consider.

If, indeed, interplanetary magnetic field fluctuations, the oscillations of the magnetosheath field and cosmic ray fluctuations with frequencies in the 6 to 30 cycles per hour range are regarded as related to one another, it is necessary to establish a mechanism which could produce all three. An obvious process which suggests itself is that interplanetary

periodicities measured by magnetometers on space probes are most likely the result of a spatial structure in the plasma wind. For a wind with a radial velocity of 400 km/sec. the observed 18-cycle/h fluctuations correspond to a scale length of 0.5×10^{-3} A.U. of the irregularities in the plasma wind. The fluctuations of the energy density impinging on the magnetosphere resulting from these irregularities could be the means through which the periodicities are generated in the geomagnetic field.

Dhanju and Sarabhai (1967) in proposing the mechanism indicated above have also remarked on the apparently larger amplitude of the 18 cycles per hour spectral density in the cosmic ray data when the detector was looking at the anti-solar direction compared to the solar direction. This experimental result however has not stood up when more extensive data over a period of 8 months has been considered.

The frequencies of short period fluctuations which appear prominently during any particular three-hourly period vary quite markedly from period to period. It has been shown in Figure 4.4. that when spectral density estimates for large number of three hourly sets are superposed certain frequencies appear prominently and when spectral density estimates calculated from the data for all the eight months are superposed there is evidence for oscillations with the frequencies 16 and 27 CPH standing out significantly above

the other frequencies. This raises interesting implications if indeed the evidence is to be deemed as suggestive of some preferential mode for the presence of frequencies of the noted types. In order to explain the persistency of frequencies we could either attribute these to the source at the sun or due to some particular behaviour of the magnetosphere. If consideration is given to the magnetosphere, we find that the theoretical spectrum (Figure 5.1) of the magneto-acoustic oscillations of the magnetosphere shows a peak corresponding to a period of 200 seconds (Prince and Bostick 1964).

We have observed earlier in Chapter IV that there is a very interesting and significant relationship between the level of geomagnetic disturbance and the average power of the cosmic ray short period oscillations in the frequency range 6 to 30 cycles per hour. High level of geomagnetic disturbance, as characterised by K_p , is associated with a low average power of the fluctuations in cosmic rays in the 6 to 30 cycles per hour range. However, during this time, prominent peaks appear at the frequencies of 9, 17 and 28 cycles per hour. Low level of geomagnetic activity, corresponding to small K_p , is characterised by a high average power in the spectral range 6 to 30 cycles per hour and a prominent frequency only at 27 cycles per hour. We also observe that the average power is reduced during periods of large cosmic ray intensity changes. The prominent

frequencies are rather more evident in the case of positive intensity when compared to the negative intensity changes (Table No.4.3).

Howard (1967) has recently summarised the study of power spectrum analysis of velocity fields observed in the solar photosphere. His observations reveal that oscillatory motions with a period of 300 seconds come in fairly well defined bursts that may last in phase as long as 30 minutes. Howard states: 'Both the power spectrum and the visual observations of the tracings show that a wide range of periods between 200 and 400 seconds are present. There appears to be no relation between the periods seen and the presence or absence of a magnetic field in the region being observed. Near the limb, shorter periods are found - down to about 100 seconds'.

De Jager (1965) has summarised current ideas on the spectra of the solar photosphere in Figure 5.2. He observes that the spectral region covered by our analysis viz. 6 to 30 cycles per hour is one in which the sun seems to be constantly active. Moreover, the particular periods of 200 to 300 seconds seem to be associated with the scale size of the granules.

Troitskaya and Gul'elmi (1967) in a recent review of geomagnetic micropulsations have pointed out characteristics of PC 4 and PC 5 pulsations as indicated in the

Appendix I.. The occurrence of the geomagnetic activity of PC 4 is reduced with high Kp. This similarity with what we observe in cosmic rays is perhaps indicative of a general correlation between these two phenomena.

The simultaneous onset of geomagnetic disturbance producing high Kp and a Forbush decrease of large magnitude, signifies the passage across the earth of a sharp discontinuity in the interplanetary plasma and the magnetic field configuration. During the period under review, there were 106 epochs of high Kp while there were only 9 epochs for which Forbush decreases with intensity changes of more than 2% also occurred at Deep River in the neutron monitor. For high Kp occurring without a Forbush decrease, the short period fluctuations of cosmic rays have prominent peaks but low average power. On the other hand for geomagnetic storms, accompanied by large Forbush decreases, we have high average power in the cosmic ray fluctuations and generally an absence of prominent peaks. This would seem to suggest that blast waves producing cosmic ray Forbush decreases sweep galactic cosmic rays in the interplanetary space but are followed by a turbulent pusher gas which has a whole range of irregularities and scale lengths corresponding to the excitation of the entire range of frequencies from 6 to 30 CPH. Indeed this is fully consistent with the model suggested by Parker (1965).

We would like to assume that the main driving force for the cosmic ray oscillations in the range 6 to 30 cycles per hour arises on the sun. When the Kp is low, we can assume on the average that the magnetic field lines connecting the earth and the sun are relatively undisturbed with few magnetic field irregularities. Under these conditions, solar excitation is communicated without selective attenuation of any particular spectral frequencies. However, when magnetic field lines have got irregularities, they provide a preferential passage for transmission of certain frequencies and not others. Under these conditions, the power spectrum analysis that we see in cosmic rays has got certain peaks and the average power is reduced. At the same time, the irregularities associated with the interaction of wind of higher velocity with slower velocity plasma contributes to a higher Kp.

The prominent peaks at 16 and 27 cycles per hour in cosmic rays in the overall data is remarkably close to the preferred frequencies at the sun as well as to the resonant frequency observed in the magnetosphere.

Clinching the interpretation suggested here requires a more detailed comparison of the frequencies observed in individual three-hourly intervals with frequencies observed simultaneously in the interplanetary plasma and in the

magnetosheath. In our present analysis, we had available only one sample each for the two measurements in space. However, it is expected through the collaboration of workers engaged in the measurement of magnetic fields in interplanetary space and in the magnetosphere to extend the interpretation by more detailed analyses on three-hourly interval basis.

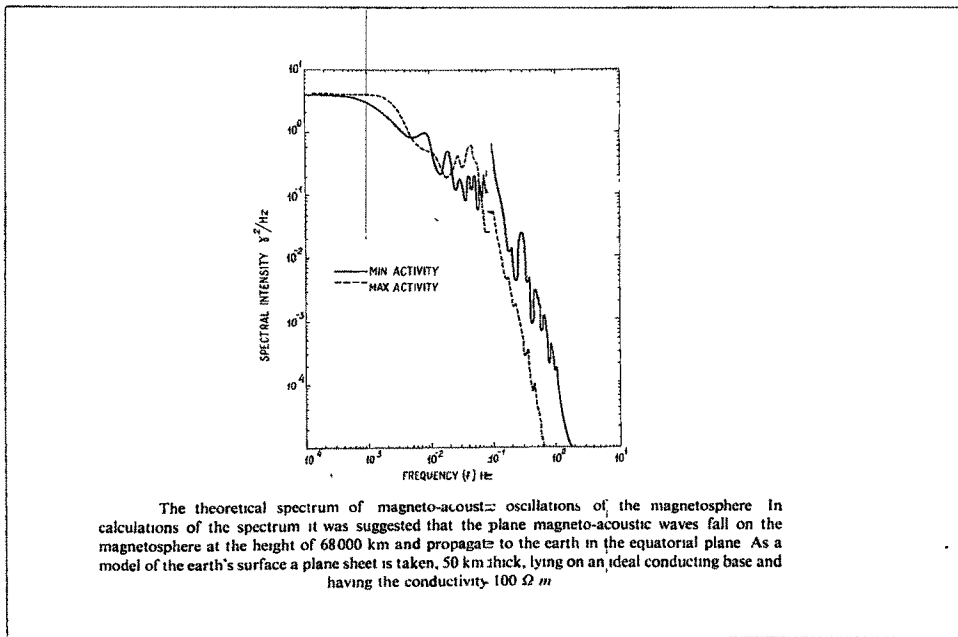


FIG. 5.1

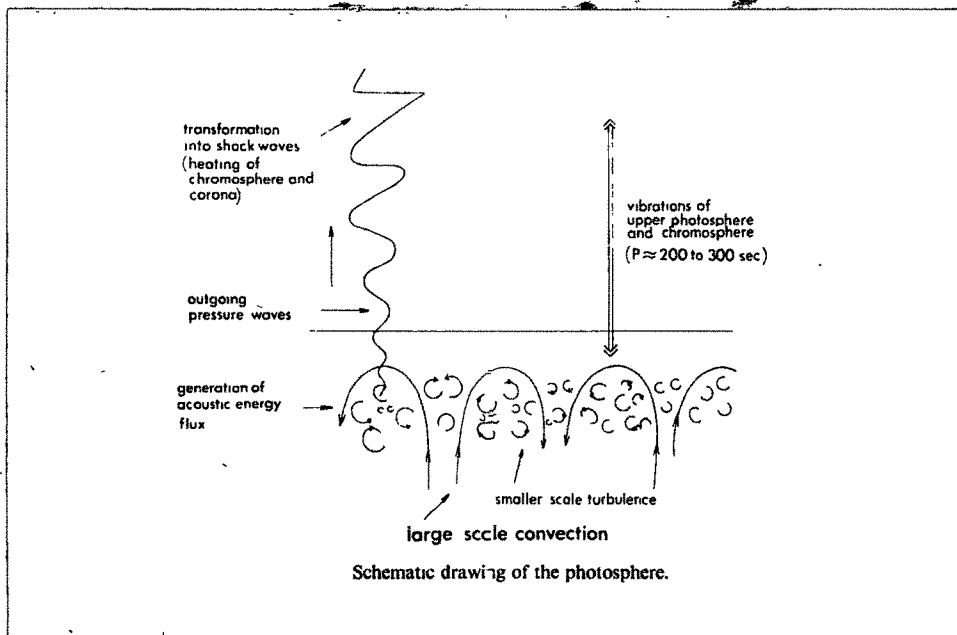


FIG. 5.2

A P P E N D I X I

From table No.VII (Troitskaya and Gul'elmi 1967)

Type of classification	: Pc 5, Pc 4, Pc 3.
Period (second)	: 150 to 600, 45 to 150, 10 to 45.
Additional characteristics and names	: Pg.
Amplitude average(gamma)	: 1-10
Characteristic of the spectrum	: Relatively regular spectrum.
Time of occurrence	: Morning and evening hours.
Character of planetary distribution	: Local in latitude and not greatly extended in longitude; strong correlation in conjugate points; dependence of the period from the latitude.
Connection with different type of magnetic activity	: Most typical for moderate magnetic activity.

From table No. VIII

Type of micropulsation : Pc 5.

Interpretation:

Generation : Interaction of solar wind with magnetosphere on the morning and evening sides.

Propagation : Toroidal oscillations.

Diagnostics:

Parameters of magnetosphere : Plasma density.

Methods of diagnostics : Using the dependence of the period of oscillations on the latitude.

A P P E N D I X II

Using the following simplified relation for estimating the changes in the cut off rigidity

$$\frac{\delta I}{I} = - \delta E_{\min} \cdot W$$

where $\frac{\delta I}{I}$ is the cosmic ray intensity change in %,

δE_{\min} is the change in cut off rigidity,

and W is the coupling coefficient in % BeV,

for $\frac{\delta I}{I}$ of .04% and taking a value of W equal to 1.5%/BeV (Dorman, Cosmic Ray variations, page 117) one finds that a change of about .03% is required in the E_{\min} . Thus .03% change in the earth's magnetic moment should occur if we use the formula

$$E_{\min} = \frac{M}{4 r_e^2} \cos \lambda^4$$

where M is the earth's magnetic moment

r_e is the radius of the earth

and λ is the geomagnetic latitude.

The station is situated almost at the geomagnetic equator, so $\lambda = 0$.

A P P E N D I X III

1. Fortran programme : P.S.A. Part I (A),
Input 12 sec. data ; Output 1 minute deviations.
2. Fortran programme : P.S.A. Part I (B),
Input 5 minute data; Output 5 minute deviations.
3. Fortran programme : P.S.A. Part II,
Input P.S.A. Part I; Output raw and refined
spectral density estimates.

```

C     POWER SPECTRUM ANALYSIS PART I(A)
C     DEVIATION FROM 1 MINUTE DATA
C     DIMENSIONA(15),X(2005)
C
C     READ CONTROL CARD,LAG INTERVAL,NO. OF LAGS,AND H
C
10  READ 11,DELT,M,H
11  FORMAT(F3.2,I2,F3.2)
C
C     READ DATA CARDS
C
1000 READ 12,A(1),A(2),A(3),A(4),A(5),A(6),A(7),A(8),A(9),A(10),
1A(11),A(12),A(13),A(14),A(15),IMS,IHS,IDS
12  FORMAT(3F4.0,1X,3F4.0,1X,3F4.0,1X,3F4.0,1X,3F4.0,I3,I2,I3)
    SX=0.
    N=0
    IMN=IMS
    IHR=IHS
    IDY=IDS
    GO TO 30
120  READ 12,A(1),A(2),A(3),A(4),A(5),A(6),A(7),A(8),A(9),A(10),
1A(11),A(12),A(13),A(14),A(15),IMN,IHR,IDY
    IF(IDY)30,80,30
30   S=0.
    DO 40 I=1,15
40   S=S+A(I)
    N=N+1
    X(N)=S
    SX=SX+S
    IF(SENSE SWITCH 1)50,60
50   PUNCH 1,N,X(N)
51   FORMAT(I5,F10.0)
60   IME=IMN
    IHE=IHR
    IDE=IDY
    IF(N-2000)20,20,70
70   PRINT 71
71   FORMAT(32HNO.OF VALUES ARE MORE THAN 2000).
    PAUSE
    GO TO 10
80   C=N
    XM=SX/C
    IPP=N-1
C
C     HEADING CARD
C
    PUNCH 90,IMS,IHS,IDS,IME,IHE,IDE,H,DELT,M,IPP,XM
90   FORMAT(2I3,I4,1X,2HTO,2I3,I4,2F6.1,2I4,3F11.3)
C
C     CALCULATION OF DEVIATION
C
    DO 110 I=1,N,5
    DO 100 J=1,5
    K=I+J-1
    IF(K-N)100,100,110
100  X(J)=X(K)-XM
110  PUNCH 120,X(1),X(2),X(3),X(4),X(5),K
120  FORMAT(5F7.2,I5)
    GO TO 1000
    END

```

```

C      POWER SPECTRUM ANALYSIS PARTI(B)
C      DEVIATION FROM 5 MINUTE DATA
C      DIMENSIONA(3),X(2005)

C      READ CONTROL CARD,LAG INTERVAL,NO. OF LAGS,AND H
C
10 READ11,DELT,M,H,MNT
11 FORMAT(F3.2,I2,F3.2,I3)

C      READ DATA CARDS
C
12 READ13,A(1),A(2),A(3),A(4),A(5),A(6),A(7),A(8),A(9),IMS,IHS,IDS
13 FORMAT(3F6.0,6X,3F6.0,6X,3F6.0,6X,2I2,I3)
    SX=0.
    N=0
    IMN=IMS
    IHR=IHS
    IDY=IDS
    GOTO30
20 READ13,A(1),A(2),A(3),A(4),A(5),A(6),A(7),A(8),A(9),IMN,IHR,IDY
    IF(IDY)30,80,30
30 DO40I=1,9,3
    N=N+1
    S=A(I)
    S=S+A(I+1)
    S=S+A(I+2)
    X(N)=S
40 SX=SX+S
    IF(SENSE SWITCH 1)50,60
50 PUNCH51,N,X(N-2),X(N-1),X(N)
51 FORMAT(I5,5F10.0)
60 IME=IMN
    IHE=IHR
    IDE=IDY
    IF(N-2000)20,20,70
70 PRINT71
71 FORMAT(32HNO. OF VALUES ARE MORE THAN 2000)
    PAUSE
    GOTO12
80 C=N
    XM=SX/C
    IPP=N-1

C      HEADING CARD
C
    PUNCH90,IMS,IHS,IDS,IME,IHE,IDE,H,DELT,M,IPP,XM
90 FORMAT(2I3,I4,1X,2HTO,2I3,I4,2F6.1,2I4,3F11.3)

C      CALCULATION OF DEVIATION
C
    DO110I=1,N,5
    DO100J=1,5
    K=I+J-1
    IF(K-N)100,100,130
100 X(J)=X(K)-XM
110 PUNCH120,X(1),X(2),X(3),X(4),X(5),K
120 FORMAT(5F7.2,I5)
    GOTO12
130 DO 140 J=J,5
140 X(J)=0.
    K=K-1
    GO TO 110
END

```

```

C POWER SPECTRUM ANALYSIS PART II WITH FILTER AND PREWHITENING
  DIMENSIONX(2000),C(200),V(200),U(200),Z(2000)
C
C READ HEADING CARD
C
100 READ423,IT,IZ,IDAY,IM1,IH1,IDAY1,H,DELT,M,IPP
    IH=H
    IF((IPP-1)/IH-M)1,2,2
    1 PRINT3
    PAUSE
    GOTO100
    2 DO543I=1,IPP,5
C
C READ VALUES OF DEVIATION FROM P.S.A 1
C
543 READ123,X(I),X(I+1),X(I+2),X(I+3),X(I+4)
    MR=M+1
    MM=M-1
    NA1=IPP+1-MM
    PM=M*M
    NN=NA1-MM
    HDELT=H*DELT
    NA2=NA1-1
C
C APPLICATION OF HIGH PASS DIGITAL FILTER
C
DO200I=M,NA1
    FEX1=0.
    IM=I-M
    DO35J=1,MM
    AJ1=J
    IMJ=IM+J
    AJ2=M-J
    IJ=I+J
    35 FEX1=FEX1+AJ1*X(IMJ)+AJ2*X(IJ)
    FEX1=FEX1+(AJ1+1.)*X(IMJ+1)
    DFEX=FEX1/PM
    Z(I)=X(I)-DFEX
200 CONTINUE
C
C APPLICATION OF PRE-WHITENING
C
DO 10 I=M,NA2
    J=I-MM
    X(J)=Z(I+1)-0.6*Z(I)
10 CONTINUE
C
C CALCULATION FOR MEAN LAGGED PRODUCT C(R)
C
DO500IR=1,MR
    SX=0.
    IRR=IR-1
    IHR=IH*IRR
    MQ=IPP-IHR
    DO400IQ=1,MQ
    IQHR=IQ+IHR
    400 SX=SX+X(IQ)*X(IQHR)
    AMQ=MQ
    C(IR)=SX/AMQ
500 CONTINUE

```

```

C
C   CALCULATION FOR RAW SPECTRAL DENSITY V(R)
C
      AM=M
      DO300I=1,MR
      R=I-1
      RPI=3.14159*R/AM
      SC=0.
      DO301J=2,M
      AJ=J-1
301  SC=SC+C(J)*COS(RPI*AJ)
300  V(I)=DELT*(C(1)+2.*SC+C(MR)*COS(R*3.14159))
      U(1)=0.5*(V(1)+V(2))
      U(MR)=0.5*(V(M)+V(MR))
      PDM=3.14159/AM
C
C   CALCULATION FOR REFINED SPECTRAL DENSITY U(R)
C
      DO302J=2,M
      AJ=J
      U(J)=0.25*(V(J-1)+V(J+1))+0.5*V(J)
C
C   COMPENSATION FOR PRE-WHITENING
C
      DIV=1.36-1.2*COS(AJ*PDM)
302  U(J)=U(J)/DIV
      DEN=2.*AM*DELT
      DO900J=1,MR
      R=J-1
      FR=R/DEN
      I=R
C
C   OUT PUT GIVING C(R),V(R),U(R) AND FREQUENCY
C
      PUNCH5,IT,IZ,IDAY,IM1,IH1,ICDAY1,H,DELT,M,I,C(J),V(J),U(J),FR
900  CONTINUE
      PAUSE
      GOTO100
      3  FORMAT(19HM IS GREATER THAN N)
      5  FORMAT(2I3,I4,1X,2HT0,2I3,I4,2F3.0,I4,I4,3F11.2,F6.3)
123  FORMAT(10F7.2)
423  FORMAT(2I3,I4,1X,2HT0,2I3,I4,2F6.1,2I4,3F11.3)
      END

```

-
REFERENCES

- Akimov, Yu.K., 1965 Scintillation counters in high energy Physics, (Academic Press).
- Anderson, K.A. and N.F.Ness, 1966 Jour.Geophys. Res. 71, 3705.
- Axford, W.I., 1964 The solar wind, page 231, Edited by Mackin and Neugebauer (J.P.L),(Pergamon Press).
- Balasubrahmanyam, V.K., and F.B.McDonald, 1964 Jour.Geophys. Res. 69, 3289.
- Barrett, P.H., L.N.Ballinger, G.Cocconi, Y.Eisenberg, and K.Greisen, 1952, Rev.Mod. Phy., 24, 133.
- Bercovitch, M., 1966 Can.Jour.of Phys. 44, 1329
- Bethe, H., 1933 Handbuchder Phy:Vol 24(1), (Springer, Berlin).
- Biermann, L., 1957 Observatory, 77, 109.
- Blackman, R.B., and J.W.Tukey, 1959 The measurement of Power Spectra, (Dover Publications, New York).
- Bland, C.J., 1962 Phil. Mag. 7, 1487.
- Bonetti, A., H.S.Bridge, A.J.Lazarus, B.Rossi, and F.Scherb, 1963 Jour.Geophys. Res. 68, 4017.
- Brice, N.M., 1967 ibid, 72, 5193.
- Bridge, H.S., 1964 The solar wind, page 123, Edited by Mackin and Neugebauer, (J.P.L), (Pergamon Press).
- Brunberg, E.A., 1953 Tellus, 5, 135.

- Buck, W.L., and R.K. Swank, 1953 Nucleonics, Vol.11, No.11, 48.
- Cahill, L.J., and P.G. Amazeen, 1963 Jour. Geophys. Res., 68, 1835.
- Cahill, L.J., and D.H. Bailey, 1965 Trans. A.U.G. 46, 116.
- Cahill, L.J., and V.L. Patel, 1967 Planet. Space. Sci. 15, 997.
- Chapman, S., 1957 Smithsonian Contr. Astrophys. No.1.
- Chapman, S., 1959 Proc. Royal Soc. A 253, 462.
- Chapman, S., and V.C.A. Ferraro, 1931 Terr. Mag. 36, 77, 171, and 37, 147.
- Charakhch'yan, A.N., and T.N. Charakhch'yan, 1959 Soviet Phy-JETP, 8, 761
- Clark, G., J. Earl, W. Kraushaar, J. Linsley, B. Rossi and F. Scherb, 1957a Nature, 180, 353 and 406.
- Clark, G., I. Escobar and J. Hersil 1962 Proc. Fifth Interamerican Seminar (Lapaz), Vol. II, 36.
- Clark, G., F. Scherb and W.B. Smith, 1957b Rev. Sci. Inst. 28, 433.
- Coleman, P.J., 1966 Jour. Geophys. Res. 71, 5509.
- Davidson, M.J., 1964 Jour. Geophys. Res. 69, 5116.
- De Jagar, C., 1965 Int. to Solar Terrestrial Relations, Edited by Ortner and Maseland (Reidal Holland), page 13.
- Dhanju, M.S., and V.A. Sarabhai, 1967 Phy. Rev. Letters, 19, 252.
- Dorman, L.I., 1957 Cosmic Ray Variations (State Publishing House, Moscow).

- Dorman, L.I., 1960 Proc. Moscow Conf., 4, 21.
- Dorman, et al, 1961 Results I.G.Y. (Moscow),
Cosmic Rays, No.4, 5.
- Dorman, L.I., 1963 Progress in Elementary particles
and cosmic ray Phys.Vol.VII, 7
(North Holland).
- Duffus, H.J., 1954 Jour.Geophys. Res. 64, 581.
J.A.Shand, C.S.Wright,
P.W.Nasmyth and
J.A.Jacobs,
- Duperier, A., 1948 Proc.Phy.Soc. 61, 34.
- Duperier, A., 1949 Proc.Phy.Soc. 62A, 684.
- Elliot, H., and 1951 Jour.Atm.Terr.Phy. 1, 205.
D.W.N.Dolbear,
- Elliot, H., 1952 Progress in Elementary particles
and cosmic ray Phy.Vol. 1, 455
(North Holland).
- Fairfield, D.H., and 1967 Jour.Geophys.Res. 72, 2379.
N.F.Ness,
- Field, E.C., and 1966 Jour.Geophys.Res. 71, 3223.
C.Greifinger,
- Finch, H.P., and 1957 Monthly Notices of Roy.Astr.Soc.
B.R.Leaton, (Geophy.Suppl.) 7, 314.
- Firor, J., 1954 Phy.Rev. 94, 1017.
- Fischer, J., 1955 Nucleonics, 13, No.5, 52
- Forbush, S.F., 1957 Proc.Mat.Acad.Sci. 43, 28
- Forbush, S.F., 1958 Trans. Am.Geophy.Union 39, 1004
- Forbush, S.F., 1966 Handbuchder Phys.Vol.49/1, 159,
(Springer, Berlin).

- Freir, P.,
E. J. Lofgren, E. P. Nay
and F. Oppenheimer, 1948 Phy. Rev. 74, 1818.
- Gold, T., 1959 Jour. Geophys. Res. 64, 1665.
- Heppner, J. P.,
N. F. Ness,
C. S. Scearce, and
T. L. Skillman, 1963 Jour. Geophys. Res. 68, 1.
- Hessler, V. P., 1967 High Altitude Geophysical Data,
UAG-C 43 and 44. Published by
Geophysical Institute, University
of Alaska.
- Hessler, V. P., and
E. M. Wescott, 1959 Nature, 184, 627.
- Howard, R., 1967 Solar Phys. 2, 3.
- Jacobs, J. A.,
Y. Kato, S. Matsushita
and V. A. Troitskaya, 1964 Jour. Geophys. Res. 69, 180.
- Jensen, D. C., and
J. C. Cain, 1962 Jour. Geophys. Res. 67, 3568.
- Johnson, T. H., 1938 Rev. Mod. Phys. 10, 193.
- Jokipii, J. R., 1966 Ap. J., 146, 480
- Jokipii, J. R.; 1967 ibid, 149, 405
- Jory, F. S., 1956 Phy. Rev. 102, 1167.
- Judge, D. L., and
P. J. Coleman, 1962 Jour. Geophys. Res. 67, 5071.
- Kaminer, N. S.,
S. F. Ilgatch, and
T. S. Khadakhanova, 1965 Proc. London Conf. Vol. 1, 486.
- Kane, R. P., 1963 Nov. Cim. 27, 441.
- Kane, R. P., 1964 Nov. Cim. 32, 273

- Kaplon, M.F.,
D.M.Ritson and
E.P.Woodroff, 1952 Phy.Rev., 85, 933.
- Kato, Y., 1965a Proc. Jap.Acad.Vol.41, No.7, 582.
- Kato, Y., 1965b Proc. Jap.Acad.Vol.41, No.8, 711.
- Kato, Y., 1967 Proc. Conjugate Point Symposium
(Boulder) III-6-1.
- Katz, L., P.Mayer,
and J.A.Simpson, 1958 Nov.Cim. 8 Suppl.II, 277.
- Kellogg, P.J., 1960 Jour.Geophys.Res. 65, 2701
- Kodama, M and
Y.Miyazaki, 1957 Rep.Ion.Res., 11, 99.
- Kondo, I., K.
Nagashima, S.Yoshida
and M.Wada, 1960 Proc.Moscow Conf. Vol.IV, 208.
- Lemaitre, G., and
M.S.Vellarate, 1933 Phy.Rev., 43, 87.
- Lemaitre, G., and
M.S.Vellarate, 1936. Phy.Rev., 50, 493.
- Lust, R., 1957 Phy.Rev., 105, 1827.
- Lyon, E.,
H.S.Bridge, A.Egidi,
and B.Rossi, 1964 Trans.Am. Geophy.Union 45, 605.
- Making, T., and
I.Kondo, 1965 Proc.London Conf.Vol.I, 564.
- Malmfors, K.G., . 1945 Ark.Mat.Astr.Fy. 32A, No.8.
- Malmfors, K.G., 1949 Tellus, Vol.1, No.2, 55.
- Mason, R.G., 1963a Trans.Am.Geophy.Union, 44 No.1,
40.
- Mason, R.G., 1963b Sci.Rep.63-13, Uni.of Calif.
Scripps Inst.San Diego,(Calif).
- Mathews, T., 1963 Phil. Mag., 8, 387.

- Mayer, P., and J. A. Simpson, 1957 Phy. Rev., 106, 568.
- McCracken, K. G., 1962 Jour. Geophys. Res., 67, 423.
- McCracken, K. G., U. R. Rao, and M. A. Shea, 1962 M. I. T. Tech. Report No. 77.
- Mead, G. D., 1964 Jour. Geophys. Res., 69, 1181.
- Mead, G. D., and D. B. Beard, 1964 Jour. Geophys. Res., 69, 1169.
- Midgley, J. E., and L. Davis, 1963 Jour. Geophys. Res., 68, 5111.
- Muirhead, H., 1965 Phy. of Elementary Particles, page 7, (Pergamon Press).
- Mustel, E. R., 1964 Space Research Vol. IV, 77.
- Ness, N. F., 1965 Jour. Geophys. Res., 70, 2989.
- Ness, N. F., and J. M. Wilcox, 1964 Phy. Rev. Letters, 13, 461.
- Ness, N. F., C. S. Scearce, and J. B. Seek, 1964 Jour. Geophys. Res., 69, 3531.
- Ness, N. F., C. S. Scearce, and S. Cantarano, 1966 Jour. Geophys. Res., 71, 3305.
- Neugebauer, M., and C. W. Snyder, 1966 Jour. Geophys. Res., 71, 4469.
- Obayashi, T., 1958 Ann. Geophys. 14, 464.
- Obayashi, T., 1959 Rep. Ion. Spa. Res., Japan, 13, 201.
- Ol', A. I., 1963 Geomag. and Aero., Vol. 3 No. 1, 113.
- Olbert, S., 1953 Phy. Rev. 92, 454.
- Pai, G. L., and V. A. Sarabhai, 1964 Planet. Spac. Sci., 12, 855.
- Parker, E. N., 1957 Phy. Rev., 107, 924.

- Parker, E.N., 1958a *ibid*, 110, 1445.
- Parker, E.N., 1958b *Ap. Jour.*, 128, 664.
- Parker, E.N., 1961 *Ap. Jour.*, 133, 1014.
- Parker, E.N., 1963 *Interplanetary Dynamical Processes*,
(Interscience Publishers, New York).
- Parker, E.N., 1965 *Spa. Sci. Rev.*, 4, 666.
- Patel, V.L., 1967 Private Communication.
- Patel, V.L., and 1964 *Phy. Rev. Letters*, 12, 213.
L.J. Cahill,
- Pomerantz, M.A., and 1962 *Phil. Mag.*, 7, 1503.
S.P. Aggarwal,
- Prince, C.E., and 1964 *Jour. Geophy. Res.*, 69, 3213.
F.X. Bostick,
- Quenby, J.J., 1967 *Handbuch der Phys. Vol. 46/2*, 310
(Springer, Berlin).
- Quenby, J.J., and 1959 *Phil. Mag.*, 4, 90.
W.R. Webber,
- Quenby, J.J., and 1960 *Phil. Mag.*, 5, 585.
T. Thambyahpillai,
- Quenby, J.G., and 1962 *Phil. Mag.*, 7, 1457.
G.J. Wenk,
- Ramakrishnan, A. 1962 *Elementary particles and cosmic
rays*, page 395 (Pergamon Press).
- Rao, U.R., and 1961 *Proc. Royal Soc.*, 263, 127.
V.A. Sarabhai,
- Rao, U.R., 1963 *Jour. Geophys. Res.*, 68, 345.
K.G. McCracken, and
D. Venkatesan,
- Rose, D.G., 1956 *Can. Jour. Phys.*, 34, 968.
K.B. Fenton,
J. Katzman, and
J.A. Simpson,

- Rossi, B., 1960 Proc.Moscow Conf., Vol.II, 18.
- Rossi, B., and K.Greisen, 1941 Rev.Mod. Phys., 13, 240.
- Rothwell, P., 1959 Jour.Geophys.Res., 64, 2026.
- Richard, K.F., U.R.Rao, and W.B.Smith, 1963 Rev.Sci.Instr., 34, 505.
- Sarabhai, V.A., 1963 Jour.Geophys.Res., 68, 1555.
- Sarabhai, V.A., and N.Nerurkar, 1956 Annual Rev.of Nuclear Sci., Vol.6, 1.
- Shea, M.A., D.F.Smart, and K.G.McCracken, 1965 Jour.Geophys.Res., 70, 4117.
- Shockley, W., and J.F.Gibbons, 1958 Semiconductor Products Jan/Feb., 9.
- Simpson, J.A., W.Ponger, and S.B.Treiman, 1953, Phy.Rev.90, 934.
- Singer, S.F., 1958 Progress in Elementary particles and cosmic ray Physics, 4, 203, (North Holland).
- Siscoe, G.L., L.D.Davis, E.J.Smith, P.J.Coleman, and D.E.Jones, 1967 Jour.Geophys., Res., 72, 1.
- Snyder, C.W., and M.Neugebauer, 1964 Space Research, Vol. IV, 89.
- Snyder, C.W., M.Neugebauer, and U.R.Rao, 1963 Jour.Geophys.Res., 68, 6361.
- Stormer, C., 1955 The Solar Aurora (Clarendon Press, London).

- Suga, K., G. Clark, and I. Escobar, 1961 Rev. Sci. Instr., 32, 1187.
- Suga, K., I. Escobar, G. Clark, W. Hazen, A. Hendel, and K. Murakami, 1962 Jour. Phy. Soc. Japan, Vol. 17, A-III, 128.
- Swann, W. F. G., 1933 Phy. Rev., 44, 224.
- Swinnerton-Dyer, H. D. F., 1963 The Computer Jour., 16, 16.
- Treiman, S. B., 1952 Phy. Rev., 86, 917.
- Torizuka, K., and M. Wada, 1960 Sci. Papers Inst. Phys. Chem. Res. (Tokyo), 54, 168.
- Torizuka, K., and M. Wada, 1962, Proc. Fifth Interamerican Seminar (Lapaz) XXVII.
- Troitskaya, V. A., and A. V. Gul'elmi 1967 Spa. Sci. Rev., Vol. VII, 689.
- Venkatesan, D., 1958 Nov. Cim., Suppl., 8, 285.
- Wada, M., 1961 Jour. Sci. Res., Inst., 55, 7.
- Webber, W. R., 1963 Jour. Geophys. Res. 68, 3065.
- Webber, W. R., and J. J. Quenby, 1959 Phil. Mag., 4, 654.
- Wilcox, J. M., and N. F. Ness, 1965 Jour. Geophys. Res., 70, 5793.
- Winckler, J. R., 1960 Jour. Geophys. Res., 65, 1331.
- and also;
- Masley, A. J., T. C. May, and J. R. Winckler, 1962 Jour. Geophys. Res., 67, 3243.
- Yoshida, S., and M. Wada, 1959 Nature, 183, 381.

.....

LIST OF TABLES

<u>Table No.</u>	<u>Contents</u>	<u>Page No.</u>
1.1	The values of the exponent γ in the integral energy spectrum in the different regions of energy of cosmic rays.	4
1.2	Classification of the important nuclear particles.	5
2.1	Pulse characteristics at the input and output of the cable from driver stage to pre-scaler.	55
2.2	Summary of the recording intervals.	63
2.3	Discriminator levels for each scintillator.	87
3.1	The durations of the recorded data.	91
3.2	Inter-relation of the P.S.A. (Power Spectrum Analysis) constants for basic data interval of 12 seconds, 1 minute and 5 minutes.	107
4.1	Prominent cosmic ray frequencies, their amplitudes, and the values of their diurnal wave, for 487, 547 and 1034 superposed three hourly samples.	114
4.2	Prominent cosmic ray frequencies, their significance levels and amplitudes for three hourly intervals of 1400 to 1700 hour and 1715 to 2015 hours, Dec.16,1965.	116
4.3 a	Prominent cosmic ray frequencies, their significance levels, and amplitudes in the superposed samples for negative and positive intensity change epochs. The average power for 6 to 30 CPH for each of the epoch is also given.	118

- 4.3 b Prominent cosmic ray frequencies, their confidence levels, and amplitudes in the superposed samples for fast and slow change epochs. The average power for 6 to 30 CPH for each of the epoch is also given. 119
- 4.4 Characteristics of the three Forbush decreases for which the spectral frequencies are investigated. 120
- 4.5 Prominent cosmic ray frequencies, their confidence limits, and amplitudes during the onset phases of the Forbush decreases: together with the average power for 6 to 30 CPH. 121
- 4.6 Prominent cosmic ray frequencies at 95% confidence limits in the pre-onset, onset and post-onset phases of the three Forbush decreases. 122
- 4.7 Prominent cosmic ray frequencies, their significance levels and amplitudes for different ΣK_p epochs. The average power for 6 to 30 CPH for each of the epoch is also given. 124

SHORT-PERIOD VARIATIONS OF COSMIC-RAY INTENSITY*

M. S. Dhanju and V. A. Sarabhai
Physical Research Laboratory, Ahmedabad, India
(Received 26 June 1967)

Hitherto it has not been possible to establish the occurrence of time variations of galactic cosmic rays with very short periods, of the order of a few minutes, because large detectors that give a really high counting rate were not available. An attempt by Torizuka and Wada,¹ with a counting rate of around 10^5 counts/min, has not yielded conclusive results. However, a large-area scintillation muon detector has been operated for several years by the Bolivian Air Shower Joint Experiment (BASJE) at Chacaltaya at an altitude of 17 200 ft, longitude $68^\circ 10'$ W and geomagnetic latitude -5.0° . The authors have been fortunate to have had the opportunity of using the output of the BASJE detector with a counting rate of a million counts/min for conducting an investigation from April 1964 to June 1966. 15 scintillation detectors each of 4 m^2 were used (Suga *et al.*²). The total array of 60 m^2 , housed in a cave, was shielded by 3 m water equivalent of galena so that the electron component was absorbed. The outputs of sets of five detectors were combined to provide three independent channels for intercomparison. Accurate time was maintained by using a crystal controlled electronic clock. Cosmic-ray data were recorded every 12 sec while one-minute recordings of barometric pressure were also made using a digital servobarometer. The 12-sec data from the three channels were intercompared and unless one or more channels exhibited erratic behavior, data from the three independent channels were combined for successive one-minute intervals. The constants used for power spectrum analysis were $n = 180$, $m = 30$, and $t = 1$ min, where n is the number of data points in each set, m is the total lag, and t is the averaging interval for each point. This gave us spectral estimates at 31 points equally spaced in frequency from 0 to 30 cycle/h. The significance of spectral-density estimates was evaluated using the method suggested by Blackman and Tucky.³ For the chi-squared distribution, we have $2(n/m - \frac{1}{3}) \sim 11$ degrees of freedom.

Spectral estimates show variability in individual samples of three-hourly intervals. As more samples are superposed, peaks in the

spectral frequency range of 1 to 6 cycle/h get smeared out by superposition. However, persistent peaks at 18 and 25 cycle/h are observed. These appear at 99% confidence limits for the superposition of 487 three-hourly sets during November 1965 to March 1966, as shown in Fig. 1. Records⁴ of the magnetic field taken by Mariner IV in the magnetosheath region a year earlier indicate that at 200-sec period (18 cycle/h), there was large spectral activity. Ness, Scearce, and Cantarano⁵ have found spectral peaks of 600-, 300-, 180-, and 120-sec periods in the interplanetary magnetic field recorded by Pioneer VI on 16 December 1965 from 1715 to 2015 h. Cosmic-ray data for the same interval show similar periodic fluctuations which are shown in Fig. 2.

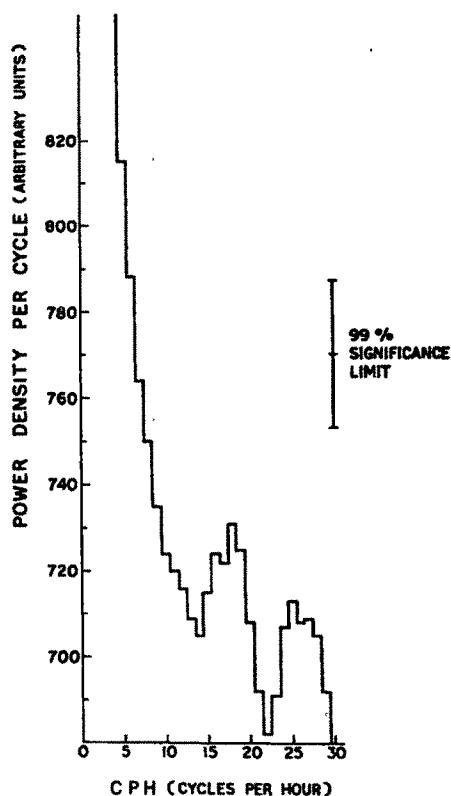


FIG. 1. The superposed spectral density for 487 three-hourly sets (November 1965 to March 1966) indicating peaks at 18 and 25 cycle/h.

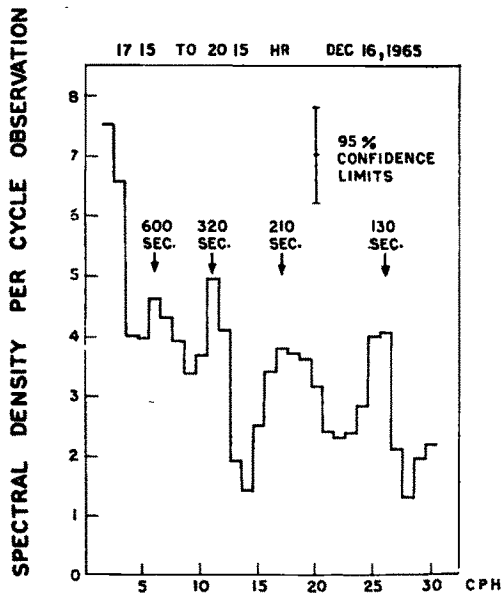


FIG. 2. The spectral density estimates for cosmic rays corresponding to the three-hourly interval when Pioneer VI was simultaneously recording interplanetary magnetic field.

Local time dependence of the spectral density has been studied for 18 cycle/h. Figure 3 corresponding to 487 intervals indicates that the variation has large amplitude when the detector is in the antisolar direction.

The barometric pressure at one-minute intervals has been subjected to power-spectrum analysis. The absence of any peaks of pressure in the region of interest corresponding to cosmic-ray peaks indicates that the cosmic-ray peaks are not due to barometric pressure changes. An attractive possibility of explaining the short-period fluctuation of cosmic rays appears through the periodic change of geomagnetic cutoff rigidities. For 487 three-hourly intervals the average amplitude of the 18-cycle/h periodicity is about $(0.04 \pm 0.01)\%$. To account for these periodic changes, which have been observed for the first time in the present investigation at the geomagnetic equator, we estimate by using the coupling coefficient given by Dorman⁶ for the meson component that there need to be periodic changes of about 20γ in the dipole field. Fluctuations of this order of magnitude in the magnetosheath have been observed⁴ for 18-cycle/h periodicity.

Related to this interpretation, three inter-

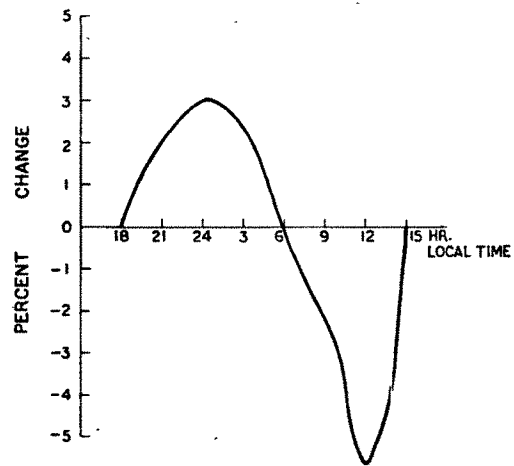


FIG. 3. The percentage change from the average of spectral density in the solar and antisolar directions for 18 cycle/h.

esting points require to be understood: First, the manner in which periodic fluctuations of the interplanetary magnetic field are translated to periodic changes of geomagnetic field relevant to changes in the cutoff rigidity of primary cosmic rays. Interplanetary periodicities measured by magnetometers on space probes are most likely the result of the spatial structure in the plasma wind. For a wind with a radial velocity of 400 km/sec the observed 18-cycle/h fluctuations correspond to a scale length of 0.5×10^{-3} A.U. of the irregularities in the plasma wind. The fluctuations of the energy density impinging on the magnetosphere resulting from these irregularities could be the means through which the periodicities are generated in the geomagnetic field. Second, there is perhaps a difference in the sharpness of the spectral peaks observed in cosmic rays at 18 cycle/h compared to the other peaks. One would like to know whether this is genuine and caused by the inherent resonant and dissipative characteristics of the magnetosheath for energy transmitted through it. Third, the larger amplitude of 18-cycle/h spectral density in the antisolar direction (3%) compared to the solar direction (-5.5%) could probably indicate the variation in the amplitude of the oscillations of the distant geomagnetic field in the tail of the cavity and in the direction of the bow shock. More quantitative analysis with additional data from space craft